POLITECNICO DI TORINO

College of Chemical and Materials Engineering

Master degree
in Chemical and Sustainable Processes Engineering

Master Thesis

Study of a prototype-biosensor effective for the screening of anticancer drugs

Supervisors

Prof. Marco Piumetti
Prof. Valentina Alice Cauda

Candidate

Lorena Elena Bobeica

November-December 2022

Index

1. Introduction

Cancer is a leading cause of death worldwide, accounting for nearly 10 million deaths in 2020. According to The International Agency for Research on Cancer and to the World Health Organization, mortality rates in 2020 are of lung cancer in the first place with 1.80 million deaths, colorectum cancer with 916 000, liver cancer with 830 000 and stomach cancer with 769 000, followed by breast cancer with 685 000 deaths. Incidence rates result to be slightly different, seeing breast cancer as the most common with 2.26 million cases. [1]

Cancer cells present a series of contradistinctive phenomena, commonly known as hallmarks of cancer. They include acquired capabilities for sustaining proliferative signaling, evading growth suppressors, resisting cell death, enabling replicative immortality, inducing/accessing vasculature, activating invasion and metastasis, reprogramming cellular metabolism and avoiding immune destruction. Furthermore, an emerging hallmark from recent studies is a reprogramming energy metabolism, characterized by that known as Warburg effect. [2] This phenomenon, better described in the following section, is generally characterized by an aerobic glycolysis which leads to lactate as its final product. Recent works have shown that lactate is also a potent signaling molecule, triggering the stabilization of hypoxia-inducible factor-1a (HIF-1a), and subsequently increasing expression of vascular endothelial growth factor (VEGF).

As high lactate levels are often associated with a worse prognosis, a solution could be constituted by anti-cancer drugs that inhibit the process of lactate production [4]. Among different ways, this can also be processed by inhibition of Lactate dehydrogenase enzyme, which, in tumoral cells, degenerates from its normal role of equilibrating any change between pyruvate and lactate through a rapid, near equilibrium reaction. So, as the final target for these drugs is Lactate dehydrogenase, the present thesis' purpose is to use of LDH to create a prototype biosensor able to detect two main LDH inhibitory drugs' efficiency: NHI-2 and Galloflavin. More precisely, they are both inhibitors of LDH-A and -B subunits; the first is the predominately expressed isoform of LDH in most cancer cells, while LDH-B is reported to regulate lysosome activity and autophagy in cancer [5] and is essential for oncogenic transformation by different mutants. [6][7][8]

At present, methods mostly used in literature to test efficiency of LDH inhibitors include LDH inhibition assays, cell-based biological evaluation assays, structure-based ligand design and protein-ligand interaction assays. LDH-inhibitor assays generally include ultraviolet absorption and fluorescence methods based on coenzyme NADH, as well as mass spectrometry based on the determination of substrate and product, methods that require a lot of enzyme and time loss. Among these techniques, hyperpolarized magnetic resonance spectroscopic imaging was also tested to evaluate the in vivo activity of an LDH inhibitor in a real-timing and non-invasive way. [9][10]

1.1 The Warburg effect and anti-cancer drug resistance

In 1957 Otto Warburg was the first to observe the anomalous characteristic of cancer cell energy metabolism. [11] Normal cells, under aerobic conditions, convert glucose to pyruvate producing ATP through a process named mitochondrial oxidative phosphorylation, while in anaerobic conditions, glycolysis is favoured and pyruvate is converted into lactate in the cytosol. On the contrary, most malignant cells, including those of lung [12], colorectum [13], liver [14] and pancreatic cancer [15], base their metabolism on an "aerobic glycolysis", meaning glycolysis operating despite the presence of sufficient oxygen. This mechanism leads to production of just 2 ATP molecules in comparison to the 36 ATP molecules produced through oxidative phosphorylation. (**Fig. 1.1**) [16] This behaviour seems to be disadvantageous from an energetic point of view, but several researches claim that tumour cells present a dual metabolism: a glycolytic phenotype under regular conditions which can switch to a non-glycolytic phenotype under lactic acidosis. This last happens under a stressful microenvironment characterized by a limited supply of glucose and helps to maintain cell proliferation. [17]

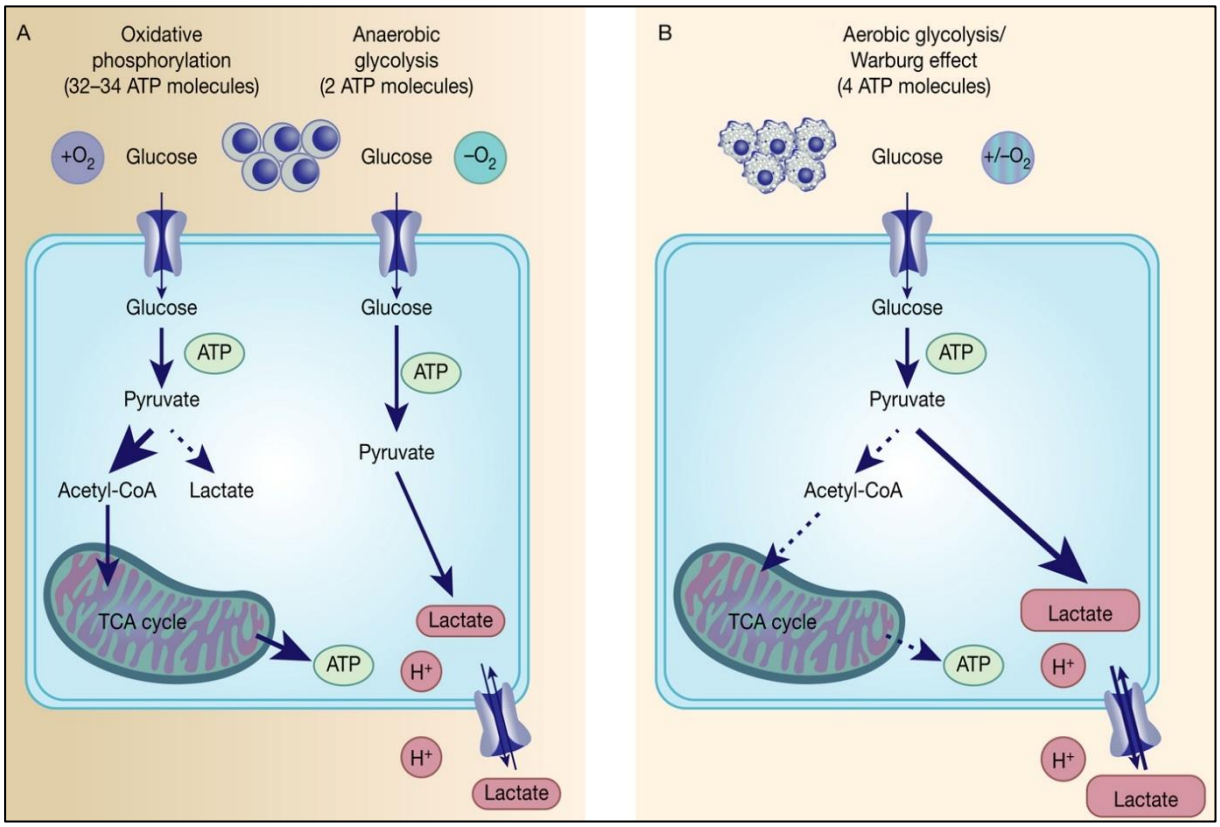

Fig. 1.1 The Warburg effect in cancer. Differentiated, normal tissues (A) metabolise glucose through oxidative phosphorylation in normoxic conditions or anaerobic glycolysis under low oxygen levels. In contrast, tumour cells (B) mainly metabolise glucose to lactate independent from intracellular oxygen (aerobic glycolysis or Warburg effect). From Unterlass *et al*, pp 2, with modifications.

Some studies sustain that the Warburg effect is a common characteristic of both cancer and normal proliferating cells, but they do it for fundamentally different reasons, in fact cancer cells need to neutralize OH- groups generated from Fenton reactions in cytosol while NPCs do it to maintain elevated cytosolic pH as an optimal condition for ribosomal proteins. [18]

Another recently studied behaviour of cancer cells regarding their metabolism is the "Reverse Warburg effect". (**Fig. 1.2**) [19] This concept implies a host-parasite relationship between cancer cells and glycolytic fibroblasts, explaining the contradictory phenomena in certain types of cancer cells with high mitochondrial respiration and low glycolysis rates. In this model of two-compartment tumor metabolism, because of oxidative stress, aerobic glycolysis occurs in stromal fibroblasts, thus becoming cancer-associated fibroblasts (CAFs).

The produced nutrients, mostly lactate, are transferred to adjacent tumor cells for supporting their fuel requirement, thus producing abundant ATP and protecting them against apoptosis. Under similar circumstances of oxidative stress cancer cells will give rise to oxidative and hypoxic cancer cells. The lasts will then be subjected to the anaerobic glycolysis, which ends up with the generation of lactic acid in a similar way as that of CAFs. The produced metabolites will be consumed by the adjacent cancer cells to meet up their metabolic requirements while the rest of the lactic acid generated will be deposited in the extracellular space (ECS), which in turn creates an acidic microenvironment. Therefore, this two-compartment tumour metabolism may contribute to chemoresistance or therapy failure in patients with cancer, as most of the conventional therapies were focusing only on the cancer cells, irrespective of the tumour microenvironment or intratumour heterogenicity. [17] [19]

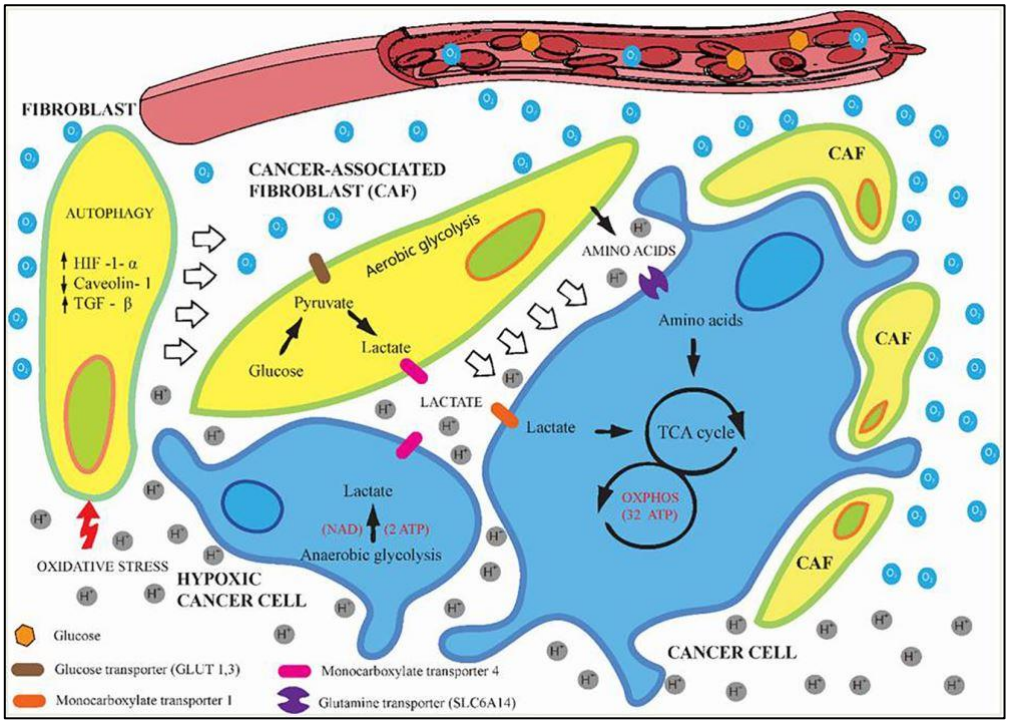

Fig. 1.2 The reverse Warburg mechanism of cancer cells and the significance of the tumour microenvironment in the progression of cancer. From Benny *et al*, pp 5.

Some of the mechanisms that could also provide a chemoresistant phenotype are glucose transport, and glycolytic enzymes such as pyruvate dehydrogenase (PDH) and lactate dehydrogenase (LDH). The last one in particular, which converts pyruvate in lactate as the end product of glycolysis was object of studies and resulted to confer resistance to a specific anti-cancer drug in breast cancer. [20] That might be why some cancer drugs have their principle based on LDH detection and inhibition, as the ones studied in this thesis activity.

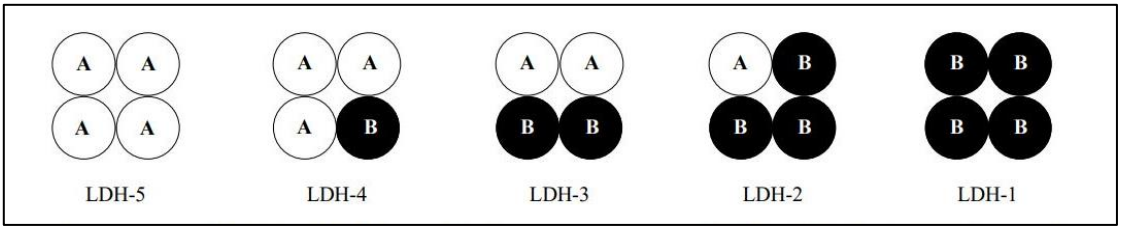

Fig. 1.3 The two homotetramers (LDH-1 and LDH-5) and the three heterotetramers (LDH-2, LDH-3 and LDH-4) are schematically represented. A (or M) and B (or H) are the kinds of the subunits. From Granchi *et al*, pp 675.

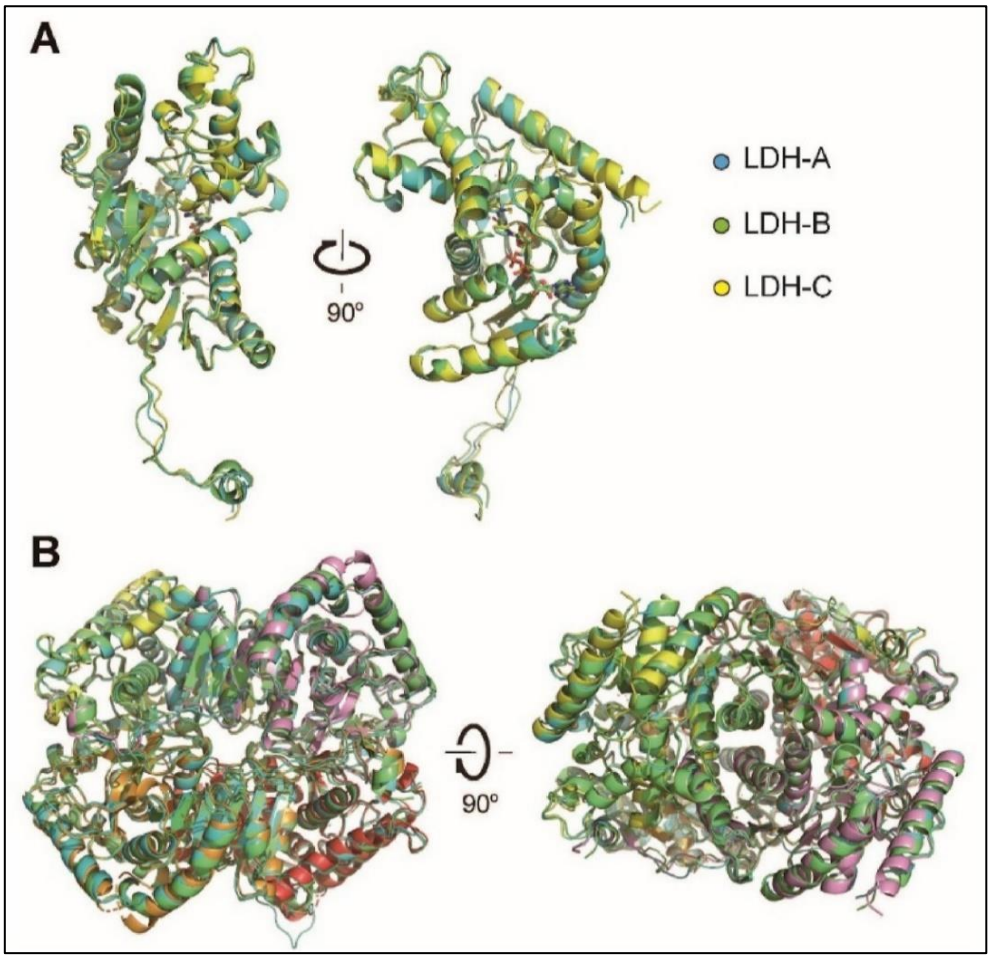

Fig. 1.4 Comparison of crystal structures of human LDH-A, LDH-B and LDH-C. (A) Superpositions of the protomers of three LDH isoforms. The cofactors and substrate-like inhibitors are shown as sticks. (B) Superpositions of the tetramers of three LDH isoforms. For clarity, the cofactors and substrate-like inhibitors are not shown. From Tan *et al*, pp 2355.

1.2 Lactate dehydrogenase as object of the study

LDH is a cytoplasmic enzyme present in almost all tissues but at high concentrations in muscles, liver, and kidney cells. It exhibits five isomeric forms assembled in tetramers of the two types of subunits, namely muscle (A or M) and heart (B or H). The isoforms, called isozymes, are named LDH-1 through LDH-5, each having differential expression in different tissues. (**Fig. 1.3**) [21] The genes that encode LDH are LDH-A, LDH-B, LDH-C, and LDH-D. LDH-A, LDH-B, and LDH-C encode for L-isomers of the enzyme (**Fig. 1.4**) [22], whereas LDH-D encodes the D-isomer.

Lactate dehydrogenase (LDH) is an important enzyme of ordinary cells' anaerobic metabolic pathway. It belongs to the class of oxidoreductases, with an enzyme commission number EC 1.1.1.27. Lactate Dehydrogenase is one of the H transfer enzymes - (oxidoreductase), which catalyses the reversible conversion of pyruvate to lactate using NADH (reduced form of Nicotinamide adenine dinucleotide). (**Fig. 1.5)** [23] Basically, the enzyme is involved in the anaerobic metabolism of glucose when oxygen is absent or in limited supply. LDH-A subunit carries a net charge of -6 and exhibits a higher affinity towards pyruvate, thus converting pyruvate to lactate and NADH to NAD^+. On the other hand, LDH-B has a net charge of +1 and demonstrates a higher affinity towards lactate, resulting in a preferential conversion of lactate to pyruvate and NAD^+ to NADH. [24][25]

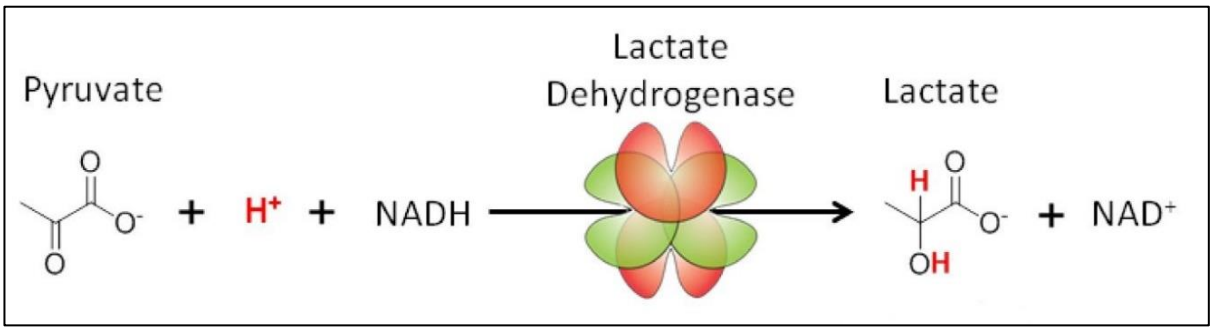

Fig. 1.5 The function of the LDH is to catalyse the reversible conversion of pyruvate to lactate with the oxidation of NADH to NAD+. From Acharya *et al*, pp 2, with modifications.

When cells become exposed to anaerobic or hypoxic conditions, the production of ATP by oxidative phosphorylation becomes disrupted. This process demands cells to produce energy by alternate metabolism. Consequently, LDH is upregulated in such conditions to cater to the need for energy production. However, lactate produced during the anaerobic conversion of glucose meets a dead end in metabolism. It cannot undergo further metabolism in any tissue except the liver. Hence, lactate is released in the blood and transported to the liver, where LDH performs the reverse reaction of converting lactate to pyruvate through the Cori cycle. (**Fig. 1.6**) [26] [27]

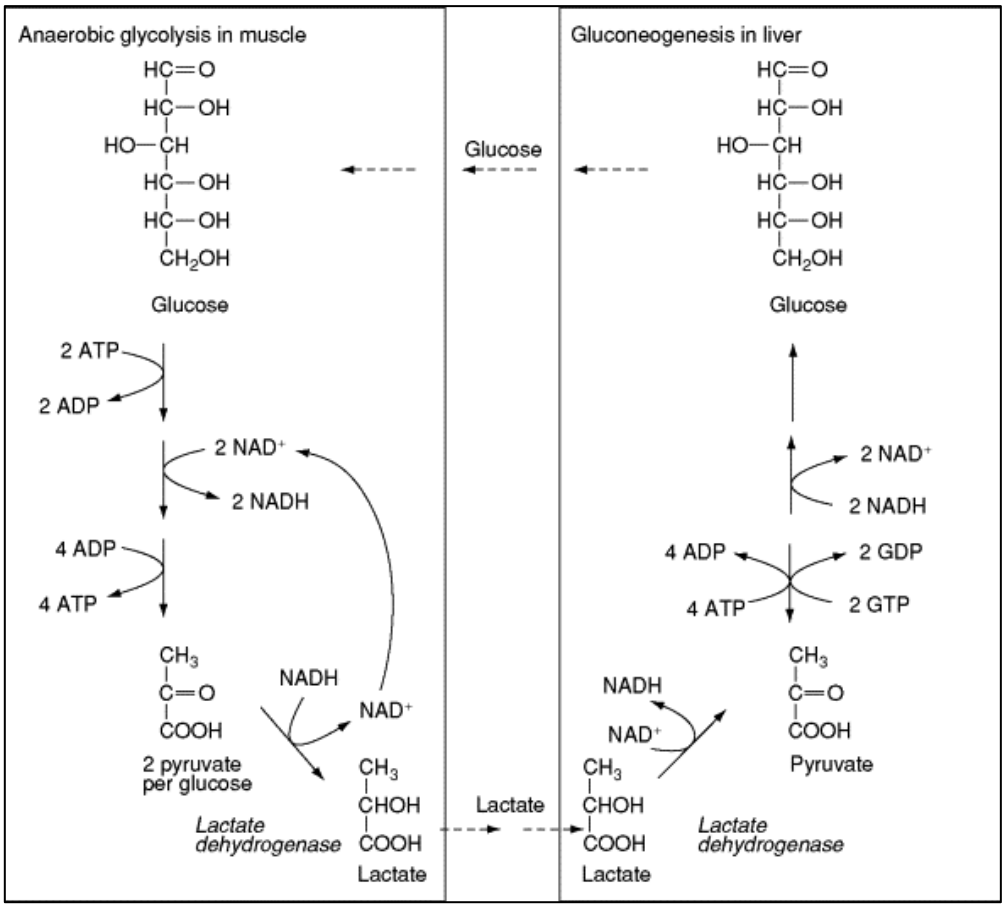

Fig. 1.6 The Cori cycle - anaerobic glycolysis in muscle and gluconeogenesis in the liver. From Bender *et al*, pp 2906.

1.3 Enzyme and LDH immobilization

Enzyme immobilization is generally adopted as means to improve enzyme stability to meet industrial requirements. Apart from gaining stability, attachment of an enzyme to a support attracts attention as a strategy that also allows the reuse of the biocatalyst and facilitates the product separation of reaction mixtures as well as enabling the use of biocatalysts in different types of reactors. [9]

Immobilized enzymes refers to “enzymes physically confined or localized in a certain defined region of space with retention of their catalytic activities, and which can be used repeatedly and continuously”. [28]

Among several immobilization techniques, the covalent coupling is the one exploited in this thesis work concerning LDH immobilization on the mesoporous silica MCM-41.

Regarding this porous material, different ways of functionalization can be processed to allow the attachment of LDH through specific functional groups such as aldehydic and aminic groups.

1.3.1 Immobilization techniques

A series of immobilization techniques have been successfully developed and are present in literature, including physical adsorption, entrapment in solid matrices, cross linking, and covalent coupling.

Physical adsorption and entrapment are classified as physical interactions, in fact the enzyme does not chemically interact with the support in these cases. Adsorption can occur through weak non-specific forces such as van der Waals forces, hydrophobic interactions, and hydrogen bonds, determining reversible links, while for entrapment, enzymes are physically and irreversibly enclosed in a support or inside of fibres, either the lattice structure of a material or in polymer membranes. In some cases, affinity binding is also included as one of the physical methods for the immobilization of enzymes through adsorption.

Cross-linking and covalent coupling provide bonds classified ad chemical, irreversible interactions. They are generated between enzyme molecules and between enzymes and carrier matrix respectively. Cross-linking is performed by the formation of intermolecular cross-linkages among the enzymes using of bi- or multifunctional reagents. The most commonly used cross-linking reagent is glutaraldehyde as it is economical and easily obtainable in large quantities. GA might as well be used in the support's functionalization. Covalent coupling, instead, is one of the most widely used methods for enzyme immobilization, it is based on chemical interactions between functional groups. Covalent bonds provide a powerful link between the enzyme and its carrier allowing its reuse more often than with other available immobilization methods. [29]

Among them, covalent enzyme immobilization has been proven to be more effective, leading to a more stable biocatalyst. [30] Through reversible covalent bonding, also the advantage of reusing the support after the inactivation of the enzyme is reached is one of the purposes of immobilization.

1.3.2 Siliceous materials for immobilization

Mesoporous materials as support for immobilized enzymes have been explored extensively during the last two decades, primarily for biocatalysis applications, but also for biosensing and biofuels. Mesoporous materials are defined as porous inorganic solids with a pore diameter range of 2-50 nm. Several types vary in particle size and structural ordering of the pores: mesoporous silica is by far the most studied mesoporous material regarding enzyme immobilization applications. MCM-41 (Mobil Composition of Matter No. 41) belongs to the M41S family: a group of materials prepared with cationic surfactants with alkyl chains ranging from 8 to 22 carbons, as templates. MCM-41 has hexagonally ordered pores with a diameter between 1.5 and 10 nm. [31] This mesoporous silica presents several characteristics such as high textural properties, mesoporous ordered structure, adjustable morphology, biocompatibility, and ease of functionalization. [32]

Two functionalization types resulted to be very advantageous for LDH immobilization, for this reason, a monofunctional and an heterofunctional support were generated.

Monofunctional MCM-41 presents amino groups derived from reaction with APTES (3-aminopropyl triethoxysilane), an organosilane with an aminic group, a functionalization commonly used to create systems for different applications. [33]

Heterofunctional MCM-41 presents aldehydic and aminic groups due to reaction with GPTMS (3-Glycidyloxypropyl trimethoxysilane) and APTES.

The architecture of the enzyme structure should also be taken into consideration when addressing the stabilization of enzymes, as inactivation mechanisms for multimeric enzymes usually start by subunit dissociation. Structural analyses have revealed that LDH tetramers can be treated as a dimer of dimers, due to differential chemical crosstalk between the monomers. [34]

2. Enzymatic studies for biosensor development

As sustainable and efficient alternatives, enzymes have been extensively applied as biocatalysts in a series of environments spacing from medicine to fuels and industrial processes. However, the flexible nature of natural enzymes makes them difficult to be used in the harsh conditions in which industrial processes usually take place, causing poor stability and low activity. Moreover, any change in their native cellular environment or new interactions may inhibit enzymes or cause instability. Methods including chemical modifications of enzymes, enzyme immobilization, chemo/enzyme hybrid catalysts, and medium engineering of biocatalysts have been used to generate industrial biocatalysts with exceptionally improved qualities.

This work mostly focuses on making the correct choice of immobilization support and its functionalization to enhance enzyme activity and reusability. The purpose of this thesis is also an appropriate knowledge of the process of enzymatic inhibition to better understand the biological mechanism this biosensor will exploit.

2.1 Supports for enzyme immobilization

As mentioned in the previous paragraph, developing biosensors requires a process for immobilizing biomolecules on a solid surface to obtain a stable biocatalyst. The choice of the support materials can strongly affect the properties of enzymes (increase enzymatic activity, improve stability and reusability), support selection has been considered as a hot topic in the field of enzyme immobilization. To date, various materials, such as graphene, carbon nanotubes (CNTs), metal-organic frameworks (MOFs), DNA nanostructures, polymers, and silica, have been applied for enzyme immobilization, which can efficiently protect enzymes from heavy metals, high temperatures, and other biologically challenging conditions. Their characteristics can vary from one to another and many of them have also been tried with LDH; a brief description of the main categories is provided in Appendix A. [35][36] Among these materials, mesoporous silica has been extensively utilized for enzyme immobilization.

2.1.1 Mesoporous silica

Meso, the Greek prefix, meaning *in between*, has been adopted by IUPAC to define porous materials with pore sizes between 2.0 and 50.0 nm. Mesopores are present in aerogels and pillared layered clays which show disordered pore systems with broad pore-size distributions. Except for these, micro and macroporous materials exist and they space from pore diameters of less than 2 nm (micropores) to pore diameters greater than 50 nm (macropores) respectively. [37]

The self-assembled porous structure allows for high enzyme loadings and creates a protective environment where the enzymes can tolerate more extreme pH, elevated temperature, and higher salt concentrations. Enzyme immobilization by physical adsorption is highly affected by the electrostatic interactions between enzymes and this type of support.

Proper characterization of the pore structure and particle morphology of the mesoporous materials demands a combination of analytical techniques, among which, the spectrum obtained from X-ray diffraction (XRD) indicates whether a hexagonal, cubic, lamellar, or disordered structure is present.

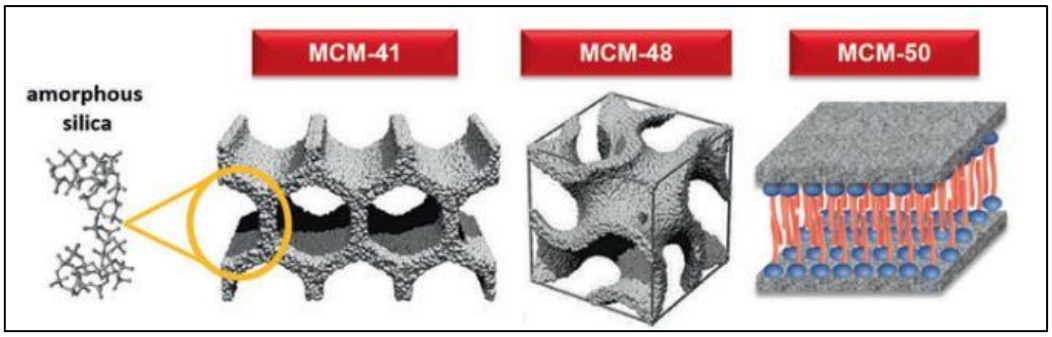

Fig. 2.1 Members of the M41S family. MCM-41(hexagonal), MCM-48 (cubic) and MCM-50 (lamellar with the presence of surfactant molecules between lamellae). From Schwanke *et al*, pp 6.

In 1992, researchers at Mobil Corporation discovered the M41S family of silicate/aluminosilicate mesoporous molecular sieves with exceptionally large uniform pore structures. Three different mesophases in this family have been identified: lamellar (MCM-50), hexagonal (MCM-41), and cubic (MCM-48) phases. MCM-41 has been the most investigated as the other two are either thermally unstable or difficult to obtain. (**Fig. 2.1**)[38] [39]

MCM-41 mesoporous silica's characteristics mentioned in subsection 1.3.2 make already clear why it has been chosen for the present work, but there are further features that have to be mentioned to better understand this choice from a chemical point of view. Except for its good thermal, hydrothermal and hydrolytic stability, this support presents a surface area of about 1,000 m^2/g and pore volumes greater than 0.5 mL/g, which indicates that a large number of enzymes can be attached to this support's surface and inside pores. Surface modification can be performed with both organic or inorganic groups to achieve properties as hydrophilicity, hydrophobicity, acidity, or basicity. The framework of MCM-41 mesoparticles has SiO_2 tetrahedra terminating in either siloxane (Si–O–Si) or silanol (Si–OH) groups on the surface, as it can be seen in **Fig 2.2**. [32]

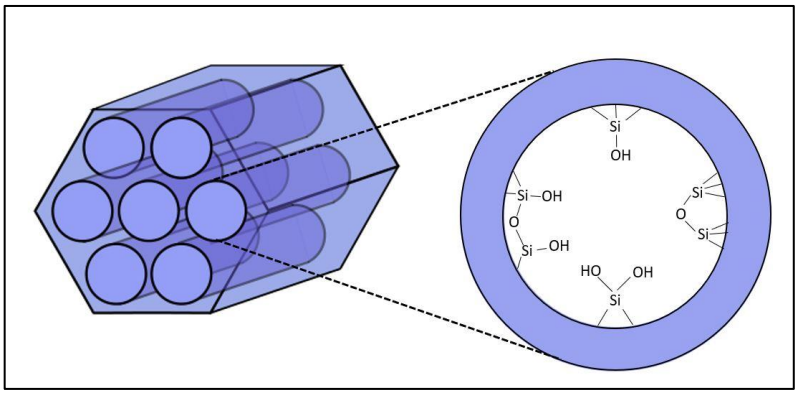

Fig. 2.2 Pure MCM-41 and a detail of types of silanol groups on its surface.

2.1.2 Support functionalization

The functionalization of nanomaterials plays critical roles in their physical and chemical properties, as well as their application. Surface modification is conducted to improve the properties of these materials for a specific application. Different types of compounds are considered for this purpose, depending on the field of use. One key aspect of functionalization is the introduction of various types of functional groups to the material surface. Supports cited before can all serve as the base for functionalized materials, and many compounds are used to modify their surface introducing aminic, carboxylic, hydroxyl, and sulfhydryl groups. The functionalization process is of great importance when a material is intended for use as a support for enzyme immobilization. In some cases, support materials are inert and require further activation. Functionalization allows the formation of stable covalent bonds between the functional groups of the enzyme and the functional groups on the surface of the support material. Enzymes on the surface of functionalized materials can be immobilized by both physical (adsorption and entrapment) and chemical (covalent and cross-linking) methods. This is related to the physicochemical properties, the structure of the material, and the types of functional groups introduced to their surface. [40]

The surface of mesoporous silica nanoparticles (MSNs) with high amounts of silanol groups guarantee the easy multi-functionalization through several strategies to improve their biocompatibility, targeted activity, and control release of cargoes inside. Two of the most studied and applied functionalization techniques on mesoporous silica support are silanization with APTES (**Fig. 2.3**) [41], to introduce primary amino groups on the support surface followed by glutaraldehyde activation, and treatment with GPTMS (**Fig. 2.4**) [42], to functionalize it with epoxy organic groups. Their ethoxy groups can react with hydroxyl groups on the surface of mesoporous molecular sieves and graft the amino and epoxy functional groups onto the surface of mesoporous molecular sieves. [43]

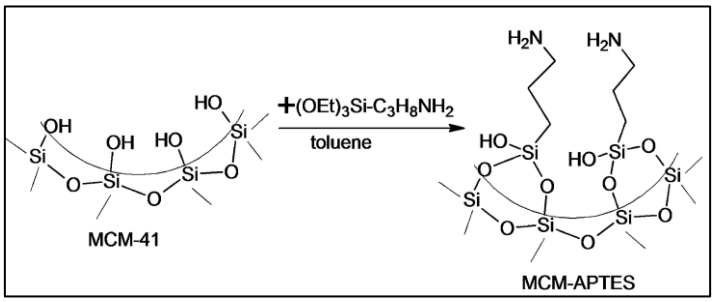

Fig. 2.3 MCM-41 pore wall functionalization with APTES. From Mitran *et al*, pp 2993, with modifications.

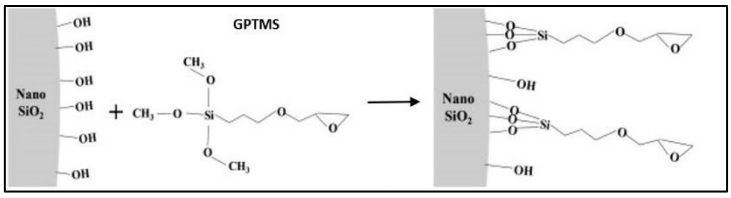

Fig. 2.4 Schematic reaction of the nano silica surface and GPTMS. From Ghanbari *et al,* pp 21.

2.2 Immobilization most efficient bonding techniques

As mentioned in subparagraph *1.3*, enzymes are immobilized to reach a certain stability and renewability. The driving forces for enzyme immobilization are also incremented by volume, specific enzyme loading, and simplification of biocatalyst recycling and downstream processing. Regarding stability, this could mainly be explained as an enzyme that is not able to undergo any intramolecular process: autolysis, proteolysis, aggregation, or undesirable interactions with large hydrophobic interfaces: air/oxygen bubbles, immiscible organic solvents, etc. In this way, under certain experimental conditions, these random immobilization protocols may promote very important stabilizations of immobilized soluble enzymes. Many techniques, processes, and materials have been studied to achieve this purpose and some of them emerged as optimum immobilization solutions also due to the possibility of associating immobilization of enzymes and improvement of functional properties. [28]

The immobilization methods exploit the fact that proteins possess amino acids with different features, whereby functional groups in side chains of these amino acids can be involved in binding to the support through various types of linkages and interactions. The enzymes can be attached by interactions ranging from reversible physical adsorption, ionic and affinity binding, to the irreversible but stable covalent bonds. Immobilization methods can be divided into two general classes: chemical and physical methods. Physical methods are characterized by weaker interactions such as hydrogen bonds, hydrophobic interactions, van der Waals forces, affinity binding, ionic binding of the enzyme with the support material, or mechanical containment of enzyme within the support. In the chemical method, the formation of covalent bonds achieved through ether, thioether, amide, or carbamate bonds between the enzyme and support material are involved. There are four principal techniques for immobilization of enzymes namely, adsorption, entrapment, covalent and cross-linking. (**Fig. 2.5**) [44] [45]. However, not one method is ideal for all molecules or purposes considering the inherently complex nature of the protein structure. Among the parameters affecting activity and stability in immobilized enzymes, the intensity of the interaction between the enzyme and the support plays a key role in the immobilization results. What should be taken into consideration is enzyme deactivation due to modification in the tertiary structure, toxicity of immobilization reagents, and costs of immobilization [34]. Principal characteristics of immobilization interactions have already been described, but to have a more complete idea, some advantages and disadvantages are presented below.

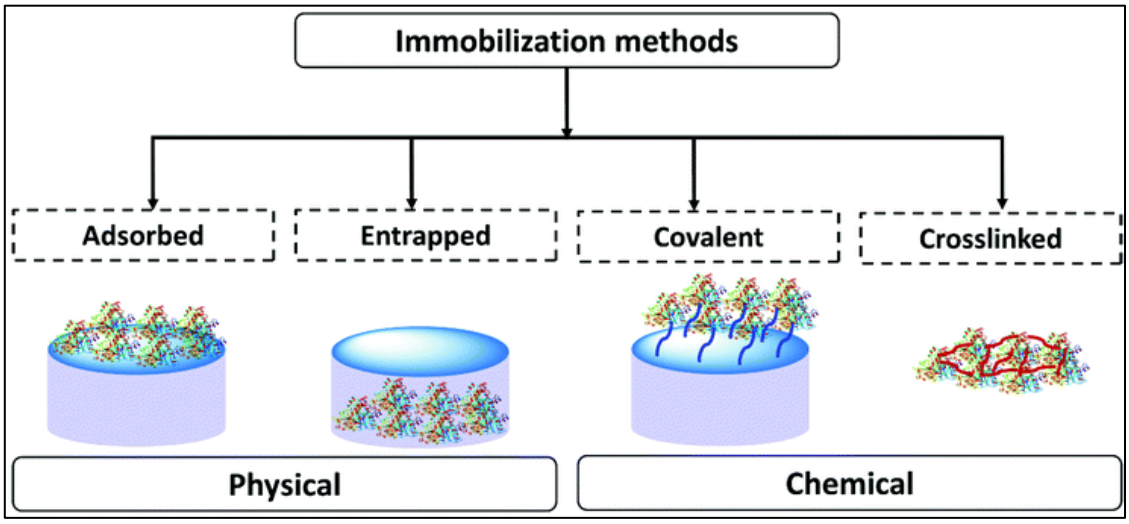

Fig. 2.5 The classification of enzyme immobilization methods. From Imam *et al,* pp 4982.

As a reversible interaction, in physical adsorption immobilized enzymes can be removed from the support under gentle conditions, a method highly attractive as when the enzymatic activity has decayed, so the support can be regenerated and reloaded with fresh enzyme. This is allowable by economic reasons, as the cost of the support is often a primary factor in the overall cost of immobilized catalysts. But on the other side of it, weak or non-specific forces imply drawbacks such as enzyme leakage from the matrix. In general, this technique is quite simple and may have a higher commercial potential due to its simplicity, low cost, and retaining high enzyme activity, but it might result to be too weak to keep the enzyme fixed to the carrier and is prone to leaching of the enzyme.

Entrapment can improve mechanical stability and minimize enzyme leaching. Nonetheless, the practical use of this method is rather limited as it tends to incur mass transfer limitations of substrate or analyte to the enzyme active site. Other disadvantages include the possibility of enzyme leakage, typical when the pores of the support matrix are too large, deactivation during immobilization, low loading capacity, and abrasion of support material during usage.

Cross-linking is another irreversible method of enzyme immobilization where the bonds are formed directly among enzymes, and pure enzymes are theoretically obtained eliminating the advantages and disadvantages associated with carriers. Technically, cross-linking is performed by the formation of intermolecular cross-linkages between the enzyme molecules using bi- or multifunctional reagents.

Covalent bonding is one of the most widely used methods for irreversible enzyme immobilization. It has been used for different enzyme immobilizations, also on innovative support, such as glucoamylase onto κ-carrageenan modified surface [46], α-chymotrypsin onto polyethylene glycol [45] and several enzymes onto paper fibers. [47]

2.2.1 Covalent coupling

During covalent coupling, the functional group that takes part in the binding of the enzyme usually involves binding via the side chains of lysine, cysteine, aspartic and glutamic acids; stable complexes are formed between the functional groups of the substrate and the functional groups of the biomolecule. The functional groups that can partake in the reaction are the amino, carboxylic, thiol, imidazole, indole, and hydroxyl groups. [29] The deprotonated amine groups of LDH possess a free electron pair that makes them highly reactive as nucleophilic agents. They can easily react with electrophiles like carbonyl, epoxy, or vinyl groups present at the carrier surface. [48]

Both one-point and multipoint covalent immobilizations are possible: last cited results to promote a dramatic stabilization of the three-dimensional structure of the enzyme. In the case of complex multimeric enzymes, formed by several subunits (two or three), can first be covalently attached to the support and the other subunits of each enzyme molecule can then be further cross-linked to the immobilized subunits by using bifunctional or poly-functional cross-linking agents (e.g., glutaraldehyde, aldehyde-dextran, etc.) In this way, complex multimeric structures can be fully stabilized. [28] The present thesis' involved groups on the functionalized support were carbonyl and amino groups, these last were activated before the immobilization process, so in both cases interaction happened between deprotonated amine groups present on LDH and carbonyl groups on support.

The formation of multiple linkages between the enzyme and immobilization support ensures retention of the enzyme and has been shown to lead to exceptional enhancements in stability against denaturation by organic solvents, elevated temperatures, surfactants, and other environmental pressures. It has been proposed that this enhancement in stability is due to a restriction in the mobility of the enzyme, which, in turn, suppresses unfolding.

Better results are obtained if a spacer between the support and the enzyme is used. For redox enzymes with NADH cofactor requirement, such as LDH, it has been proven that the co-immobilization of the cofactor via a spacer heightens the overall catalytic efficiency since the spacers allow the facilitated docking of the cofactor to the active site and its "traveling" between two redox-enzymes that are used for the cofactor regeneration. The simplest spacer that can be used is glutardialdehyde (GDA), which reacts with amino groups, previously introduced by pre-activation, under the formation of a Schiff base (**Fig. 2.6**). [49][50][51][52]

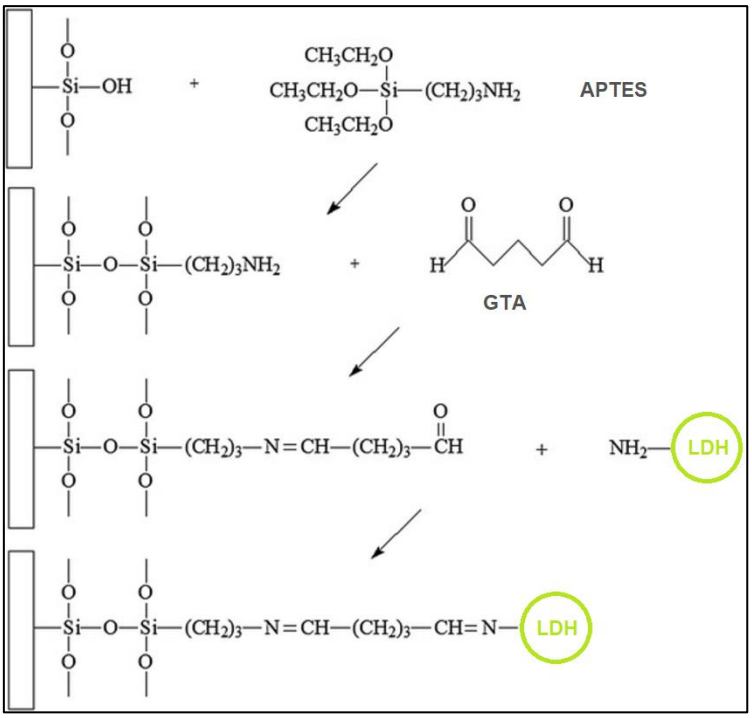

Fig. 2.6 Mechanism of immobilization of LDH with 3-APTES activated with GTA. From Zhang *et al,* pp 16, with modifications.

2.3 Enzyme stabilization

The low stability of enzymes in the presence of relatively high temperatures, organic solvents, extreme pH levels, or high ionic strengths is one of the major obstacles to their widespread usage. Therefore, to improve enzyme stability during the immobilization process, some stabilizing solutions have been added to the immobilization environment. In particular, stabilizing effects of polyethylene glycol (PEG) and trehalose have been studied in different concentrations to get better immobilization results regarding LDH on GPTMS functionalized MCM-41. Regarding PEG, two fundamental mechanisms are thought to be the cause of the improvement. i) The suppression of enzyme aggregation as a result of stronger PEG protein interactions brought on by the enhanced hydrophobicity of PEG and lysozyme at temperatures higher than conservation one is the primary reason for the stabilizing effect. ii) As seen from MD simulations, PEG stabilizes the enzyme's secondary structures to some extent by preventing their unfolding at these temperatures. As the PEG concentration rises, the effect becomes more obvious. [53][54]

Trehalose, instead, is a naturally occurring osmolyte and it is an exceptional protein stabilizer and aids in maintaining the activity of enzymes both in solution and in the frozen-dry condition. In solution, Trehalose has been found to stabilize proteins by raising the medium's surface tension, which causes the protein to preferentially hydrate. The exact nature of interactions that govern the osmolyte-mediated stability of proteins is, therefore, not yet very clear. Overall, protein stability should depend upon a fine balance between favourable and unfavourable interactions of the native and the denatured protein states with the cosolvent

molecules. [55]

From different studies, Trehalose has been suggested to form structures close to protein surfaces, and these structures may create many hydrogen bonds with a water layer on the protein surfaces. According to this model, water is trapped in a layer that lies between the surfaces of the proteins and the nearby trehalose structures. Thus, the more rigid trehalose-water complexes, which slow down protein dynamics and boost protein stability, are connected to the dynamics of the protein via the water layer. Trehalose, however, appears to attach to protein surfaces directly, according to other investigations. This describes a situation in which trehalose molecules take the place of surface water (the so-called water replacement model), and the protein is stabilized as a result of that interaction. [56]

2.4 LDH inhibition process

Recently, LDH has also started to be considered as a possible therapeutic target for pathologies as wide ranging as cancer and malaria. Interest in LDH as an anticancer therapeutic target comes from the observation that this enzyme (namely its -A isoform) becomes constantly up regulated during neoplastic change, offering the possibility of a therapeutic intervention aimed at correcting this altered activity. Moreover, in normal nondividing cells, inhibition of LDH enzymatic activity should not cause harmful effects to mitochondrial respiration, suggesting tolerability for normal cell metabolism. [57]

Enzyme inhibition is an important means of regulating activity in all living cells. There are three basic types of enzyme inhibition: competitive, non-competitive, and uncompetitive. Competitive inhibitors compete with substrates for the same binding site on the enzyme. They can be substrate analogues, alternative substrates or products of the reaction. Competitive inhibitors that are not metabolized by the enzyme are termed dead-end inhibitors. Non-competitive inhibition involves a molecule binding to a site other than the active site (an allosteric site). The binding of the inhibitor to the allosteric site causes a conformational change to the enzyme's active site, thus, the active site and substrate no longer share specificity, meaning the substrate cannot bind. As the inhibitor is not in direct competition with the substrate, increasing substrate levels cannot mitigate the inhibitor's effect. Uncompetitive inhibition occurs when the inhibitor (I) binds only to the enzyme-substrate complex (ES) and not free enzyme (E). One can hypothesize that on binding the substrate (S), a conformational change in E occurs, which presents a binding site for I. Inhibition occurs since ESI cannot form product. It is a dead-end complex which has only one fate, to return to ES. [58]

LDH is a very difficult target for the development of new inhibitors, and in past years several attempts have been characterized by a very low success rate. Among the most successful ones, Gossypol, a natural phenol derived from the cotton plant, inhibits LDH by competition with NADH, but it is not specific for this enzyme.

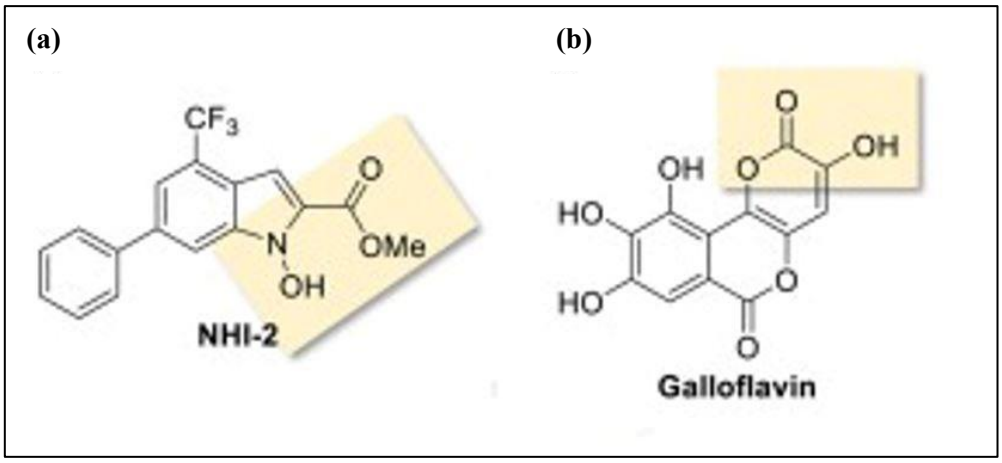

Fig. 2.7 LDH-A inhibitors: NHI-2 **(a)** and Galloflavin **(b)**. From El Hassouni *et al*, pp 51, with modifications.

Until recently, the only well-characterized and specific inhibitor of LDH was oxamic acid, a small molecule that inhibits both the A and B isoforms of LDH by competing with pyruvic acid, the enzyme's natural substrate. Although it displays good selectivity for LDH and weak toxicity in healthy animals, oxamic acid has the drawback of poor cellular penetration; as a consequence, it was found to inhibit aerobic glycolysis and the proliferation of tumour cells cultured in vitro only at high concentrations, which cannot be expected to be reached in vivo. To find novel inhibitors, different studies were carried out on the structure of the LDH-A, as this isoform is up-regulated in the majority of human cancer cells.

By using structure-based virtual screening, a research team from the University of Bologna identified galloflavin (GF), a gallic acid derivative that inhibits both the A and B LDH isoforms. (**Fig 2.7-b**). [59]

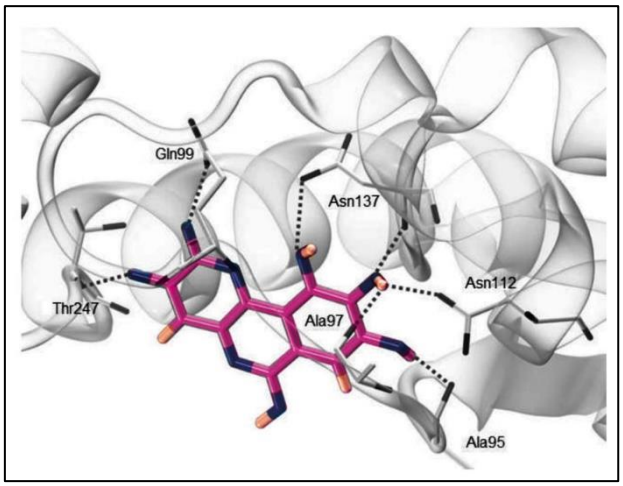

Fig. 2.8 Putative binding mode of galloflavin (pink) at the human LDH-A binding site. From Manerba *et al*, pp 314, with modifications.

It was found to inhibit both the enzymatic activity of purified LDH and lactate production in cultured cells, proving good cell permeability. This molecule binds mainly to the enzyme by hydrogen bonds. In particular, the carbonyl oxygen atoms of galloflavin act as hydrogen bond acceptors with Thr247 and Gln99, and the compound's hydroxy groups establish hydrogen bond interactions with Asn137 and Ala95. Finally, the 9- hydroxy group could make contact with either Ala97 or Asn112 and with the backbone nitrogen atom of Asn137 as well, as shown in **Fig. 2.8**. According to researchers, galloflavin seems to preferably bind the free enzyme, without being competitive with either pyruvate or NADH. [6] Another emerging LDH inhibitor was designed by University of Pisa and is described as a new chemical structure obtained by inserting –OH and –COOH groups into an N-hydroxyindole (NHI) scaffold. [59] Several derivatives of the original structure were obtained and tested: increased sensitivity of NHI-1 and NHI-2 in pancreatic cancer cells growing under hypoxic conditions were reported. [60] In particular, NHI-2 (**Fig 2.7-a**) proved to be stable after uptake by cancer and is a subject of the present study.

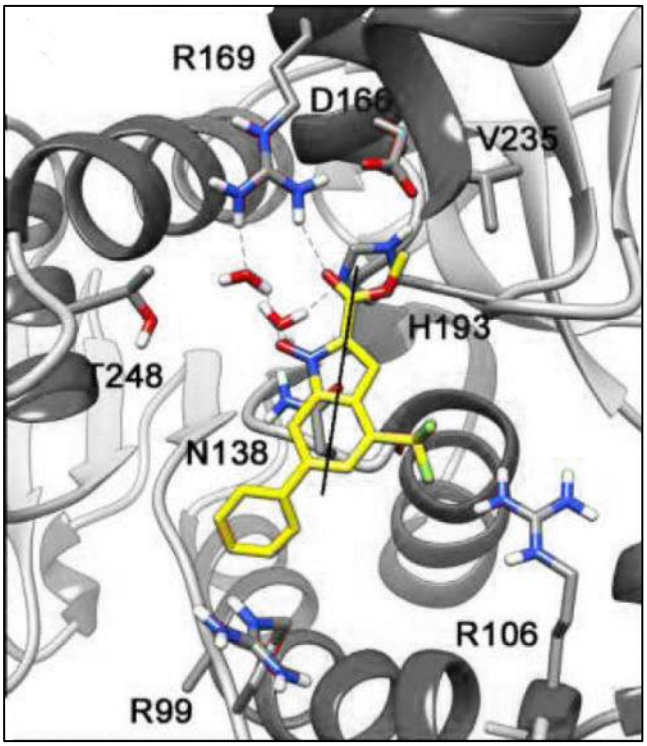

Fig. 2.9 Overall disposition of the ligand NHI-2 (yellow) into LDH-A. From Granchi *et al*, pp 13, with modifications.

It is a competitive inhibitor of LDH-A by binding to the NADH binding pocket. In the study of Granchi *et al*, molecular dynamics (MD) simulation of the complex with NHI-2 highlighted a ~30° rotation along the axis perpendicular to the main plane of the molecule when the COOH group of NHI-1 is replaced by COOMe. The ester group of NHI-2 forms an H-bond with R169, whereas the methyl substituent is directed toward lipophilic residue V235. The rotation of the molecule leads to the formation of a new water-mediated interaction between the N-hydroxy group and the NH of R169, and this interaction proved to be stable during the

whole MD process. This spatial shift of the molecules places the electronegative terminal portion of the CF_3-group in closer proximity to the positively charged residue R106, with the plausible formation of an additional polar interaction between NHI-2 and the enzyme. The rest of the molecule showed a water-mediated H-bond between the N-OH group and H193. Interactions are better shown in **Fig. 2.9.** [61] [62]

2.4.1 Competitive inhibition of LDH

As NHI-2 is object of the present thesis and it inhibits LDH through a competitive mechanism, a more detailed explanation of this process is provided. First of all, a simplified chemical equation of the kinetics of an enzyme is shown, in which the second step is considered to be irreversible, equation (2.1):

$$E + S \underset{k_{-1}}{\overset{k_1}{\rightleftarrows}} ES \xrightarrow{k_2} E + P \tag{2.1}$$

where k_1, k_{-1} and k_2 are rate constants for the designated steps. This simple kinetic mechanism for enzyme catalysis based on equation (2.1) was proposed by Michaelis and Menten in 1913 and later modified by Briggs and Haldane to include a slightly more general set of relationships among the rate constants of the mechanism. The resulting equation is the well-known Michaelis-Menten equation (2.2).

$$v = \frac{V_{max}[S]}{K_m + [S]} = \frac{k_c[E]_t[S]}{K_m + [S]} \tag{2.2}$$

Competitive inhibition occurs when the inhibitor binds at the same site as the substrate. The molecular basis for the binding of competitive inhibitors at the active site is that the substrate and the inhibitor are structurally similar, with the result that the enzyme is "deceived" into recognizing and binding the inhibitor. Thus, two reactions are possible:

$$E + S \leftrightarrow ES \leftrightarrow E + P \tag{2.3}$$

$$E + I \leftrightarrow EI \tag{2.4}$$

The modified Michaelis-Menten equation that relates the velocity of the reaction in the presence of competitive inhibitor to the concentrations of substrate and inhibitor is as follows:

$$v = \frac{V_{max}[S]}{K_m\left(1 + \frac{[I]}{K_i}\right) + [S]} \tag{2.5}$$

In this relationship, K_m is multiplied by a term that includes the inhibitor concentration, [I], and the inhibitor constant, $(1+[I]/K_i)$. The observed "K_m," also called $K_{m(app)}$, is > K_m because S and I compete for binding at the active site, and thus a higher concentration of S is required to achieve half-maximal velocity, as it can be seen from **Fig. 2.10**. [63]

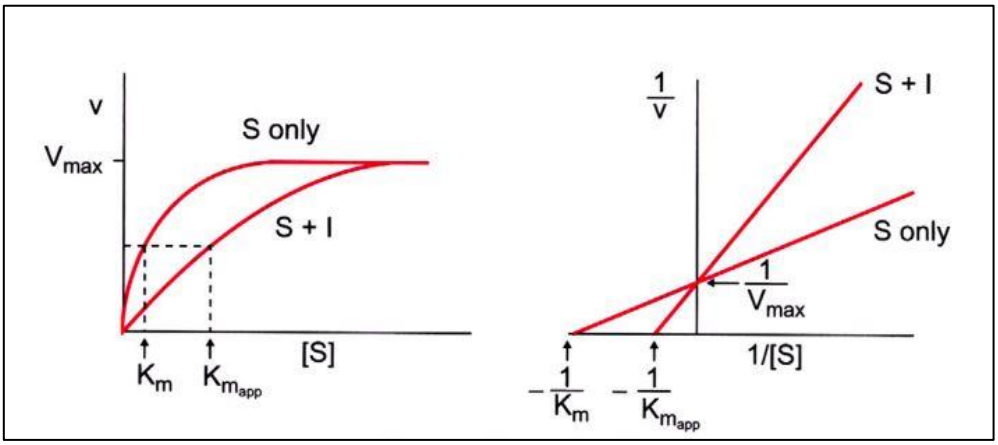

Fig. 2.10 Competitive inhibition: plots of velocity versus substrate concentration or 1/velocity versus 1/substrate concentration (Lineweaver Burk double reciprocal plot). From Bhagavan *et al*, pp 71, with modifications.

2.5 Prototype-Biosensor for screening of anti-cancer drugs

The word "biosensor" is inclusive and refers to any analytical tool that has immobilized material, primarily biological, that precisely interacts with an analyte to produce an electrical, chemical, or physical output that can be examined and evaluated. The amount of an analyte present during the reaction is reflected in the output signals. Various parts can make up a biosensor, including an analyte, bioreceptor, transducer, electrical device, and display. The transducer or the detector element, which transforms one signal into another one, works in a physicochemical way: optical, piezoelectric, electrochemical, electrochemiluminescence, etc.

The initial phase in the creation of biosensors is the validation of biological recognition elements for signal transduction. Choosing the right bioreceptor and quantifiable signaling element transducer combination is crucial when creating biosensors. In electrochemical biosensors, the biorecognition component reacts with the analyte to produce an electrical signal that is proportional to the analyte concentration present. One of the following techniques may be used to find the signal:

Amperometric transducers track variations in current brought on by electrochemical reduction or oxidation processes. A biological recognition unit is typically mounted on electrodes made of gold, platinum, or carbon in such a biosensing system, and it also includes a reference electrode.

Potentiometric biosensors are sensors that monitor potential or charge accumulation. A reference electrode that provides constant potential regardless of analyte concentration and a membrane that interacts with charged ions are both present in a transducer that has an ion-selective electrode (ISE).

2.5.1 Characteristics of a biosensor

Every biosensor possesses a certain set of static and dynamic properties. The performance of the biosensor is affected by the optimization of these features.

Sensitivity and selectivity: the reaction of a biosensor to a unit dose of analyte concentration is referred to as sensitivity. The capacity of a bioreceptor to recognize a particular

analyte even in complicated samples is known as selectivity. The finest illustration of analyte-biorecognition in a highly selective manner is an enzyme-substrate pair. The selectivity property will improve biosensors' ability to evaluate even extremely complicated samples.

Stability: the durability of a biosensor determines how frequently and for how long it can be used. To prevent performance changes, biosensor components must remain stable after processing and during shelf life. The stability will also depend on the immobilization techniques utilized and the kind of connection the bioreceptor forms with the transducing element.

Precision is measured by comparing computed values to actual values, and accuracy is expressed as a percentage recovery. Contrarily, precision is the standard deviation of the biosensor response for the same sample when assessed at various times.

Reproducibility is the ability of a biosensor to produce identical results for repeated experimental setups. Reproducibility takes the robustness of the analytical method into account. The relative standard deviation of biosensor responses across numerous experiments is represented as the reproducibility.

Linearity demonstrates the precision of the measured response. It is connected to a biosensor's analyte range and resolution.

Response time is the amount of time it takes for a circuit or measuring device to detect a specific fraction change in response to an input signal change. As a result, every device needs time to get 95% of the responses. The two most significant and crucial performance criteria are the limit of detection (LOD) and the limit of quantification (LOQ). The amount of analyte measured by a biosensor is defined by LOD and LOQ, also known as its sensitivity. LOD is a quantitative understanding of what restricts the analyte's smallest concentration, while LOQ is the analyte’s lowest concentration that can be quantified with precision and accuracy. [64]

3. Materials and methods

LDH's density could be evaluated as the average density of proteins in general, but for a more accurate value, equation (3.1) has been used, which evaluates protein density as a function of molecular weight, instead of using the constant value ρ = 1.35 g/cm^3 independent of the nature of the protein and particularly independent of its molecular weight. [65]

$$\rho(M) = \left[1.410(6) + 0.145(28) \cdot \exp\left(-\frac{M(kDa)}{13(4)}\right)\right] g/cm^3 \quad (3.1)$$

where M is the molecular weight in kDa, which according to the literature is 35 kDa, 70 kDa, and 140 kDa for monomer, dimer, and tetramer forms respectively, resulting in a density of 1.41 g/cm^3 for the tetramer form. [66]

Through equation (3.2) volume of the protein can be obtained and, if the protein's sphericity is assumed, through the inverse formula for a sphere's volume (3.3), the radius of the minimum sphere containing the protein is obtained. [67]

$$V_{protein} = \frac{v_2}{N_A} \cdot M \quad (3.2)$$

$$R_{min\,sphere} = \left(\frac{3 \cdot V_{protein}}{4 \cdot \pi}\right)^{1/3} = 3.75\ nm \quad (3.3)$$

where

$V_{protein}$	is the volume occupied by the protein in nm^3
v_2	is the partial specific volume (inverse of density), equals to 0.71 cm^3/g
N_A	is Avogadro number
M	is the molecular weight of protein in Da
$R_{min\,sphere}$	is the radius of the minimum sphere containing the protein, in nm

The enzyme is recombinant human L-Lactate Dehydrogenase (*h*LDH-A) expressed in E. coli, acquired from Merck as an aqueous solution. The cofactor NADH was purchased from the same Merck company.

3.1 Support functionalization

Functional groups have necessarily been added on the MCM-41 support's surface to allow covalent binding between LDH and the mesoporous silica. This last has therefore undergone a series of steps to obtain two functionalized supports: a mono-functionalized one, in which a single type of functional groups was added through a reaction with APTES, and a hetero-functionalized one, where both aminic and aldehydic groups were added to the surface of the mesoporous silica through contemporaneous reaction with APTES and GPTMS.

3.1.1 Mono-functionalized support with aminic groups

A mono-functionalization of the support aims to generate one type of functional group on its surface, which in this case are aminic groups.

The process starts with 1 g of weighted support (mesoporous silica MCM-41) to which 30 mL of toluene and 1.5 mL of APTES (3-Aminopropyltriethoxysilane) are added into a balloon, under the hood. The balloon is connected to a cooling column, for evaporating toluene recovery, and reacts for 5 hours under vigorously stirring conditions guaranteed through a magnetic anchor. 105°C constant temperature is maintained thanks to a silicon oil bath stirred as well. The support is then cooled down to room temperature ad filtered through a Buchner funnel under vacuum. Filter papers 42 from Whatman^{TM} have been used for this purpose. It is eventually washed with acetone in the same amount of toluene and with abundant deionized water and it is let dry. **Fig 3.1** constitutes a schematic representation of the chemical process occurring during mono-functionalization.

A further step is required to activate the functionalized support, and it is the addition of glutaraldehyde; this step will be explained more in detail in section 3.5.2 [68][69]

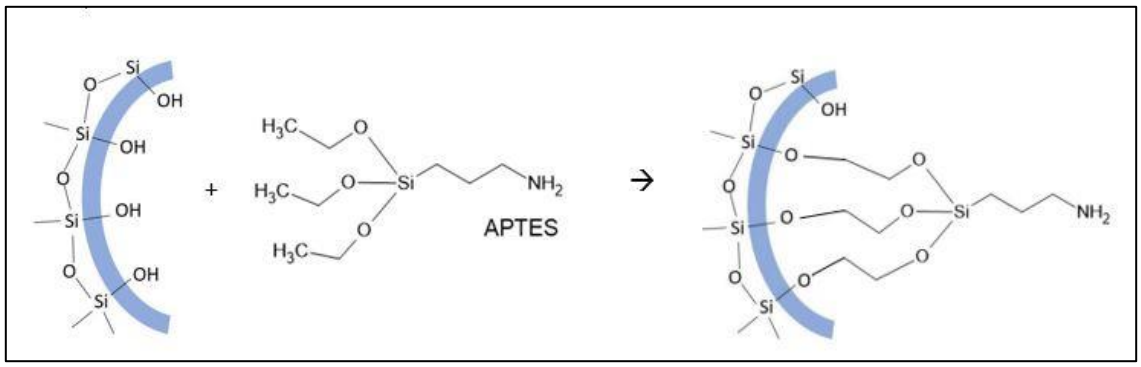

Fig. 3.1 MCM-41 mono-functionalization with APTES

3.1.2 Hetero-functionalized support with aminic and aldehydic groups

The addition of two different functional groups is meant to improve even more LDH covalent linking to the support and enhance its stability.

For 1 g of weighted support (mesoporous silica MCM-41), 30 mL of toluene, 1.5 mL of APTES, and 1.5 mL of GPTMS (3-glycidyloxypropyltrimethoxysilane) are added into the balloon under the hood. Vigorously stirring conditions at about 180 rpm are maintained, through a magnetic anchor, for 5 hours at 105°C in the presence of a cooling column. Temperature is maintained constant through a stirred silicon oil bath. In this step, aminic groups are formed in the same way it was described in subsubsection 3.1.1, GPTMS reacts with MCM-41 superficial silanol groups and determines epoxy group formation.

After the reaction time, support is cooled down and filtrated through a Buchner funnel under vacuum. It is washed at first with abundant acetone (at least 30 mL) and then with deionized water. In the following step, the obtained support is added to 30 mL of an H_2SO_4 solution 0.1 M. The balloon is again connected to a cooling column and is stirred in a silicon oil bath for 2 h at 85°C under the hood. During this time, GPTMS' epoxy groups are hydrolysed

by sulfuric acid, obtaining diols. The support is then cooled down and filtered through a Buchner funnel under vacuum and washed with distilled water again. The third and last step of this process implies that the support is added to 30 mL of a $NaIO_4$ 0.1 M aqueous solution, stirred for 2 h at room temperature, filtered in a Buchner funnel under vacuum, and washed with deionized water. In this step sodium periodate oxides diols and generates aldehydic groups. A sample of the solution is collected two times during this process, before and after the reaction, to evaluate aldehydic groups' formation and their quantity. The sample containing the suspension is then centrifugated at about 5000 rpm for 1 min and the supernatant is collected to be tested.

On the surface of this hetero-functionalized support, both aminic and aldehydic groups will be present, ready to react with LDH functional groups. **Fig 3.2** is a schematic representation of the entire process. [68][70]

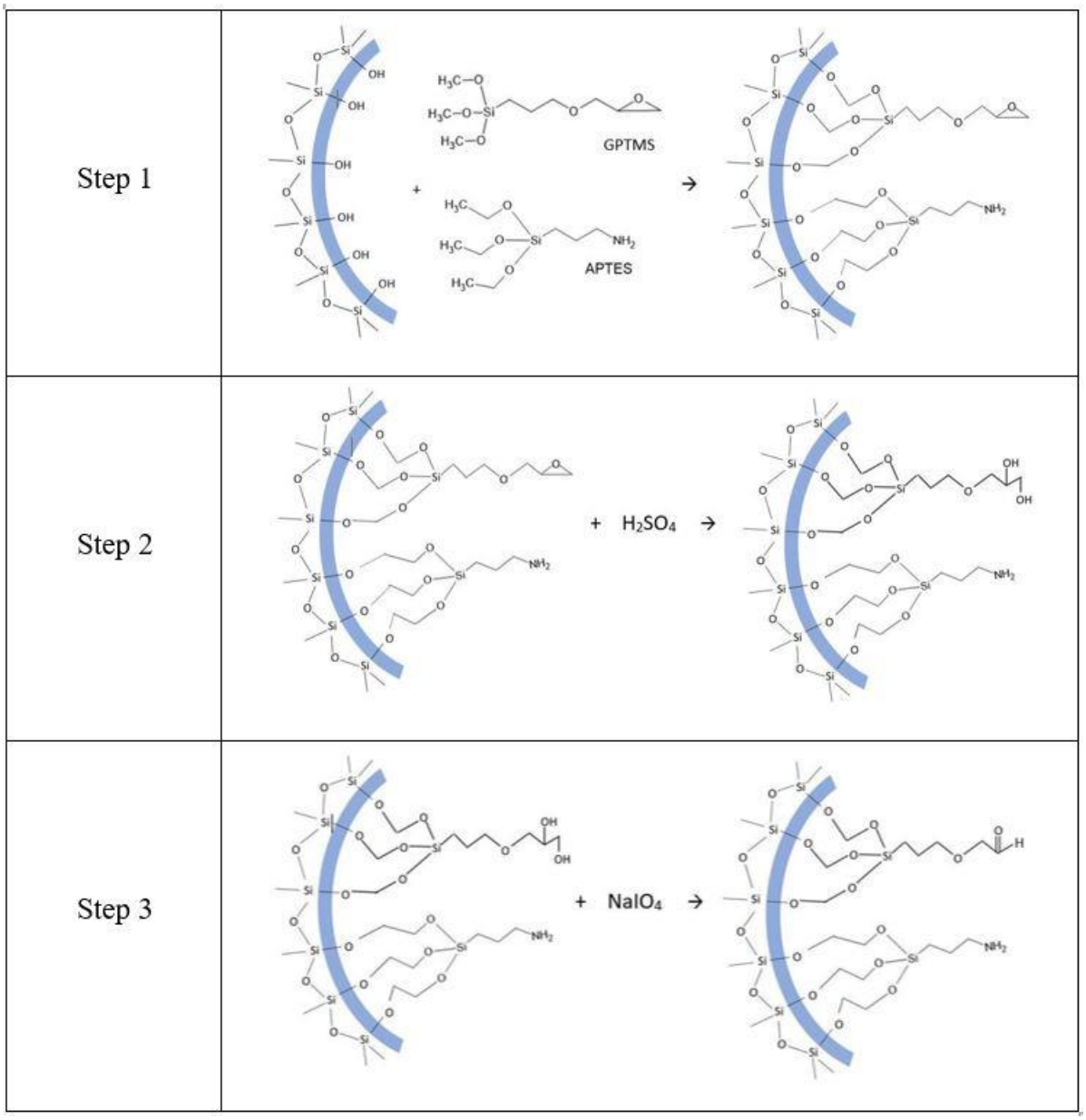

Fig. 3.2 MCM-41 hetero-functionalization with GPTMS and APTES. Step 1: aminic and epoxy groups formation; Step 2: diols formation; Step 3: aldehydic groups formation

3.1.3 Aminic groups characterization

For aminic group quantification, a 300 mM $CuSO_4$ solution has been prepared. 1.5 mL of this solution was mixed with 0.05 g of APTES mono-functionalized MCM-41. It was stirred at room temperature for 1 hour to put support and $CuSO_4$ solution in contact. The interaction between the support's silanol groups and copper sulphate is schematically represented in **Fig. 3.3**. 1.2 mL of solution is then collected, and centrifugated at 1000 rpm for 3 minutes, and 900 µL of the supernatant is collected as the final.

Previously a calibration line was constructed by diluting the initial solution. Each cuvette was filled with 100 µL of a known concentration solution and 900 µL of distilled water; their absorbance was measured by a spectrophotometer DR500 at 750 nm wavelength. Eventually, the absorbance of a solution composed of 900 µL of distilled water and 100 µL of the supernatant of the reacted one is measured. Using the calibration curve, mols of aminic groups per gram of support are determined.[71]

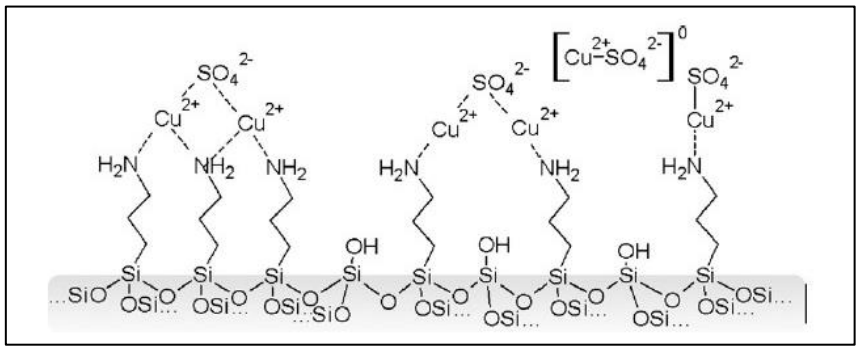

Fig. 3.3 Possible coordination of copper ions by functionalized matrix and stabilization by sulphate anions. From Lombardo *et al,* pp 58

3.1.4 Aldehydic groups characterization

These groups characterization is made by back titration with $NaHCO_3$/KI as described in [70] and in [68]: absorbance at 420 nm wavelength before and after the oxidation process, carried out with $NaIO_4$, was measured and related to the aldehydic groups produced. To make this possible, 10 mL of KI 10 % solution and 10 mL of $NaHCO_3$ saturated solution were prepared. The samples collected before and after the oxidation reaction were diluted (1:50) by mixing 980 µL of distilled water and 20 µL of the samples. Two cuvettes were then prepared with 0.1 mL of diluted samples, 0.5 mL of $NaHCO_3$ solution, and 0.5 mL of KI solution, and the absorbance was measured with a spectrophotometer DR500 setting the *Fixed Wavelength* mode at 420 nm. These measurements were then integrated into equation (3.4) to determine the number of aldehydic groups present on the support surface. [72]

$$\frac{\mathrm{mol_{ald}}}{\mathrm{g_{sup}}} = \frac{\mathrm{V_{IO_4^-}}[\mathrm{IO_4^-}]_{\mathrm{in}}\left(1-\frac{\mathrm{Abs_{fin}}}{\mathrm{Abs_{in}}}\right)}{\mathrm{g_{sup}}} \quad (3.4)$$

where

$\mathrm{mol_{ald}}$	are the moles of aldehydic groups formed on the surface
$\mathrm{g_{sup}}$	is the mass of MCM-41 support in grams
$\mathrm{V_{IO_4^-}}$	is the volume of initial solution of sodium periodate in mL
$[\mathrm{IO_4^-}]_{\mathrm{in}}$	is the initial concentration of sodium periodate solution in mmol/mL
$\mathrm{Abs_{fin}}$	is the absorbance at 420 nm of the sample at the end of the oxidation reaction
$\mathrm{Abs_{in}}$	is the absorbance at 420 nm of the sample at the beginning of the oxidation reaction

3.2 Physical-chemical material characterization

3.2.1 N_2 physisorption at 77 K

The process known as physical adsorption or physisorption implies that a specific number of N_2 molecules are attracted to the surface of a solid by van der Waals forces when these get in contact at 77 K (nitrogen's liquefaction temperature at atmospheric pressure). Low interaction energy separates physisorption from chemisorption in this process and, thermodynamically, physisorption is reversible at isothermal conditions, which is not the case for chemisorption.

This technique allows the determination of the material's surface area, pores' volume, and their dimensional distribution. Before the measurement in the analysis apparatus Micrometrics TriStar, a pre-treatment on the samples is carried out, raising the temperature to 200 °C and leaving the catalyst under nitrogen flow for 2 hours, to clean the surface and eliminate any foreign substance that could alter the results of the experiment.

Samples are analysed by measuring the volume of adsorbed nitrogen as a function of the partial pressure of N_2 at -196 °C; it is a phenomenon of physical adsorption followed by a subsequent desorption, which sees the gas and the solid surface interact through Van der Waals forces. At a given relative pressure, the amount of gas at a specific part of the surface of a solid depends on local surface-energetic properties and on the geometry of the surface. To interpret physisorption measurements of porous systems, surfaces are classically assumed to be homogeneous, so the amount adsorbed at a specific relative pressure is determined by pore size/geometry. These two aspects are intimately related, so assumptions have to be made about geometry to obtain pore size. The most common assumption is that of a cylindrical pore system. At low pressures ($P/P_\circ < 0.2$), micropores are filled with N_2; at increasing pressure, mesopores fill and macropores are filled from pressures around $P/P_\circ \sim 0.96$. Mechanisms of desorption of N_2 are partially different. Physical models of these adsorption and desorption mechanisms constitute the basis for the interpretation of isotherms in terms of porosity and pore structure. Therefore, by plotting the adsorbed volume of N_2 as a function of its normalized partial pressure

concerning the vapor pressure, the adsorption isotherms are obtained, which can be grouped into 6 classes, according to the IUPAC classification. Type I isotherms are typically employed to represent adsorption on microporous adsorbents because they "approach a limiting value". Strong and weak adsorbate-adsorbent interactions are described in Types II and III, respectively, of adsorption on macroporous adsorbents. Types IV and V represent capillary condensation in addition to mono- and multilayer adsorption. (**Fig. 3.4**) [73][74][75]

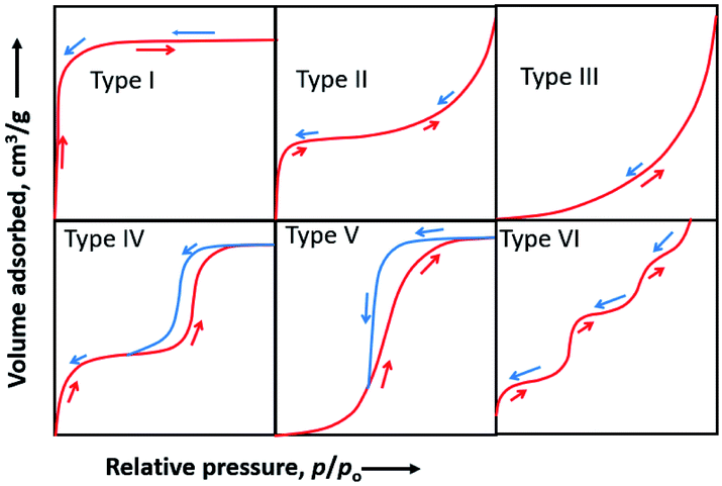

Fig. 3.4 The IUPAC Classification of Adsorption Isotherms. From Kumar *et al*, pp 36

It is well known that there is a correlation between the microstructure of a mesoporous material (such as pore size distribution, pore geometry, and connectivity) and the shape of the hysteresis loop. The IUPAC provided also an empirical classification of hysteresis loops. (**Fig. 3.5**) According to IUPAC, type H1 is frequently associated with porous materials consisting of well-defined cylindrical-like pore channels or agglomerates of roughly homogeneous spheres. Type H2 materials are described as frequently disordered, with poorly defined pore size and shape distributions, as well as bottleneck constrictions. Materials that give rise to H3 hysteresis feature slit-shaped holes (the isotherms showing type H3 do not show any limiting adsorption at high P/P°, which is observed with non-rigid aggregates of plate-like particles). Due to the so-called tensile strength effect, which may occur for nitrogen at 77 K in the relative pressure range of 0.4 to 0.45, the desorption curve of H3 hysteresis contains a slope that is linked to a force on the hysteresis loop. However, type H4 hysteresis is also frequently linked to tiny slit pores. [38][76]

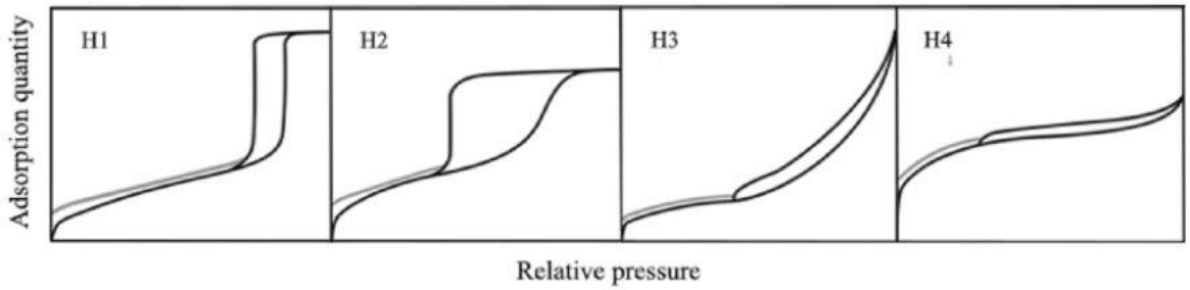

Fig. 3.5 The relationship between the pore shape and the adsorption–desorption isotherm. From Xiong *et al*, pp 13

The Brunauer-Emmet-Teller (BET) equation allows the calculation of the specific surface area values; it is a model that takes into account the formation of multilayers, non-uniform surfaces and the interactions between the adsorbent molecules in adjacent layers. The equation of the BET model in linear form is as follows:

$$\frac{P}{V\cdot(P^0-P)} = \frac{C-1}{V_m\cdot C}\cdot\left(\frac{P}{P^0}\right) + \frac{1}{V_m\cdot C} \qquad (3.5)$$

where

V is the total specific adsorbed volume

V_m is the specific volume adsorbed by a monolayer

P^0 is the saturation pressure

P is the dynamic equilibrium pressure

C is a constant that expresses the difference between the adsorption enthalpy of the first and second or upper layers, obtainable from equation (3.6)

$$C = \exp\left(\frac{E_1-E_L}{RT}\right) \qquad (3.6)$$

where

E_1 is the adsorption heat of the first layer

E_L is the adsorption heat of the following layers or liquefaction heat

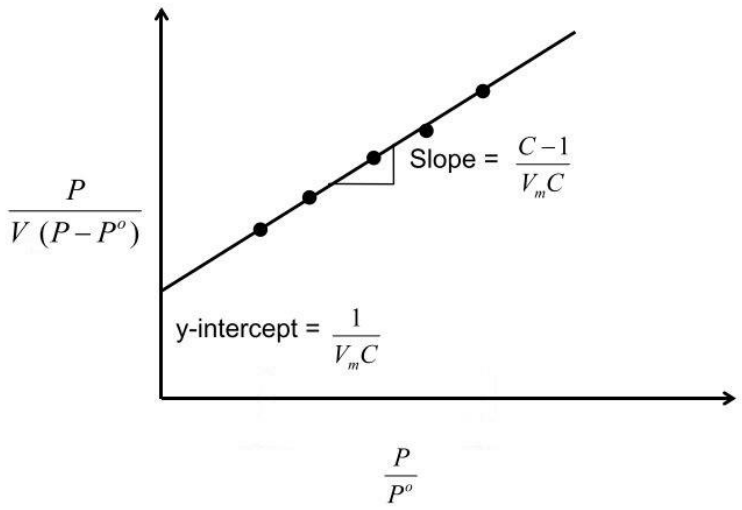

Fig. 3.6 BET theory illustration. From Kumar *et al,* pp 42 with modifications.

Specific surface area (S_{BET}) can be calculated through equation (3.7) evaluating the adsorbed gas by one monolayer (V_m) from the slope and intercept (**Fig. 3.6**). [77]

$$S_{BET} = \frac{V_m \cdot N_A \cdot S}{\tilde{V}} \cdot \frac{1}{m} \qquad (3.7)$$

where

$\tilde{V}$	is the molar volume of the adsorbed gas
S	is the adsorption section
N_A	Avogadro number
m	is the solid mass

3.2.2 X-ray diffraction (XRD)

X-ray diffraction is used to identify the crystalline phases of a material; X-rays have a wavelength that can vary between 0.5 and 2.0 Å, a dimension comparable with the interplanar distances of the crystalline material.

The crystalline phases, which possess a skeleton of ordered atoms, are irradiated with X-rays, which, interacting with the crystalline plane, generate a scattering phenomenon: if there is a constructive diffraction, following the satisfaction of Bragg's law (3.8), a signal is generated. **Fig. 3.7** represents a scheme of the X-ray diffraction process and Bragg's law. [78]

$$n \cdot \lambda = 2 \cdot d \cdot \text{sen}\,\theta \qquad (3.8)$$

where

n	is the diffraction order and it is a positive integer
λ	is the wavelength of the incident Beam
d	is the distance between parallel crystalline planes
θ	is the incident angle

Once the analysis is performed, a diffractogram is obtained and it is compared with a database built over the decades, which contains more than a million patterns of crystalline solids; thanks to this comparison it is possible to trace the different phases that make up the sample analysed.

As described in the previous paragraph, X-ray diffraction is typically used for crystalline solids. Although MCM-41 is an amorphous solid, it presents a very ordered pattern characterized by hexagonally ordered mesopores. As just said, the wavelength of electromagnetic radiation is comparable to the distance between the centres of the channels.

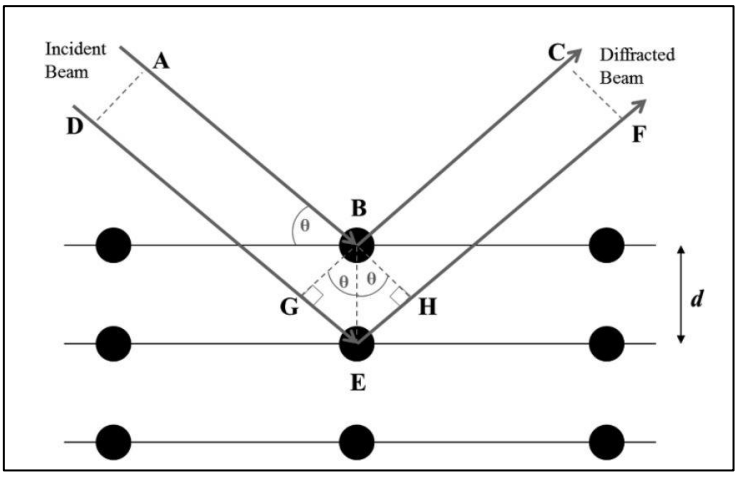

Fig. 3.7 Diffraction of the incident X-ray beam by atomic planes in a crystalline solid. From Forbes *et al*, pp 217.

Sample analysis is performed with the Empyrean 3.0 diffractometer equipped with an anticathode in Cu (K_α, λ = 1.54 Å, 40 kV and 40 mA); in this case, the 2θ angle was made to vary between 0.75° and 5° with an angular step of 0.013°. By rotating the sample, the angle θ with which the X-rays collide is varied and, consequently, the intensity of the diffracted signal is changed, which in turn is measured by a detector. The latter is mounted on an arm that rotates at a 2θ angle as shown in **Fig. 3.8**.

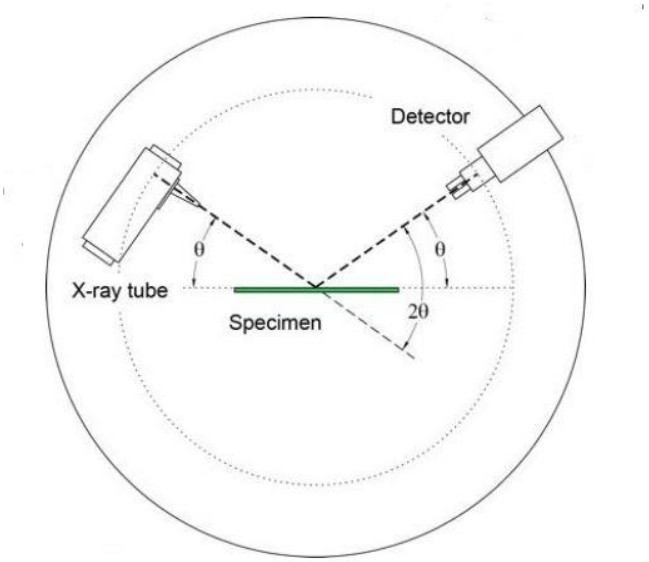

Fig. 3.8 Schematic of the goniometer configuration widely used for XRD analysis. From ITWG, pp 1.

Once diffractogram is composed, θ angle is determined from data as the angle corresponding to absorbance maximum value.

Referring to **Fig 3.9**, to determine the characteristic parameters of the cell composing the material, a series of equations are listed below.

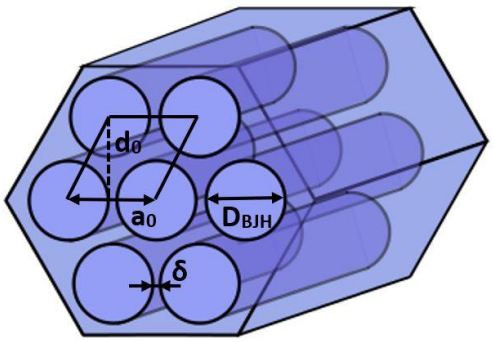

Fig. 3.9 Scheme of cell parameters.

$$d_0 = \frac{\lambda}{2 \cdot \text{sen}\theta} \tag{3.9}$$

$$a_0 = \frac{2 \cdot d_0}{\sqrt{3}} \tag{3.10}$$

$$\delta = a_0 - D_{BJH} \tag{3.11}$$

where

d_0	is the inter-reticular distance
λ	is the wavelength of the incident Beam
a_0	is the cell parameter
θ	is the diffraction angle corresponding to the peak
δ	is the wall thickness
D_{BJH}	is the pore diameter evaluated with the BJH method [79]

3.2.3 Fourier-transform infrared spectroscopy (FTIR)

Fourier transform infrared spectroscopy (FTIR) uses the mathematical process (Fourier transform) to translate the raw data (interferogram) into the actual spectrum. FTIR method is used to obtain the infrared spectrum of transmission or absorption of a materials. Under specific conditions, the nanoparticles' surface chemical composition can be determined, and additionally, the reactive surface sites responsible for the surface reactivity can be identified, depending on the infrared absorption frequency range of 400 and 4,000 cm^{-1}. [33]

The process consists of an infrared spectrum of a sample made by passing a beam of infrared light through a sample or reflecting off of the surface of the sample. The infrared light is absorbed in specific frequencies representing the vibrations of bonds or groups in the molecule. For a vibrational mode in a molecule to be infrared active, it must have a permanent dipole. An absorbance spectrum is produced, showing the wavelengths that the sample absorbs, revealing details about the molecular structure of a sample. It happens that, when an infrared photon is absorbed by a molecule, this transits from a basal vibrational state to an excited one. Molecular vibrations fall into two main categories: *stretching* and *bending*. The stretching

vibration entails a change in the inter-atomic distance along the bond axis, whereas in bending vibrations the bond lengths remain constant, but the bond angles change. There are four types of bending vibrations: rocking, scissoring, wagging, or twisting. Stretching absorptions are of two types: symmetric and asymmetric (**Fig. 3.10**) and usually produce stronger peaks than bending in the infrared spectrum; however, bending absorptions can be useful in differentiating similar types of bonds. [80] Moreover, a section corresponding to functional groups, from 3,800 to 1,300 cm^{-1} and a section corresponding to fingerprints – characteristic bands for each molecule - from 1,300 to 650 cm^{-1} are present. A summary of these regions can be seen in **Fig. 3.11**.

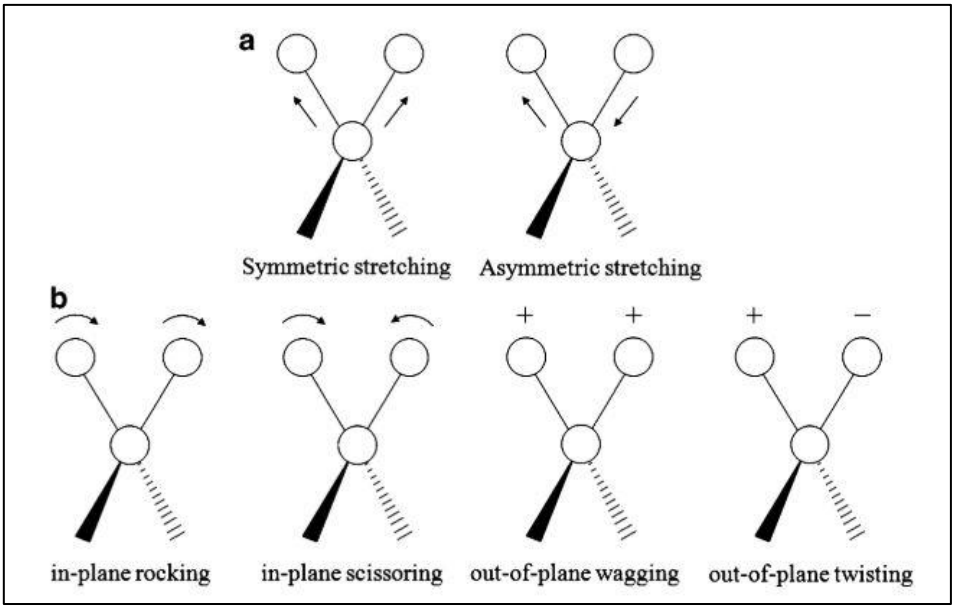

Fig. 3.10 Types of molecular vibrations: (a) Stretching vibrations and (b) bending vibrations. "+" and "-" symbols indicate motion towards the paper and away from the paper, respectively. From Dittrich *et al*, pp 189.

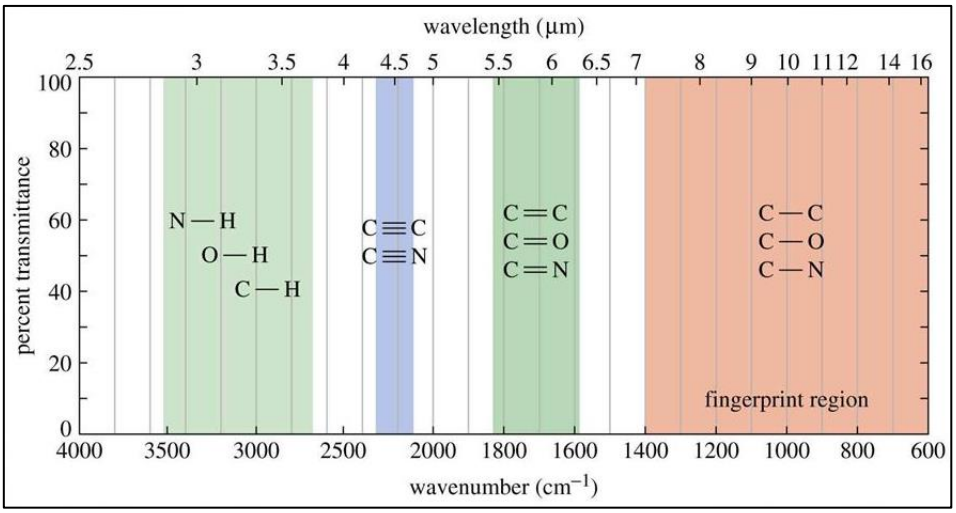

Fig. 3.11 Summary of IR absorption regions. From Wade *et al.*

3.2.4 Transmission Electron Microscopy (TEM)

Transmission electron microscopy is an analysis that allows to obtaining information on the morphology of a material, the size of the crystallites, and the elementary composition. This technique consists in accelerating the electrons from 100 keV up to 1 MeV (as regards the most advanced transmission electron microscopes) and making them interact with the sample. The energy with which the electrons are accelerated is important, as the resolution of the images is related to it. For TEM analysis we work in an extremely high vacuum and the sample is prepared in such a way that the thickness is extremely small, but it is also possible to use the sample in the form of powder which is then dispersed on a screen of copper.[81]

The accelerated electrons, directed along the column of the microscope, are deflected by a suitable system of electromagnetic lenses, interact with the sample, and are finally projected onto a fluorescent screen, which collects and sends the signal to a monitor on which to display a 2D, black and white image of the sample. **Fig. 3.12** shows the scheme of a modern TEM: it is possible to see a condensing lens that serves to direct the electron beam toward the sample, an objective lens, an intermediate lens, and a projection lens. The use of the GMS3 software made it possible to rework the TEM images and calculate the distance d between the different crystalline planes, or, in the case of MCM-41, the pores' average diameter.[81]

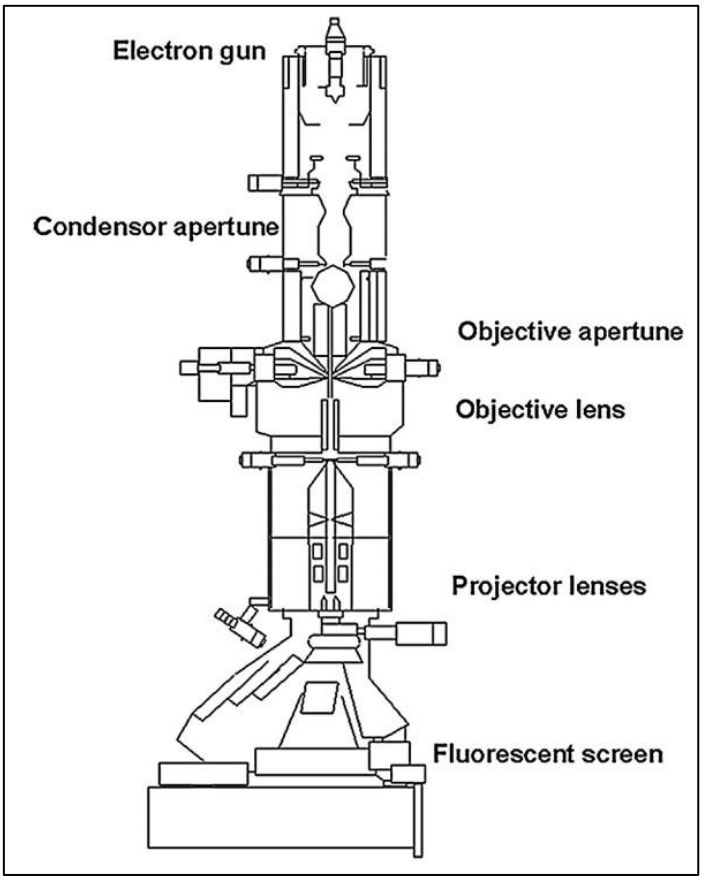

Fig. 3.12 TEM microscope. From Tang *et al,* pp 147.

3.3 Free LDH characterization through activity assay and optimal operation conditions

Enzymes are labile and instable, properties that usually hampers in vitro studies. To reduce the risk of activity loss some parameters' influence on LDH was studied. The aim was to determine values among which LDH has its peak of activity, so several enzymatic assays were processed at different temperatures and pH. In addition, an activity enzymatic assay was made in the following way, measuring the enzyme's absorbance through a spectrophotometer Jasco V-730 (**Fig. 3.13**) in the *Time Course* mode, at the beginning and at the end of a 60 seconds reaction.

Enzymatic activity can, of course, be influenced by enzyme, substrate, and cofactor concentrations, they play an important role as regarding process costs, measurements, and dynamics. Concentrations used in these enzymatic assays have been previously analysed and compared, obtaining as optimal concentrations of 7 mM for NADH and 49 mM for pyruvate, regarding the reaction occurring from NADH to NAD^+. Enzyme concentration only regards costs of the process, which tend to increase if a huge amount of enzyme is employed, and analysis difficulties if its concentration is too low.

3.3.1 Temperature and pH

To obtain information about the optimal pH and temperature of the enzyme, nine different conditions were tested varying the temperature between 25 and 65 °C and the pH between 5 and 11. The middle point having 45°C temperature and pH 8 was tested in triplicate to have a more accurate measure around the point expected to be the optimal one in terms of both temperature and pH. The temperature of both buffers and the analysis room was kept constant through the Julabo instrument (**Fig. 3.13**).

The environment's pH was determined by the pH of the employed buffer, 0.1 M phosphate buffer for pH 5 – 8, and 0.1 M carbonate buffer for strongly alkaline environments. The correct pH was obtained through correction with HCl and NaOH. Literature evidence how the maximum LDH activity lies between pH values of 4 and 9, depending also on the tested isomer of human LDH, its foreign original organism, or a cancerous environment. [82][24][83][84]

Fig. 3.13 Jasco V-730 spectrophotometer and Julabo instrument

3.3.2 Enzymatic activity assay

Reaction occurred in a cuvette containing 2.7 mL of phosphate buffer 0.1 M pH 7.5 at the optimal temperature of 45°C, 100 µL of pyruvate solution 49 mM, 100 µL of NADH solution 7 mM and 100 µL of a LDH solution 0.01 mg/mL. Absorbance spectrum of NADH presents two peaks, one at a wavelength of 260 nm and the second at 340 nm, while NAD^+ only shows a peak at 260 nm. During the reaction, the cofactor NADH is converted to NAD^+ through an oxidation process, thus, the peak of NADH's absorbance at 340 nm should decrease during the reaction. Therefore, the analysis is conducted in *Time Course* mode at 340 nm to observe the peak's decreasing slope in 60 seconds. [85]

Final values of absorbance slope have been eventually inserted in equation (3.12) which aim is to determine free enzyme activity, meant as the quantity of enzyme needed to convert one substrate micromole or to form one product micromole in one minute.

$$A_{FE} = \frac{\Delta Abs}{\Delta t} \cdot \frac{1}{\varepsilon} \cdot \frac{V}{m_{enzyme}} \tag{3.12}$$

where

A_{FE}	is the free enzyme activity in IU (international units)
$\frac{\Delta Abs}{\Delta t}$	is the absorbance variation in 60 s
ε	is the molar attenuation coefficient (6.22 $mM^{-1}cm^{-1}1$ cm)
V	is the reaction solution's total volume in mL
m_{enzyme}	is the enzyme mass into solution in mg

3.4 Free LDH Bradford assay for concentration determination

Bradford protein assay is the simplest and most efficient way to determine a protein's concentration in a solution. The principle of this assay is that the binding of protein molecules to Coomassie® Brilliant Blue G-250 dye under acidic conditions results in a colour change from brown to blue and, therefore, shifts its absorbance peak to 595 nm. This method actually measures the presence of the basic amino acid residues, arginine, lysine, and histidine, which contribute to the formation of the protein-dye complex.

A calibration curve is needed. This curve is created through absorbance measures of bovine serum albumin (BSA) solutions having different concentrations. Absorbance is measured at 595 nm wavelength with a DR500 spectrophotometer and a curve, using phosphate buffer 25 mM pH 7, is determined.

The same procedure is applied to each type of analysed buffer. Starting from a BSA and buffer solution having 1 mg/mL BSA concentration, 5 different solutions are created: 0.01 mg/mL, 0.02 mg/mL, 0.05 mg/mL, 0.1 mg/mL, and 0.2 mg/mL BSA concentration. Measured solutions inside cuvettes were formed by 1 mL of Bradford reagent and 100 µL of each of the solutions just cited.

3.5 LDH immobilization

One support, MCM-41, and two different functionalization procedures of this support have been exploited to immobilize LDH enzyme through covalent binding. Hetero-functionalized MCM-41 with APTES and GPTMS and mono-functionalized MCM-41 with only APTES, both previously described in subsection 3.1, have been used.

For the final evaluation of the immobilization percentage, equation (3.13) has been used.

$$\%I = \frac{\text{Initial activity} - \text{Activity in supernatant}}{\text{Initial activity}} \cdot 100 \qquad (3.13)$$

where

%I	is the enzymatic immobilization percentage
Initial activity	is the initial activity of the free LDH
Activity in supernatant	is the final activity of the supernatant solution

3.5.1 LDH immobilization on hetero-functionalized support

Procedure steps regarding immobilization on support presenting aminic and aldehydic functional groups follow in part FDH immobilization described by Pietricola *et al*. [68][86] As described in section *2.3,* different stabilizing solutions were used as immobilization environment: 50 ppm, 500 ppm, 1% and 5% w/v PEG solutions and a 300 mM trehalose solution.

PEG solutions were obtained starting from 9 mL of specified PEG concentrations in carbonate buffer 25 mM pH 9. As cited previously, PEG (Polyethylene glycol) results to improve the tertiary structure of a protein's stability as it reduces the water accessible surface area of the protein to protect the intrapeptide hydrogen bonds. [54][34]

200 mg of functionalized support is added to the solution to reach an enzymatic load of 1 $mg_{enzyme}/g_{support}$. After 15 minutes of reaction at a temperature between 4 and 10°C the first sample is collected, and from then every 15 minutes. In particular a sample of the suspension has to be analysed to understand if besides pH and temperature, the interaction with the support also destabilizes the enzyme. A sample of the free LDH is collected to analyse the evolution of its activity during the immobilization time. This value cannot decrease below a threshold value that is arbitrarily set at 75% of the initial enzymatic activity. Eventually, the suspension sample is centrifugated at 500 rpm for 2 minutes in CAPP CR1512 centrifuge (**Fig. 3.14**). and the supernatant is analysed to understand if pH and temperature condition destabilize the enzyme and, based on the obtained activity, to evaluate the concentration of free enzyme still present in solution which did not attach to the support. Samples are collected until enzymatic activity in the supernatant solution tends to zero or until it presents two successive constant values. This overall immobilization time varies from 30 to 120 minutes, depending on the variation of free enzyme activity in time.

Absorbance measures are made through the spectrophotometer Jasco-V730 utilizing *Time Course* mode for 60 seconds at a wavelength of 340 nm. Test is performed in the same conditions as the previously described enzymatic assay.

After this first phase, at an almost zero activity of the supernatant, the complement to 20 mL of buffer-PEG solution is added together with a weighted quantity of $NaBH_4$, enough to have a 0.1 mg/mL concentration of $NaBH_4$ in the solution. The obtained solution reacts for 15 minutes at a temperature between 4 and 10°C without being covered so the developed hydrogen can be released. [34]

Fig. 3.14 Centrifuge CAPP CR1512

Support with immobilized LDH is then filtered through a Buchner funnel under vacuum and washed first with 20 mL of phosphate buffer pH 7.5 25 mM and then with distilled water. One samples from the filtrated solution and one from the washing buffer are collected and analysed to determine if any relevant residue activity is present. A schematic representation of the immobilization process is provided. (**Fig. 3.15**)

The aldehydic groups, present on the support, tend to form, in alkaline conditions, the so-called Schiff's bases, characterized by the presence of a double bond linking carbon and nitrogen atoms between aminic and glyoxyl groups resent on the support's surface. This is the reason $NaBH_4$ is added: to convert Schiff's bases into secondary amino bonds; the remaining glyoxyl groups are then converted into inert and hydrophilic hydroxyl groups. [87][88]

Immobilization mediated by trehalose follows almost the same steps as the previous one. Immobilization occurs in 9 mL of Carbonate buffer pH 9, 25 mM with a 300 mM concentration of trehalose. The alkaline value of the utilized buffer's pH is due mainly to glyoxyl groups that do not immobilize enzymes at a neutral pH, while in alkaline conditions they form a multipoint covalent immobilization. The immobilization occurs exactly as the one described in the previous section and the same concentration of $NaBH_4$ is used to reduce Schiff's bases is utilized. (**Fig. 3.15**)

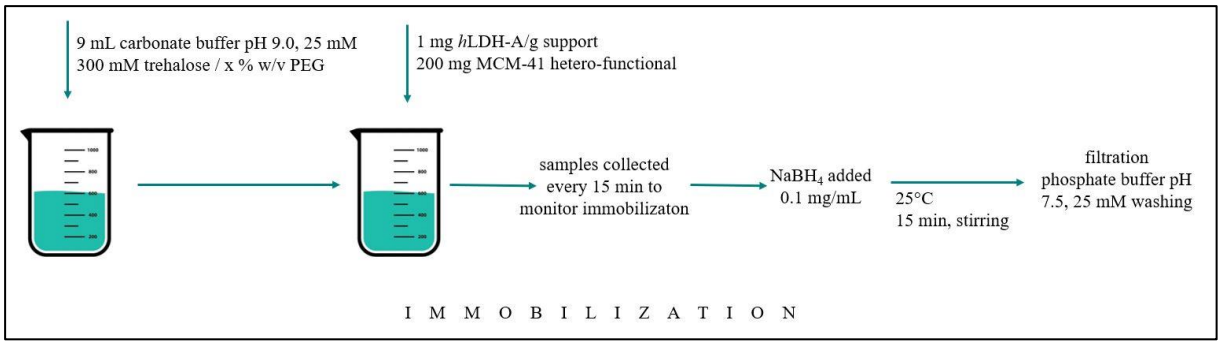

Fig. 3.15 Scheme of *h*LDH-A's immobilization on hetero-functionalised MCM-41

3.5.2 LDH immobilization on mono-functionalized support

There is an important main difference from the previous immobilization that implies an initial activation with Glutaraldehyde of the functionalized mesoporous silica with only aminic groups.

25 mL of a 2.5% v/v (and successively 1% v/v) glutaraldehyde solution in 50 mM sodium phosphate buffer at pH 7.0 and 25°C were used for the activation: 1 g of the mesoporous silica is suspended into 25 mL of the 2.5% v/v glutaraldehyde 50 mM pH 7.0 solution and let react for 2 h in continuous stirring conditions and at room temperature. Immobilized preparation was then filtered under vacuum and washed with deionized water. After this step, support was ready for the immobilization process. It was redispersed into 9 mL of a solution made by phosphate buffer 25 mM pH 7.0 and a weighted amount of LDH to have an enzymatic load of 2 $mg_{enzyme}/g_{support}$. [30] Similarly to the immobilization on hetero-functionalized support described in subsection 3.5.1, every 15 minutes samples were collected and analysed both as suspension and supernatant. The analysis consisted of a *Time Course* analysis of absorbance at 340 nm wavelength for 60 seconds. Cuvettes to be analysed into Jasco V-730 spectrophotometer contained 2.7 mL of phosphate buffer 0.1 M pH 7.5 maintained at optimal temperature through Julabo instrument, 100 µL of a 7 mM NADH solution, 100 µL of a 49 mM pyruvate solution and 100 µL of the sample to be analysed. Eventually, when the activity of the filtrate approach zero, the immobilization solution is filtrated under vacuum and it is washed with 20 mL of phosphate buffer 25 mM pH 7.5 and with deionized water. (**Fig. 3.16**)

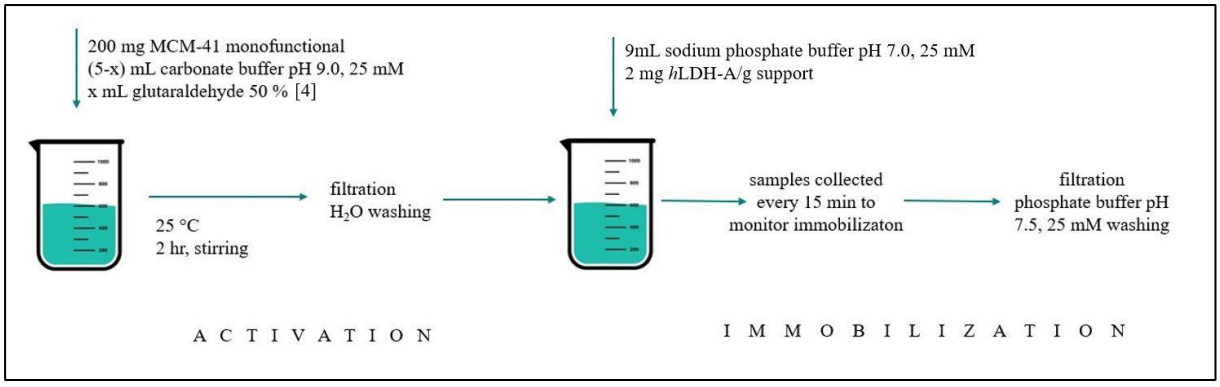

Fig. 3.16 Scheme of *h*LDH-A's immobilization on mono-functionalised MCM-41

3.5.3 Concentration determination and Bradford assay

In mono-functionalized MCM-41 immobilization case, at the end of the procedure, Bradford assay is processed. It consists in the lecture of absorbance through a spectrophotometer DR500 at a fixed wavelength of 595 nm of the sample, then a relationship between these values and the Bradford calibration curve determined in subsection 3.4 is determined. Samples analysed in the spectrophotometer are composed by 1 mL of Coomassie® Brilliant Blue G-250 colorant and 100 µL of the free LDH sample and filtered samples collected from time t_{15} to end of the immobilization (100 µL of buffers for blank).

It is expected that, as during time immobilization occurs, concentration of protein in the supernatant, starting from a maximum in the free LDH solution, decreases, so values of absorbance decrease as well. This measurement of concentration in the supernatant is determined in a different way for LDH's immobilization on hetero-functionalised support as it has been noticed how Bradford assay turns out to be more efficient at a neutral pH instead of pH 9 utilised for hetero-immobilization. Percentage concentration calculus in this case was processed through activity measurement utilizing for this purpose equation (3.13), as activity and concentration are two directly proportional variables.

3.5.4 Retained activity of immobilized enzyme

Immobilization monitoring every 15 minutes and Bradford assay to determine enzyme concentration into the filtrated sample are techniques that provide important data regarding LDH immobilization. Nevertheless, an additional parameter is calculated with the purpose of universally compare all types of immobilizations regarding their activity with respect to the free LDH one, either is has been done on mono or hetero-functionalized support or utilizing different concentrations of stabilizing solutions and additive. The percentage Retained activity makes this calculus possible, as it is determined from equation (3.14).

$$R_{act} = \frac{A_{IE}}{q \cdot A_{FE}} \cdot 100 \qquad (3.14)$$

where

R_{act}	Percentage Retained activity
A_{IE}	Immobilized enzyme activity
q	Enzymatic loading
A_{FE}	Free enzyme activity

The enzymatic loading corresponds to 1 mg of enzyme over gram of support for the hetero functionalized MCM-41 and to 2 mg of enzyme over gram of support for the mono functionalized one.

To evaluate these two activities, an enzymatic assay is processed for the free enzyme (previously described in section 3.3.2) and for the immobilized enzyme. After the immobilization, the enzyme is dried at 4°C for 2 to 4 days before the activity test. The first step of this assay consists in adding 1 mL of Phosphate buffer pH 7.5, 0.1 M to 20 mg of weighted

biocatalyst. The solution is then mixed through a vortex and 100 µL of it is tested in a cuvette containing 2,700 µL of the same buffer cited earlier, 100 µL of a 7 mM NADH solution and 100 µL of a 49 mM pyruvate solution. Everything is maintained at the physiologic temperature, which corresponds to about 37 °C, in stirring conditions during the analysis. This is, theoretically, the optimal operation temperature for free LDH. Values of activity are taken through a *Time Course* analysis at 340 nm wavelength after 60 s. Three measures are taken to better define the error affecting measurements. Absorbance values are then evaluated through equation (3.15) to determine the immobilized enzyme activity.

$$A_{IE} = \frac{\Delta Abs}{\Delta t} \cdot \frac{1}{\varepsilon} \cdot \frac{V}{m_{bio}} \qquad (3.15)$$

where

A_{IE}	is the immobilized enzyme activity
$\frac{\Delta Abs}{\Delta t}$	is the absorbance variation in 60 s
ε	is the molar extinction coefficient (6.22 $mM^{-1}cm^{-1}1$ cm)
V	is the solution volume inside the reaction cuvette
m_{bio}	is the biocatalyst mass

3.5.5 Optimum working pH and temperature for immobilized enzyme

As for the free enzyme procedure previously described in subsection 3.3.1, the 50 ppm PEG immobilised enzyme's activity has been tested for temperatures of 25°C, 35°C, 45°C and 65°C and for pH between 5 and 11, to determine its optimal working conditions. These intervals and values have been specifically chosen to be tested to obtain information about the entire map of pH and temperature at which the enzyme might operate. Measurements have been taken in the same way described for the Retained activity calculus, meaning the analysed suspension has been made from 20 mg of weighted biocatalyst and 1 mL of phosphate buffer pH 7.5 0.1 M, then mixed through a vortex. Central points (35°C and 45°C, at pH 8) have been tested in triplicate to have a more accurate value for the expected activity peak.

3.5.6 Fluorescence microscopy of the immobilized enzyme

To evaluate the effective presence of the *h*LDH-A enzyme on the functionalised support's surface, a fluorescence microscopy has been processed with the Nikon Eclipse Ti microscope. The enzyme has been coloured following the procedure presented by ATTO 488 Protein Labelling Kit acquired from Merck based on N-hydroxysuccinimidyl (NHS)-esters. They are the reagents most frequently employed to react with amines. NHS-esters easily interact with substances that contain amino groups, resulting in the formation of a chemically stable amide bond between the dye and, for example, a protein. To be reactive, the amino group must be deprotonated. As a result, the pH of the solution needs to be raised enough to produce a significant amount of unprotonated amino groups. Among characteristic features of the fluorescent label there is an excellent water solubility, strong absorption, high fluorescence

quantum yield, high photo-stability and very little triplet formation. The fluorescence is most effectively stimulated between 480 and 515 nm (**Fig. 3.17**). [89][90]

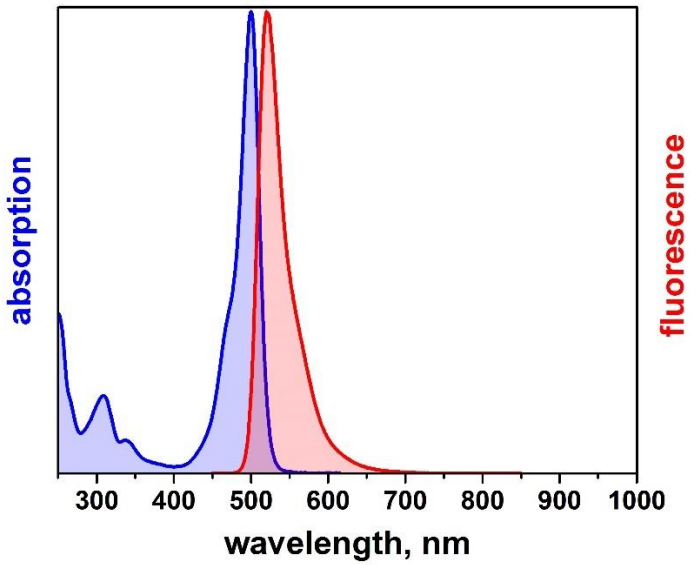

Fig. 3.17 ATTO 488 absorption and fluorescence spectra. From ATTO 288 Product information, pp 1.

Since the utilized enzymatic solution presents a concentration of 1.99 mg/mL in buffer at pH 7.5, a solution of 0.995 mg/mL in carbonate buffer pH 9.5 was utilized to avoid significant pH alterations of the employed buffer provided by ATTO kit at pH 9.5. This concentration value is less than what the technique predicts, which can result in a less effective staining. The labelling colour was diluted as well in 20 µL of sodium carbonate buffer pH 9.5 and, to allow the reactive dye molecules to form bonds with the amino groups of the protein, the enzyme and dye are incubated for two hours with gentle stirring at room temperature in the previous described solution of buffer pH 9.5. The fluorescently labelled enzyme is further purified via a separation column: the enzyme + dye solution passes through the column due to the addition of 5 mL of buffer pH 7.5 on the top of it. A sufficient amount of the filtrated is collected, to guarantee an enzymatic loading of 1 mg/mL and the immobilization in presence of 50 ppm PEG is conducted following the procedure previously described in subsection 3.5.1. Eventually 10 washing procedures of the dried biocatalyst with Milli-Q water are carried on.

To help the labelling performance along, both staining procedures are carried in the dark.

3.5.7 Thermal stability of free and immobilized LDH

An experimental test for determination of the thermal stability has been processed for free and immobilized enzyme. A water bath has been set at the optimum operative temperature of 45°C for a total time of 72 hours. A 0.01 mg/mL free enzyme concentration solution and a suspension of 20 mg of biocatalyst in 1 mL of phosphate buffer have been utilized for measurements. They have been tested at a time 0 for which there is no influence of the temperature, after which Eppendorf containing the solutions have been immersed in the water

bath. Tripled measurements have been processed after 1, 2, 6, 18, 24, 48 and 72 hours from time 0 for both free and immobilised LDH. Absorbance measurements have been taken at 340 nm wavelength, in 60 s, inserting100 µL of the sample to be analysed in 2,700 µL of buffer, 100 µL of a 49 mM pyruvate solution and 100 µL of a 7 mM NADH solution. The absolute error has been calculated through the standard deviation formula for each point and a trendline has been determined from equation (3.16). [68]

$$A = A_0[(1-\alpha)\cdot e^{-k_D\cdot t} + \alpha] \quad (3.16)$$

where

A	is the activity at any time
A_0	is the initial activity
α	is the asymptotic value to which the activity tends for an infinite time
k_D	is the deactivation constant
t	is the time

3.6 LDH inhibition

Inhibition operated by NHI compounds regarding LDH-A enzymatic subunit has been described in subsection *2.4.* To obtain an experimental value that proves the occurred inhibition, activity assays in absence and in presence of the inhibitor for both free and immobilized enzyme have been performed.

3.6.1 Free *h*LDH-A inhibition by NHI-2

The assay is carried on similarly to the one for the calculation of Retained activity: a solution with a concentration of 0.01 mg/mL of free enzyme is created in phosphate buffer and 100 µL of it is tested in presence of already cited 100 µL of a 7 mM NADH solution, 100 µL of a 49 mM pyruvate solution and 2,700 µL of phosphate buffer. For the one in absence of inhibitor nothing is altered while for the inhibition test, 30 µL of an NHI-2 solution 3.75 mM are introduced into the analysed cuvette. Therefore, a total reaction volume of 3.03 mL will be used in calculations. NHI-2 solution has been obtained by dissolving the anti-cancer drug in a suitable solvent such as dimethyl sulfoxide (DMSO). To determine the inhibition percentage, equation (3.17) is utilized.

$$\text{Inhibition}_{\text{free LDH}}\,\% = \frac{A_{\text{free LDH,No NHI}} - A_{\text{free LDH,NHI}}}{A_{\text{free LDH,No NHI}}} \cdot 100 \quad (3.17)$$

where

$A_{\text{free LDH,No NHI}}$	is the activity in absence of the LDH inhibitor NHI-2

$A_{free\ LDH,NHI}$ is the activity in presence of the LDH inhibitor NHI-2

They have been both calculated through equation (3.18), just changing the reaction volume as specified before for $A_{free\ LDH,NHI}$.

$$A_{free\ LDH,No\ NHI/\ NHI} = \frac{\Delta Abs}{\Delta t} \cdot \frac{1}{\varepsilon} \cdot \frac{V}{m_{enzyme}} \quad (3.18)$$

where

$\frac{\Delta Abs}{\Delta t}$ is the absorbance variation in 60 s

ε is the molar attenuation coefficient (6.22 $mM^{-1}cm^{-1}1$ cm)

V is the reaction solution total volume in mL

m_{enzyme} is the enzyme mass into solution in mg

3.6.2 Immobilized *h*LDH-A inhibition by NHI-2

The same procedure is followed for the inhibition of immobilized enzyme, a suspension of 20 mg of biocatalyst in 1 mL of buffer is created and 100 µL of this is tested with and without 30 µL of NHI-2 solution through the absorbance measurement at 340 nm wavelength. Once the triplicate assay has been completed, equation (3.19) is used for the inhibition percentage calculation, while activities are both calculated through equation (3.20) operating just a change in the reaction volume for $A_{biocatalyst,NHI}$.

$$Inhibition_{biocatalyst}\ \% = \frac{A_{biocatalyst,No\ NHI} - A_{biocatalyst,NHI}}{A_{biocatalyst,No\ NHI}} \cdot 100 \quad (3.19)$$

$$A_{biocatalyst,No\ NHI/NHI} = \frac{\Delta Abs}{\Delta t} \cdot \frac{1}{\varepsilon} \cdot \frac{V}{m_{bio}} \quad (3.20)$$

where

$A_{biocatalyst,No\ NHI}$ is the activity in absence of the LDH inhibitor NHI-2

$A_{biocatalyst,NHI}$ is the activity in presence of the LDH inhibitor NHI-2

$\frac{\Delta Abs}{\Delta t}$ is the absorbance variation in 60 s

ε is the molar attenuation coefficient (6.22 $mM^{-1}cm^{-1}1$ cm)

V is the reaction solution total volume in mL

m_{bio} is the biocatalyst mass

4. Results and discussion

4.1 Support characterization results

4.1.1 N_2 physisorption at 77 K results

A summary of the obtained results from the N_2 physisorption analysis at 77 K of commercial MCM-41, heterofunctional and monofunctional MCM-41 is presented in Table 4.1. Specific surface area (S_{BET}) has been calculated through BET (*Brunauer-Emmett-Teller*) model equation (3.7) analysis. Utilizing BJH (*Barrett-Joyner-Halenda*) method the cumulative pores' volume (V_p) and the pores' average diameter (d_p) have been obtained.

	S_{BET} $\left(m^2/g\right)$	V_p $\left(cm^3/g\right)$	d_p (nm)
MCM-41	866	0.36	3.7
MCM-41 heterofunctional	474	0.08	5.7
MCM-41 monofunctional	576	0.10	5.4

Table 4.1 MCM-41, MCM-41 heterofunctional and MCM-41 monofunctional samples' properties derived from N_2 physisorption at 77 K

MCM-41's initial morphology is altered by the hetero and mono functionalization processes, which results in a drop of S_{BET} and V_p. Pore dimension indicates that hollow pores did not change during functionalization. The decrease of the BET surface area and pore volume might be due to the destruction of a small amount of pore structure or to chemical modification. In all samples, the pore size distribution in **Fig. 4.1** is highly condensed around d_p value reported in table 4.1.

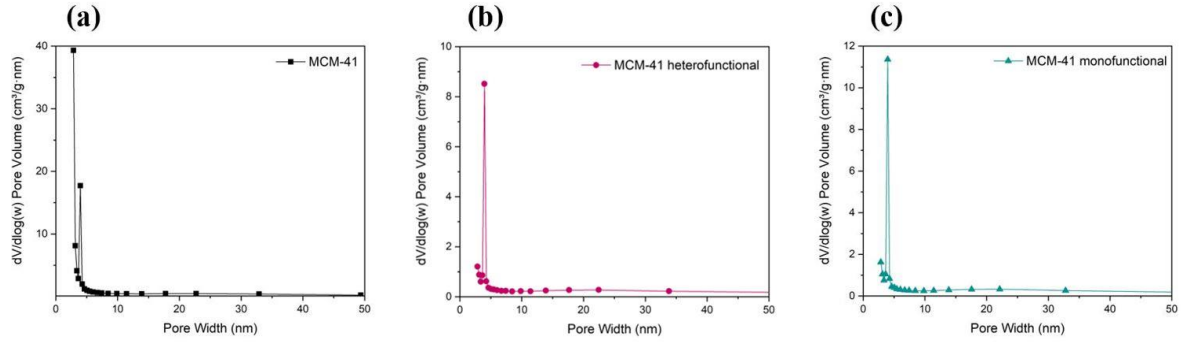

Fig. 4.1 Pore size distribution for MCM-41(**a**), MCM-41 heterofunctional (**b**) and MCM-41 monofunctional (**c**) samples

In **Fig.4.2** the adsorption and desorption isotherms of all three samples are shown. After a comparison with the IUPAC classification in **Fig. 3.4** and **Fig. 3.5**, it has been deduced these are of type IV with an H4 hysteresis cycle.

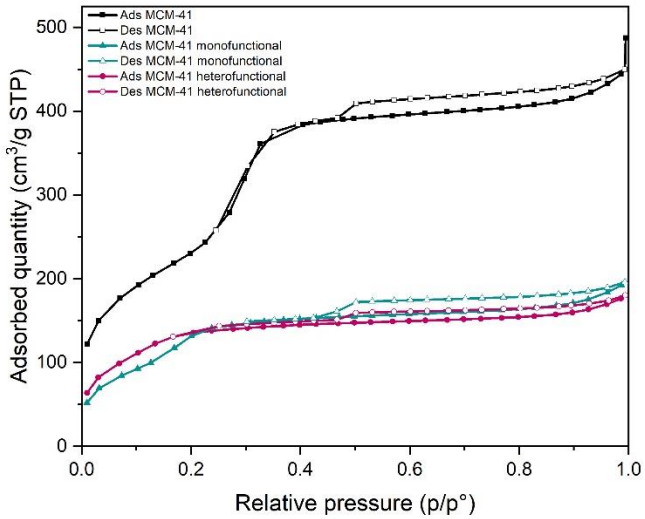

Fig. 4.2 Adsorption and desorption isotherms for MCM-41(black), MCM-41 heterofunctional (pink) and MCM-41 monofunctional (green) samples.

4.1.2 X-ray diffraction (XRD) results

Fig. 4.3 shows the XRD spectra of the MCM-41, MCM-41 heterofunctional and monofunctional samples. By the literature, MCM-41 presents in the interval 2θ considered two peaks identified with *100* and *110*, characteristic of a material's ordered structure. Intensity of the peak *100* of the functionalized MCM-41 support resulted in lower intensity after the introduction of both amino and glyoxyl groups through hetero and mono-functionalization.

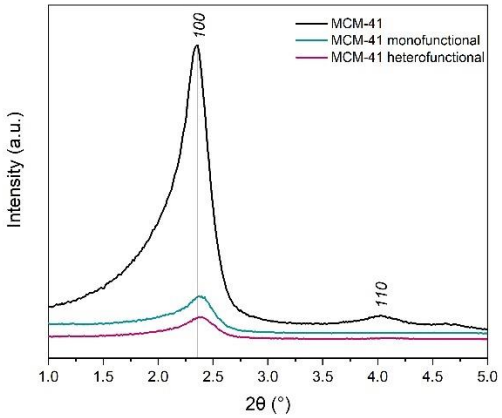

Fig. 4.3 XRD diffractogram of MCM-41 (black), MCM-41 heterofunctional (pink) and MCM-41 monofunctional (green) samples.

Table 4.2 summarizes the values of the diffraction angle θ, the inter-lattice distance d_0, the cell parameter a_0, and the wall thickness δ calculated according to equations (3.9), (3.10) and (3.11).

	θ (°)	d_0 (nm)	a_0 (nm)	δ (nm)
MCM-41	1.19	3.7	4.3	1.0
MCM-41 heterofunctional	1.18	3.7	4.3	1.8
MCM-41 monofunctional	1.19	3.7	4.3	1.9

Table 4.2 MCM-41, MCM-41 heterofunctional and MCM-41 monofunctional samples' properties derived from XRD

4.1.3 Fourier-transform infrared spectroscopy (FTIR) results

In **Fig. 4.4** there is a representation of FTIR spectra of starting silica support and both mono and hetero-functionalized silica after a thermal pre-treatment at 300°C. This is necessary for water residues to evaporate to permit a clearer view of most peaks present in the range 4,000-1,300 cm^{-1}, which would differently be hidden by water molecules or other impurities.

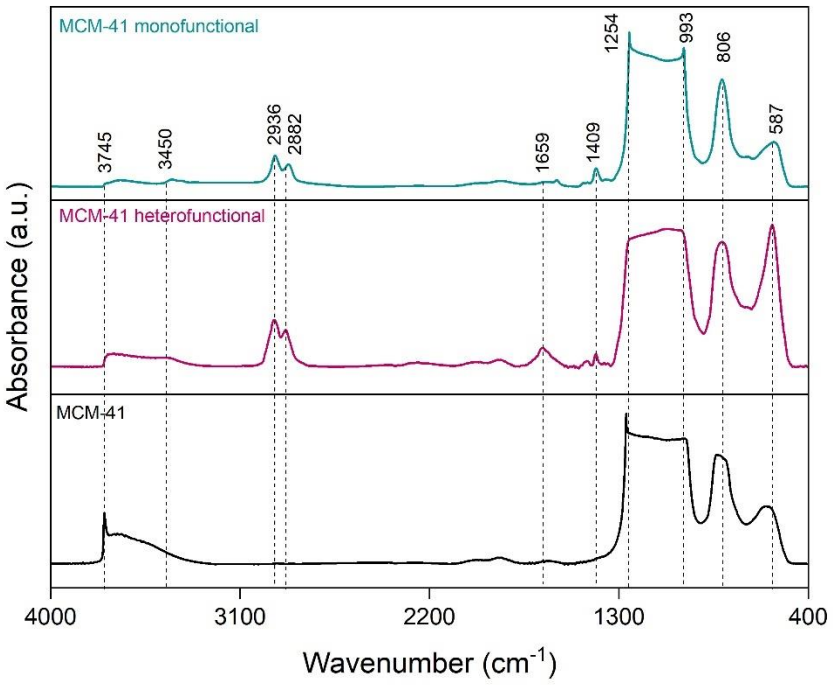

Fig. 4.4 FTIR spectra of MCM-41 (black), MCM-41 heterofunctional (pink) and MCM-41 monofunctional (green) after a pre-treatment at 300°C

At 3745 cm^{-1} there is a peak present in MCM-41 spectra, absent in the functionalized ones. This corresponds to isolated silanol groups that react with organosilanes to provide glyoxyl and ammino groups during functionalization. Other peaks are present in both mono and hetero-functionalized silica and absent in the starting one, meaning the functionalization took place. The most relevant ones are summarized in Table 4.3. [91][92]

Wavenumber (cm^{-1})	Functional group
3745	Isolated -OH groups
3450	N–H stretching vibration
2936, 2882	Asymmetrical and symmetrical stretching vibrations of CH_2 groups
1659	Bending -NH and Stretching C=O
1409	Bending CH in -CH_2- e -CH_3
1254	Si-CH_2 from GPTMS structure
1200 - 1000	Si-O-C, Si-O-Si, Si-O-H and C-O
806, 587	Si-O-Si stretching and Si-O-Si bending

Table 4.3 FTIR wavenumber range and functional groups in evidence for MCM-41, MCM-41 heterofunctional and MCM-41 monofunctional

4.1.4 Transmission Electron Microscopy (TEM) results

In **Fig. 4.5** TEM images of MCM-41, MCM-41 heterofunctional and MCM-41 monofunctional at 80000x, while in Table 5.4 a summary of the average pore diameter measured in different positions is present. Moreover, it is possible to observe how structures present on the edges of MCM-41 silica due to the presence of silanol groups are less evident in the functionalized silica. This might happen because of the functionalization treatment or the substitution of silanol groups with amino and glyoxyl ones. Although numbers do not coincide precisely, it can be seen that they are of the same order of magnitude as the ones calculated with the BJH method in subparagraph 4.1.1.

	Pore dimension (nm)
MCM-41	3.6
MCM-41 heterofunctional	3.7
MCM-41 monofunctional	3.5

Table 4.4 Pore dimensions in MCM-41, MCM.41 heterofunctional and MCM-41 monofunctional measures from TEM images

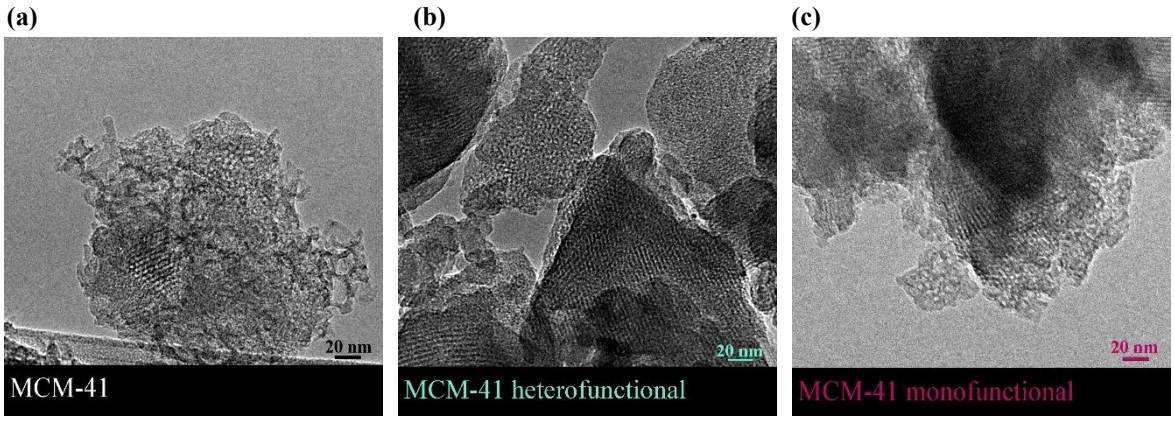

Fig. 4.5 TEM images of MCM-41 (**a**), MCM-41 heterofunctional (**b**) and MCM-41 monofunctional (**c**)

4.2 Free LDH

The occurring reaction of NADH conversion to NAD^+ has been analysed as the acquired enzymatic subunit *h*LDH-A is the one mostly responsible for catalysing this reduction, while other subunits are responsible for the reverse reaction catalysis. As all enzymatic assays within this thesis work, the process to determine the enzyme's working optimum temperature and pH is based on the measurement of absorbance at 340 nm wavelength for 60 s. A peak of this value will be obtained when a maximum NADH concentration in its reduced form is present in the solution and a constant minimum value will be reached when the reaction occurred and all NADH has been converted to NAD^+. **Fig 4.6** is the representation of the spectra just described, where the green curve represents the spectra covering all interesting wavelengths at time 0, before the reaction has occurred, and the red curve represents the same points after a 60 s reaction where the NADH specific peak is no more present.

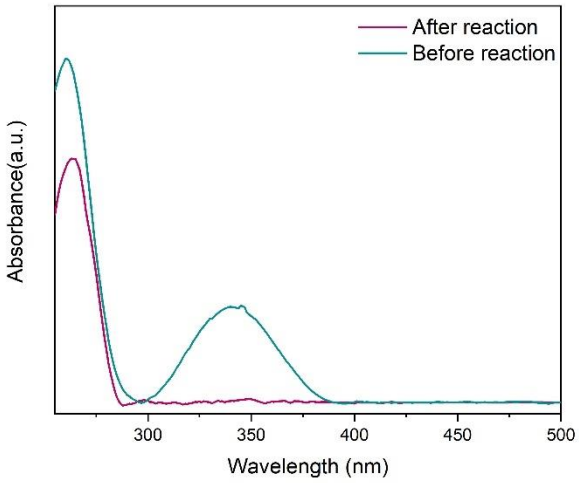

Fig. 4.6 NADH spectra, peak of absorbance at 340 nm wavelength

4.2.1 Free LDH's optimum operative temperature and pH

In **Fig. 4.7** a map of temperature and pH regarding the free enzyme is present. The analysed reaction is the one of NADH conversion to NAD^+. NADH and pyruvate starting solutions have been used in 7 mM and 49 mM concentrations respectively, which resulted as optimal from previous researches. Obtained activity peak corresponds to a pH of 7.5 and to a temperature of about 40-45°C. These values of temperature and pH have been utilized for both free LDH and immobilized one assays to guarantee the most favourable conditions for its activity.

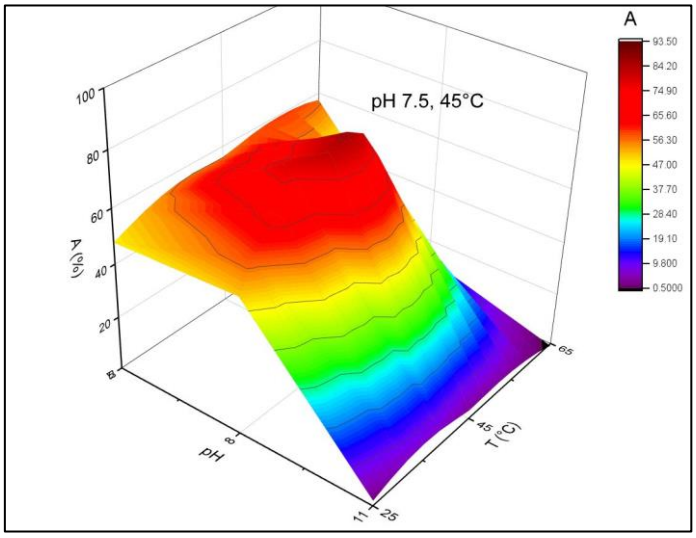

Fig. 4.7 Surface determined from analysed points of temperature and pH

4.3 Functionalization and immobilization processes results

4.3.1 Aldehydic and amino groups quantification

Functionalization processes were followed by a characterization procedure to determine the effective group quantity generated on the MCM-41 support's surface. Regarding aldehydic groups, equation (3.4) has been used to calculate group quantity while for amino groups the interaction between NH_2 groups and copper ions has been exploited. Table 4.5 summarizes the mmol of functional groups on g of support.

	$mmol/g_{support}$
Aldehydic groups for MCM-41 heterofunctional	1.44
Amino groups for MCM-41 monofunctional	0.95

Table 4.5 Aldehydic and amino groups quantification for heterofunctional and monofunctional MCM-41

As described in subsection 3.1.3, a calibration curve for the $CuSO_4$ solution (**Fig. 4.8**) has been created to confront the obtained value of groups quantity generated on the mono-functionalized MCM-41. Something more could be said about the interaction between functional groups and copper ions, as shown in **Fig. 4.9**, one link can take up one, two, or three NH_2 groups. The table reports the number obtained from a 1:1 proportion, hence it constitutes an overestimation of the effective groups formed; if 1:2 and 1:3 proportions are taken into account, the calculation of the number of amino groups will be more complex to handle.

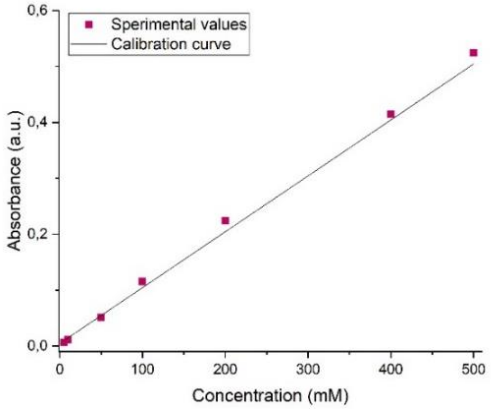

Fig. 4.8 Calibration curve based on tested different concentration solutions of $CuSO_4$.

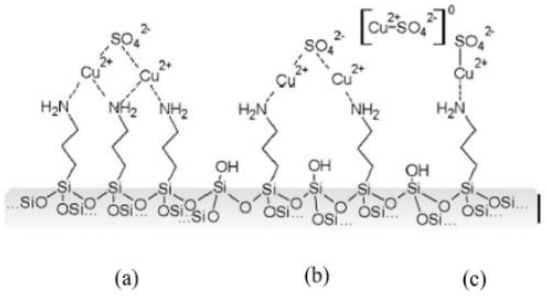

Fig. 4.9 Possible interactions between copper ions and NH_2 groups: 1:3 (a), 1:2 (b) and 1:1 (c) proportions.

4.3.2 Immobilization percentage and Retained activity

Table 4.6 presents values of immobilization percentage (I) and Retained activity (R_{act}) for all the immobilizations tested, both on heterofunctional and monofunctional MCM-41. Procedures have been described in subsections 3.5.3 and 3.5.4.

	t (min)	**I (%)**	**R_{act} (%)**
***h*LDH-A on MCM-41 heterofunctional**	40	99	13.8 ± 7.7
***h*LDH-A on MCM-41 heterofunctional 50 ppm PEG**	45	92	24.8 ± 4.2
***h*LDH-A on MCM-41 heterofunctional 500 ppm PEG**	40	95	12.7 ± 7.7
***h*LDH-A on MCM-41 heterofunctional 1% PEG**	40	77	10.4 ± 4.2
***h*LDH-A on MCM-41 heterofunctional 5% PEG**	145	80	7.2 ± 4.2
***h*LDH-A on MCM-41 heterofunctional 300 mM Trehalose**	30	93	11.5 ± 1.3
***h*LDH-A on MCM-41 monofunctional 1% GA**	30	96	13.3 ± 11.8
***h*LDH-A on MCM-41 monofunctional 2.5% GA**	30	84	8.9 ± 3.4

Table 4.6 Immobilization time (t), immobilization percentage (I) and Retained activity for experimented immobilizations.

As previously described, three measurements have been taken to monitor immobilization: the free enzyme activity, the suspension activity and the supernatant of the centrifugated solution at 500 rpm for 2 minutes. The evolution of these measurements is represented in **Fig. 4.10** for immobilization in presence of GA for monofunctional support and in **Fig. 4.11** for the one in presence of PEG and Trehalose for heterofunctional support.

To guarantee an optimal reaction environment, some considerations have been made regarding both pH, molarity, and temperature, factors that have a relevant influence on the immobilization process. pH and molarity roles are interconnected, as their variations determine a change in the surface and bulk charge distribution, with the consequent variation of the environment in which the enzyme operates. Thus, it has been demonstrated that the ideal pH of the reaction environment is typically near to the enzyme's isoelectric point, which for *h*LDH-A is equivalent to 8.4. Regarding glutaraldehyde immobilizations, the molarity, which is related to the ionic strength of the solution, must be kept low to speed up the process. Eventually, increasing the temperature might play a role in protein deactivation, although it can speed up the immobilization process, some temperature thresholds must not be overcome. [84]

During immobilization, it can be seen how both the free enzyme and the suspension activity values are kept almost constant at a value around 100%, with a minority of cases in which they drop under 75%. This can be due to a deactivation inhibition by maintaining the temperature during immobilization at 4-10°C.

Eventually, immobilization time fluctuates around a value of 35-40 minutes, with an exception for the immobilization in presence of 5% PEG and a minimum value of 30 minutes reached during the immobilization with 50 ppm PEG and the ones on the monofunctional MCM-41.

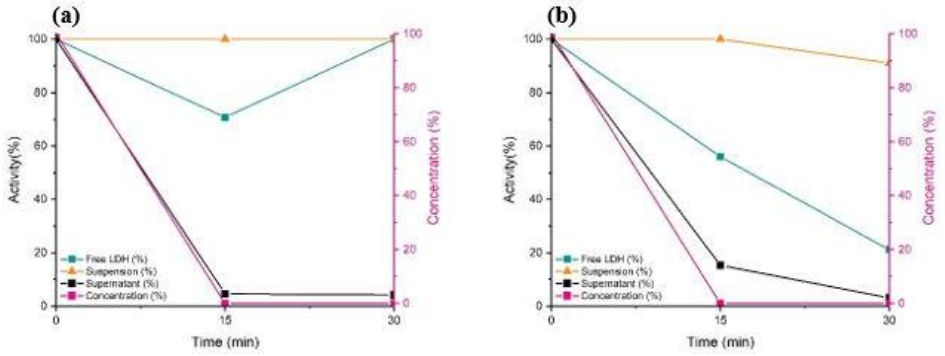

Fig. 4.10 Free enzyme, suspension and supernatant percentage activity and concentration percentage in supernatant for immobilizations on MCM-41 monofunctional with 1% GA **(a)** and 2.5% GA **(b)**

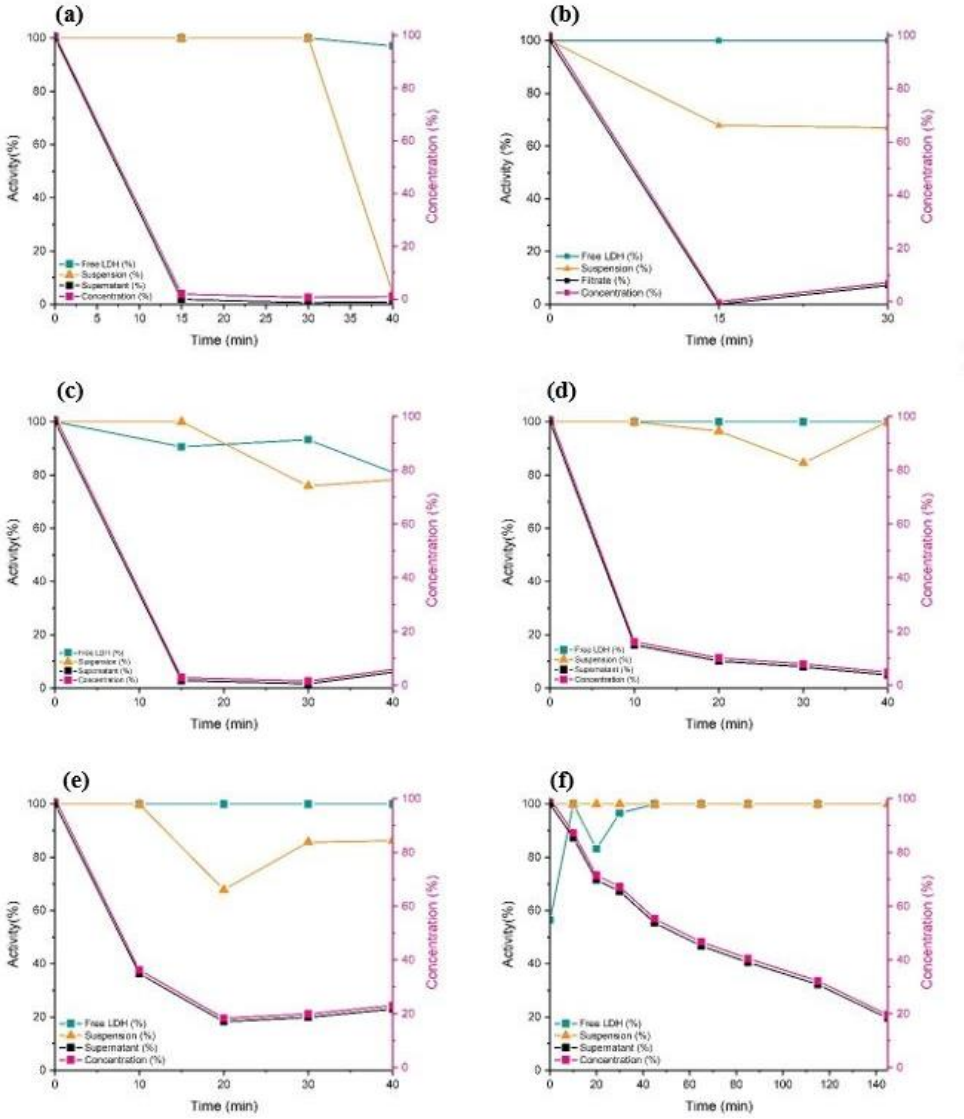

Fig. 4.11 Free enzyme, suspension and supernatant percentage activity and concentration percentage in supernatant for immobilizations on MCM-41 heterofunctional without PEG or Trehalose **(a)**, with Trehalose 300 mM **(b),** with 50 ppm PEG **(c),** with 500 ppm PEG **(d),** with 1% PEG **(e),** with 5% PEG **(f)**

It is clear how immobilizations in presence of PEG reach the highest percentage of Retained activity. If confronting both this value and the immobilization percentage (**Fig. 4.12**), the immobilization in presence of a 50 ppm PEG solution results in an acceptable compromise of the specified values among all the immobilizations tested. It also presents the minimum immobilization time which implies a limited energy waste. Further tests have been processed for this immobilization to determine other working parameters.

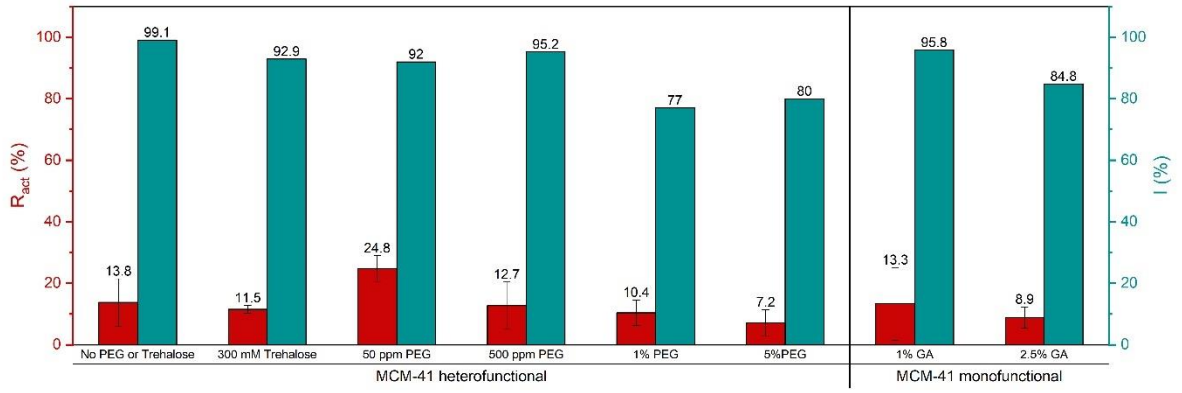

Fig. 4.12 Immobilization percentage (green) and Retained activity (red) for immobilizations on hetero and mono-functionalized MCM-41

Percentage Retained activities present a significant error, which might bring some values under a 5%. For this reason, activity values found are to be considered low. Some cases present a Retained activity over 10% with a relatively small error which can be considered more significant results. In this data evaluation, it has not been taken into consideration any issue related to the presence of the enzyme inside the silica pores or any phenomena regarding the limit to the mass transfer since both functionalized materials have a smaller pore diameter than the minimum of the enzyme. Sodium borohydride utilized in the immobilization process on MCM-41 heterofunctional to reduce Schiff's bases may play an important role, as it has a negative effect, enhancing the enzyme's denaturation process. Also, as the PEG concentration gets higher, the Retained activity tends to low down, which might indicate that the optimal value lies around 50 ppm of PEG. Two possible causes of a low R_{act} value for MCM-41 monofunctional are the percentage of glutaraldehyde used and the pH which does not represent an optimal immobilization condition. It is known that the enzymatic activity is inversely proportional to the concentration of glutaraldehyde. In fact, too many bonds between glutaraldehyde and enzyme can cause a distortion of the protein structure and, in particular of the conformation of the active sites, decreasing the accessibility of the substrate and the enzymatic activity.

4.3.3 Optimal temperature and pH for immobilized enzyme

As already cited, the temperature and pH tests have been carried out on the immobilized LDH on MCM-41 heterofunctional in presence of 50 ppm PEG. The procedure consists of the same steps as described in subparagraph 3.5.5 and it is very similar to the one applied for the free enzyme.

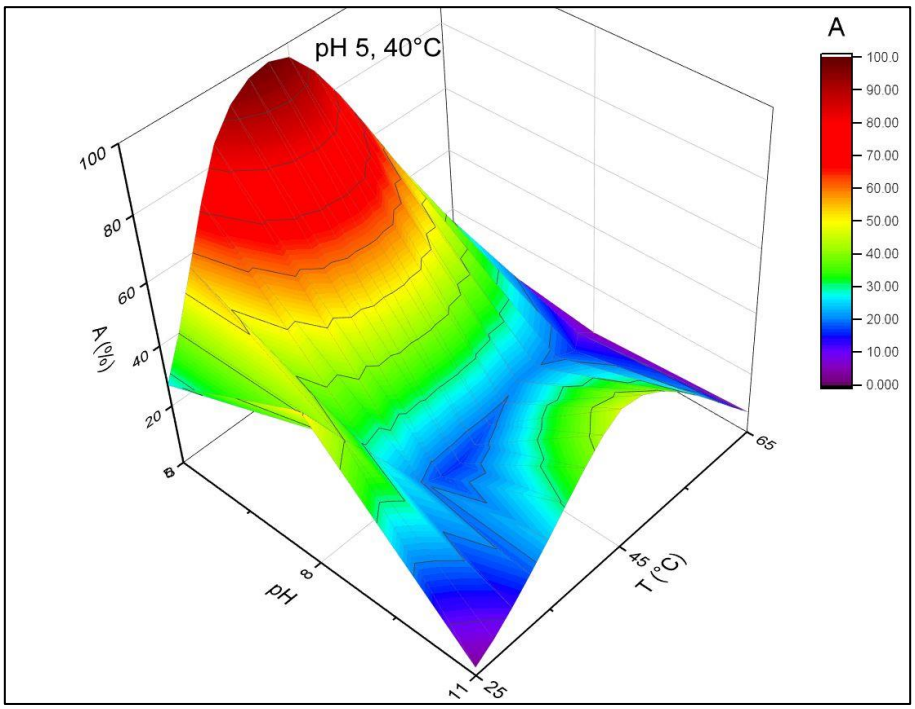

Fig. 4.13 Temperature and pH map for optimal operative conditions determination for immobilized enzyme.

From **Fig. 4.13** it is possible to see how a peak is found for a temperature of 40°C and a pH of 5. With respect to the free enzyme (40-45°C and pH 7.5), optimal operative conditions shifted to a more acidic pH for immobilized LDH. This might be explained by the fact that H^+ and OH^- concentrations usually are not equally partitioned between the microenvironment of the immobilized enzyme and bulk solution due to electrostatic interactions with the matrix, which often leads to the displacements in the pH activity profile. As the pI of LDH is 8.4, the enzyme presents a positive net charge at pH 5, 6, and 7 and is negatively charged at higher pH. The positive net charge of LDH results to be more pronounced for lower pH in the interval 5-7, but the negative surface charge of silica is, therefore, less pronounced. Thus, it is not obvious how the Columbic attraction between the enzyme and the pore walls will vary with pH. One might initially expect a repulsive interaction between the weakly negatively charged LDH and the strongly negatively charged silica surface at the greatest pH, pH 11, but this interaction might not be the dominant one. The enzyme may adopt a conformation such that it exposes positively charged groups toward the silica surface, leading instead to an attractive enzyme-silica interaction, similar to the situation at the lower pH values, a phenomenon that would justify both activity peaks at pH 5 and 11 for the immobilized enzyme. [30][98]

4.3.4 Fluorescence microscopy results

LDH has been coloured and then immobilized in the same chosen conditions (50 ppm PEG) as described in subsection 3.5.6 and therefore it was analysed through a fluorescence microscope. Labelling kit ATTO 488 emits fluorescence in the green channel, while the silica support should only present an intrinsic fluorescence in the blue channel. From the images presented, analysed with the magnificence of 60x, two main situations can be identified: in one the support can only be distinguished in the blue channel as there is a low amount of it (**Fig. 4.14-a, b**) and in the second in which the fluorescence given by the support in the green channel is significant and it could be due to the overlapping of several layers of MCM-41 functionalised support (**Fig. 4.14-c, d**). In both cases the enzyme is distinguishable from the support as its fluorescence in the green channel is very significant even in comparison to a large amount of MCM-41 (**Fig. 4.15**). Moreover, after a careful view, it is possible to notice that, when both green and blue channels present fluorescence for only the MCM-41 support, the images are perfectly superimposable, which does not happen when the labelled enzyme is present (**Fig. 4.16**).

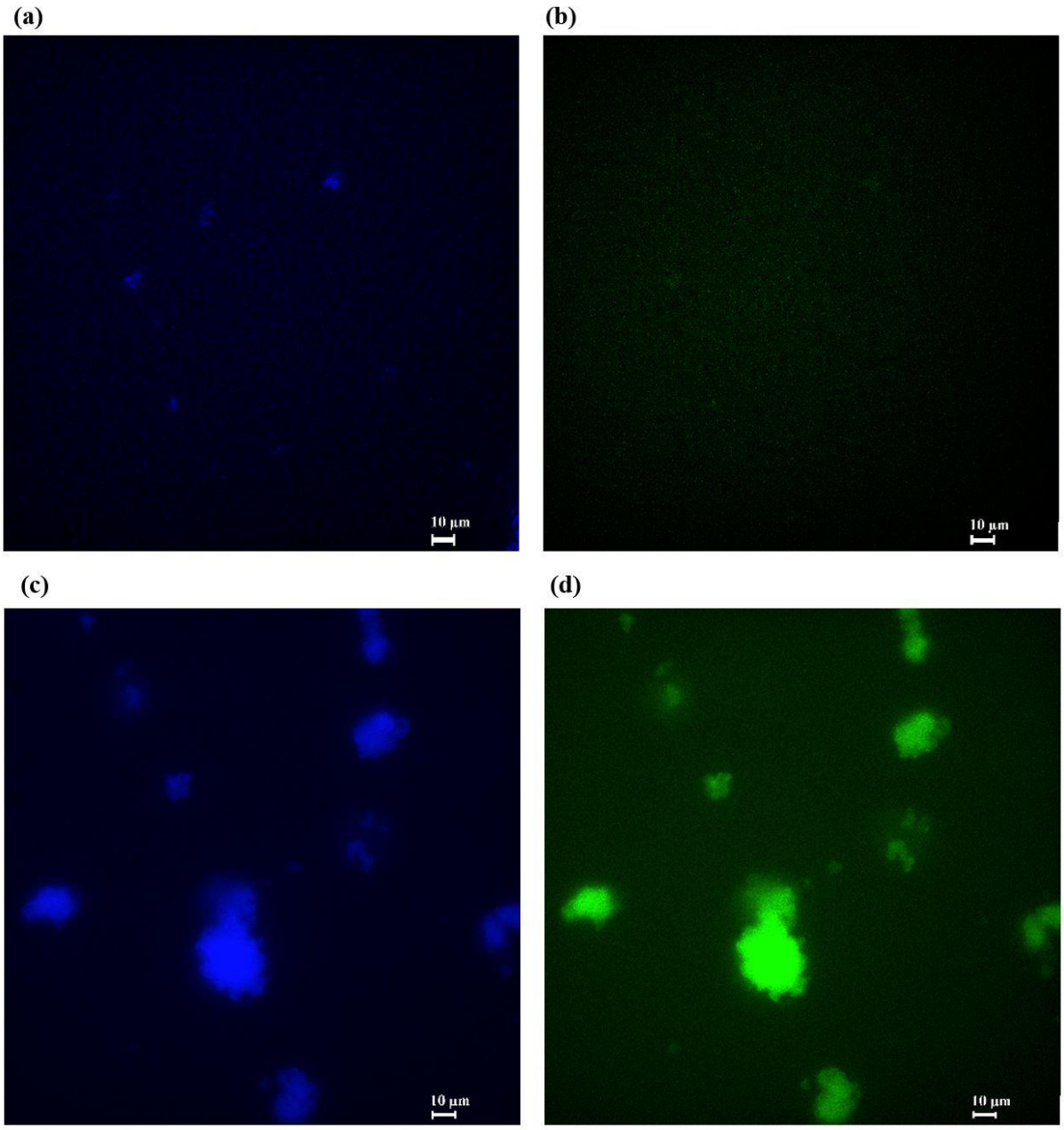

Fig. 4.14 Fluorescence microscopy images with a magnificence of 60x of MCM-41 in blue **(a, c)** and green **(b, d)** channels.

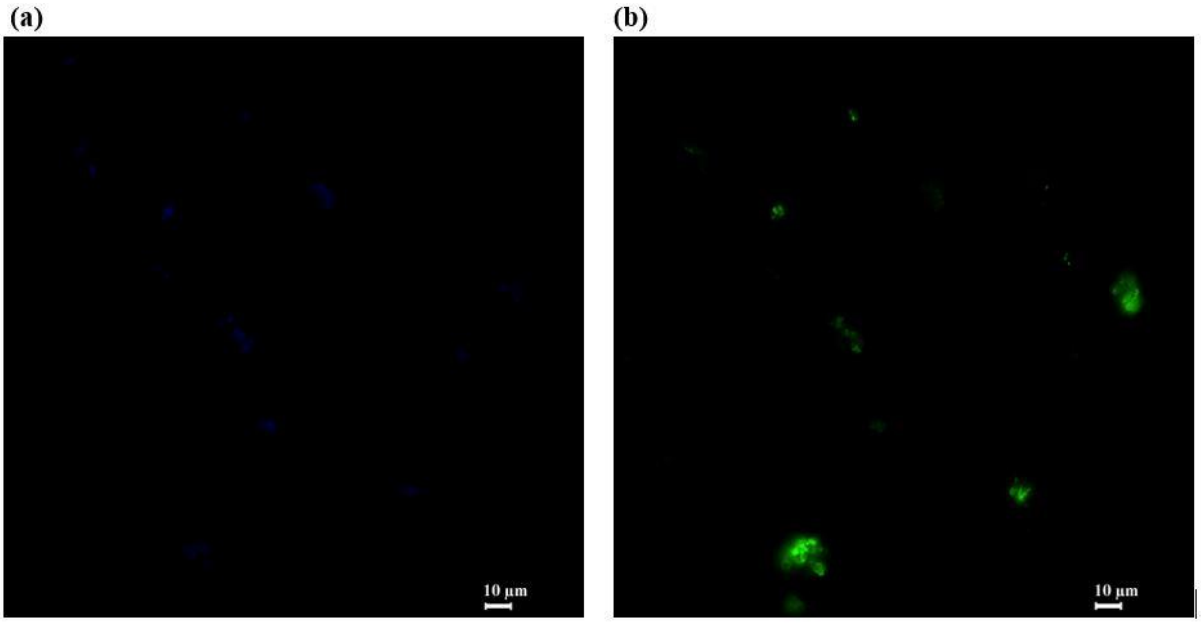

Fig. 4.15 Fluorescence microscopy images with a magnificence of 60x of *h*LDH-A immobilized on MCM-41 heterofunctional with 50 ppm PEG in blue **(a)** and green **(b)** channels.

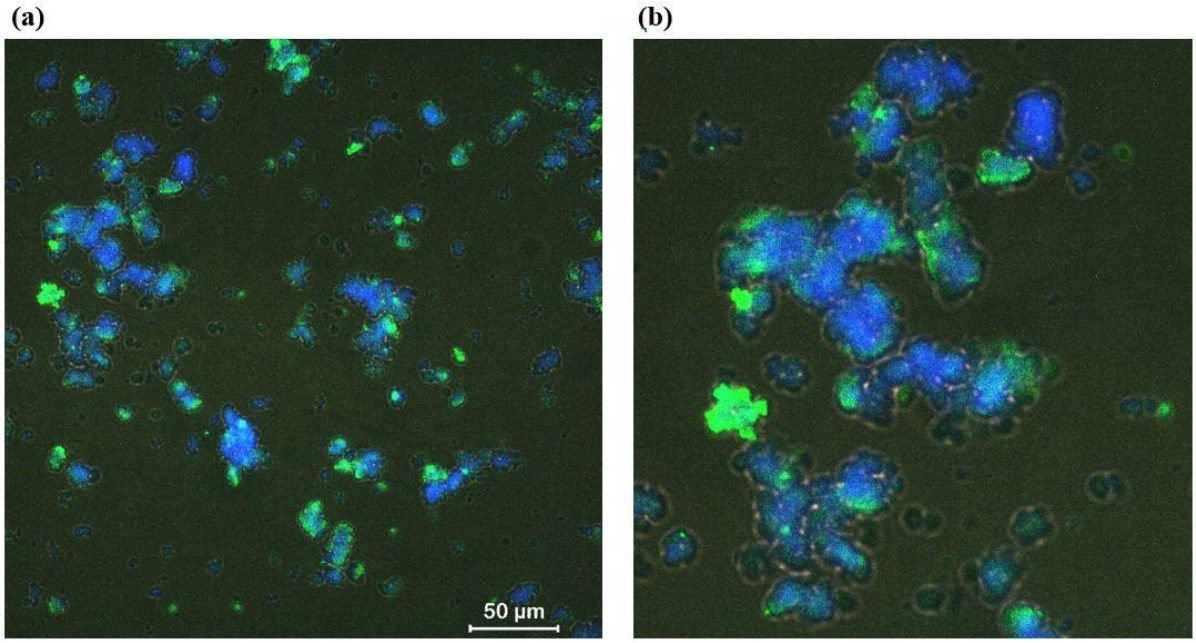

Fig. 4.16 Fluorescence microscopy images with a magnificence of 60x of *h*LDH-A immobilized on MCM-41 heterofunctional with 50 ppm PEG in overlapped blue and green channels. **(b)** is a magnificence of **(a).**

4.3.5 Thermal stability results

To determine a thermal stability for both the free enzyme and the biocatalyst, a test was processed for a total time interval of 72 hours as described in subparagraph 3.5.7.

Fig. 4.17 and **Fig. 4.18** represent the experimental points for the free and immobilized LDH respectively and a trend line calculated through equation (3.16) after parameters have been determined through a graphical way. Each point is constituted by the average of the measurements that have been taken and the error bar corresponding to the relative error calculated through the error's propagation theorem.

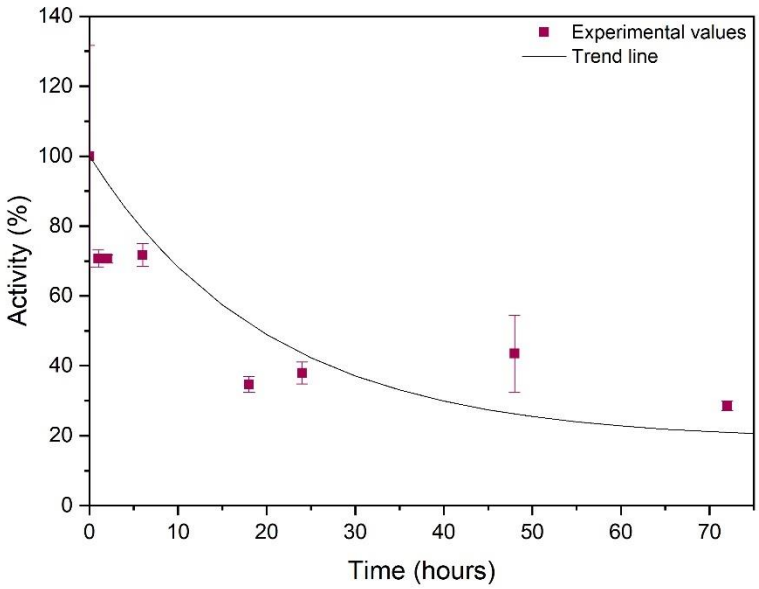

Fig. 4.17 Free LDH thermal stability experimental points and trend line.

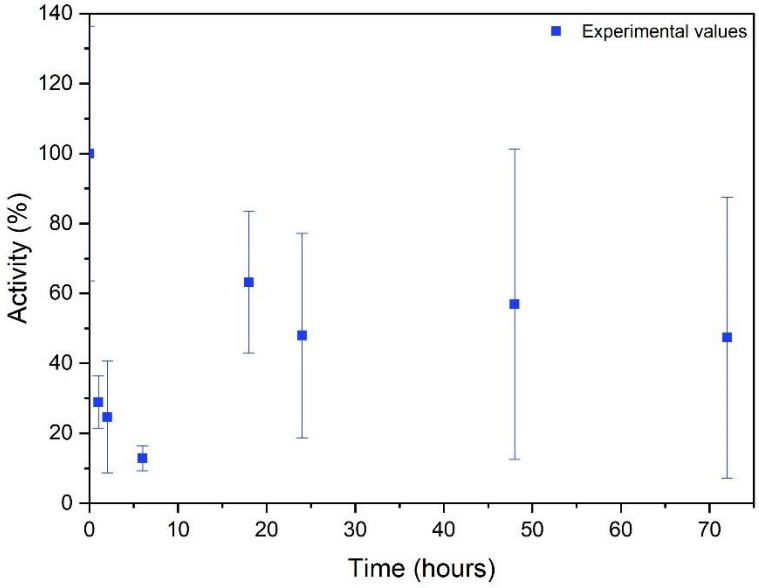

Fig. 4.18 Immobilized LDH on MCM-41 heterofunctional 50 ppm PEG thermal stability experimental points.

From the graph representing the free enzyme test, it is easy to see how experimental activities reach values of about 20% of the initial one for time approaching 72 hours, following the trend line's evolution. On the contrary, for the analysis of the biocatalyst's activity in time, it is not possible to establish a trend for the experimental points. This derives from the fact that in the initial 6 hours activity drops to values concerning the free LDH activity. In point analysed after 18, 24, 48 and 72 the activity trend seems to raise up, but an excessive error is present. This might be due to a low homogeneity during the immobilization procedure or to an unfolding of the protein leading to its inactivation in specific points on the support.

4.3.6 Results of the inhibition test with NHI-2

The inhibition test of *h*LDH-A by the anti-cancer drug NHI-2 has been processed for both the free enzyme and the immobilized one in presence of 50 ppm PEG. The test procedure is the same utilized for the activity assays conducted so far and it is described in subsection 3.6.1. For both cases, it is expected a higher activity in absence of the inhibitor than from the one in its presence, meaning that the conversion from pyruvate to lactate operated by the enzyme has been inhibited. In fact, from **Fig. 4.19** it can be seen how in the presence of the anti-cancer drug both free enzyme and biocatalyst have been inhibited. Lower activity in presence of the inhibitor, and so a more significant inhibition, has been obtained for the free LDH concerning the immobilised enzyme.

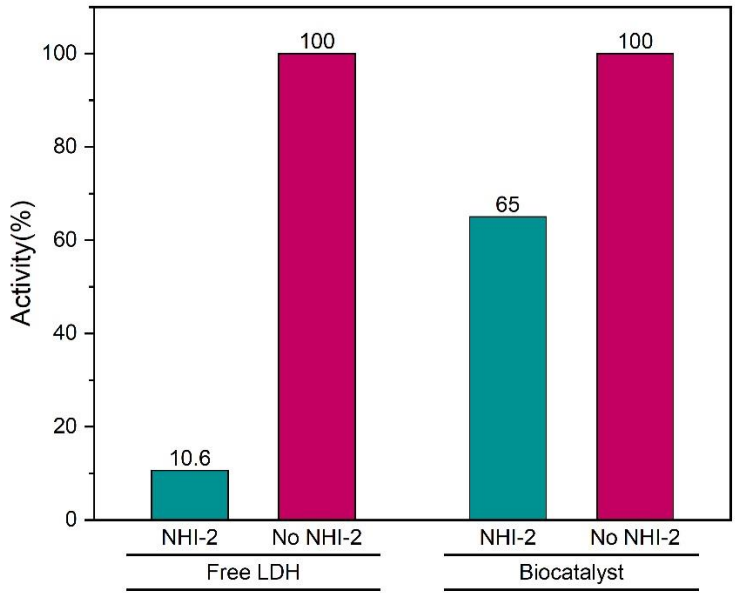

Fig. 4.19 Free and immobilized *h*LDH-A in absence and presence of inhibitor NHI-2

Percentage inhibition values presented in Table 4.7 have been calculated through equations (3.17) and (3.19) for free enzyme and biocatalyst respectively.

	Inhibition (%)
Free *h*LDH-A	89.4
***h*LDH-A/MCM-41 heterofunctional 50 ppm PEG**	35.0

Table 4.7 Inhibition percentage values from NHI-2 inhibition test of free and immobilized *h*LDH-A.

An improvement in the inhibition percentages could be obtained by optimizing the concentrations and volumes of the reagents used. However, a change in the type of quantitative analysis to perform these tests is suggested. High Performance Liquid Chromatography (HPLC) is a valid alternative to obtain more precise results.

5. Electrochemical studies for biosensor development

5.1 Biosensor's design

Several papers have been analysed to determine the feasibility of an electrochemical biosensor that exploits the immobilized LDH onto hetero-functionalized mesoporous silica MCM-41**.** The detection mechanism for quantification of lactate concentration into solution derives from the redox reaction involving the cofactor NADH/NAD^+. Among several biosensor types described in subsection *2.5*, an electrochemical biosensor prototype results to be the most suitable for this case. Recently, this sensor category has generated a lot of interest, especially for use in medical diagnostics, condition monitoring, and environmental monitoring. A brief description of its operation mode is provided below.

As cited in the initial chapters, A subunit of LDH specifically catalyses the chemical conversion of pyruvate into L-lactate and NADH to NAD^+ as equation 5.1 shows, while equation 5.2 represents the redox reaction taking place for cofactor NADH/NAD^+.

In the reaction environment a series of redox reaction involving oxygen takes place between the enzyme and the electrode surface, determining a potential difference proportional to the amount of dissolved lactate.

$$\text{Pyruvate} + \text{NADH} \longrightarrow \text{L} - \text{lactate} + \text{NAD}^+ \tag{5.1}$$

$$\text{NADH} + \text{H}^+ \longrightarrow \text{NAD}^+ + 2\text{H}^+ + 2\text{e}^- \tag{5.2}$$

It must be taken into consideration that the sensitivity of the electrochemical sensor will be affected by several aspects such as surface modification to allow ions exchange and the electrochemical transduction mechanism. The most common method to improve sensor performance is to chemically modify the working electrode's surface. To further boost the performance of electrochemical sensors in terms of their sensitivity and selectivity, extensive research is underway to find suitable modifier materials. Among them, Nafion was used as an electrode modifier for sensor electrode fabrication. It is a fluoropolymer-copolymer based on sulfonated tetrafluoroethylene and it is the first of a group of synthetic polymers known as ionomers that have ionic properties. Because of its excellent chemical and mechanical stability in the demanding conditions of this application, it has attracted a lot of attention as a proton conductor for proton exchange membrane (PEM) fuel cells, as it helps to block the anionic species from reaching the electrode surface and allows the cation conduction to pass through, thus leading to good selectivity. Additionally, Nafion helps to enhance the stability of carbon-modified electrodes due to its excellent film-forming ability.

To overcome several difficulties an electrochemical biosensor faces and to improve their analytical performance, several challenges need to be solved. These include: (i) the electrode's surface's slow electron transfer rate properties, which lead to a poor response signal; (ii) the electrode's limited sensitivity and selectivity capabilities toward target analyte detection due to the occurrence of fouling effect; and (iii) the electrode's overlapping voltametric response brought on by the coexistence of various interfering species. From researches it emerged how

a carbon-polymer-based hybrid material endows the novel properties of composites that are essential in boosting the sensing performance. [94]

The traditional experimental electrochemical setup uses a three-electrode cell made up of an electrolyte, a conductive solution that permits charge transport, a working electrode (WE), which is the biosensor where electrochemical transduction occurs, a counter-electrode (CE), which is controlled by a potentiostat and provides a path for current flow while setting a specific potential for the WE, and a reference electrode (RE), which is kept close to the WE. Screen-printed electrodes (SPEs) were recommended by Couto *et al.* [95] as a viable option for an electrochemical transducer because of their inexpensive cost and ability to be discarded after each study. Among the types of electrochemical biosensors, amperometric and potentiometric are the most employed ones.

The amperometry method is based on applying a fixed voltage to the WE and measuring the electrical current that results from the faradaic reactions involving the electroactive analyte as they occur over time. In this method, the use of a specific potential is associated with a given analyte, minimizing the interference of other electroactive species on the electrochemical response of the biosensor, and increasing its selectivity and sensitivity.

The potentiometry relies on the potential difference between the WE and the RE when a negligible current flow is recorded. The Nernst equation can be used to compute the observed potential, which is proportional to the ion activity. [95]

A good solution seems to be constituted by a Glassy Carbon Electrode (GCE) which surface has been modified with Nafion. More details about this composite's formation process can be found in the reference article [64]. Briefly, the procedure implies the enzyme immobilization onto mesoporous silica as a first step, then a reaction of the silica/*h*LDH-A complex with Nafion follows, and eventually a suspension of this final complex is dropped on the surface of the GC electrode. (**Fig 5.1**)

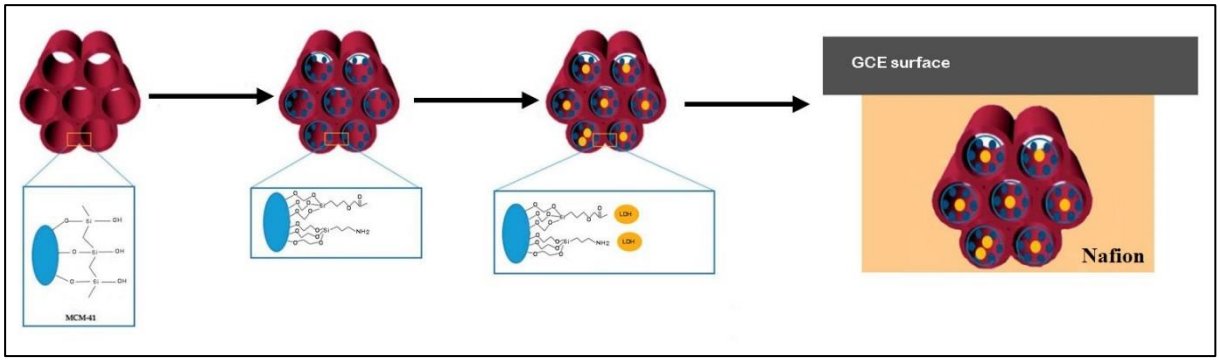

Fig. 5.1 *h*LDH-A/mono-functionalised MCM-41 leading to the complex on GCE electrode modified with Nafion

Electrochemical measurements can be processed through a conventional three electrode system comprising of the fabricated bioelectrode as the working electrode, Pt as a counter or auxiliary electrode and Ag/AgCl as a reference electrode. For this purpose, the SPE design of the biosensor could be employed. In **Fig. 5.2** there is a representation of the common features that characterise an electrochemical cell and an SPE, specifically regarding an enzyme-based biosensor. [96]

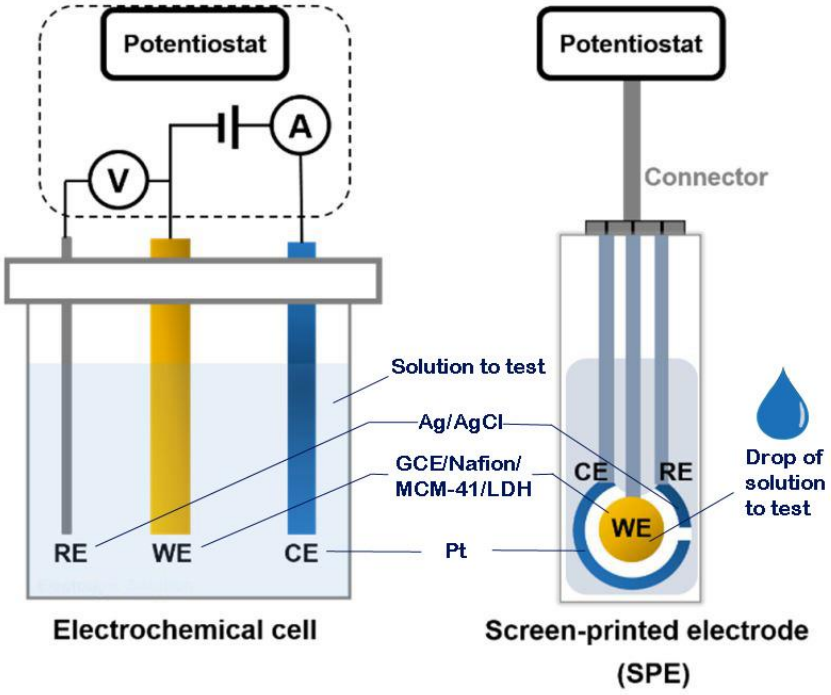

Fig. 5.2 The two types of electrochemical biosensors with three electrodes: reference (RE), working (WE), and counter (CE) connected to a potentiostat. From Damiati *et al*, pp 7 with modifications.

A similar operating principle has been applied by Romero *et al*. [97] for the development of an amperometric biosensor prototype in which the sensitive component constituted by the enzyme immobilized onto a mucin/albumin matrix is further entrapped between two polycarbonate membranes and fixed to a Pt electrode's surface. The working electrode has been as well covered with a Nafion membrane, to avoid critical issues cited before, block interferences, and to increase the specificity of the sensor. Nafion membrane preparation and the construction of the enzymatic electrode are described more in detail in the designated paper.

Utilizing the project just described as a starting model, a sketch of the biosensor prototype has been developed, involving a series of modifications mainly regarding the immobilized enzyme positioning within the biosensor. In the developed model, the biocatalyst as a powder is encapsulated in a compartment delimited by two polycarbonate membranes. Sizes of this compartment may be calculated to optimize the volume and concentration of anti-cancer drug that must be provided for the quantity of biocatalyst powder encapsulated. In **Fig. 5.3** a sketch of this compartment is provided; its dimensions are in meters and they have been obtained increasing the biocatalyst volume and maintaining the same proportions as in the inhibition tests carried on through a spectrophotometer. Dimensions of the prototype are purely esteemed.

Fig. 5.3 Sketch of the tubular compartment for the biocatalyst powder holding within the biosensor prototype. Exploded isometric 3D view on left and assembled 3D view with quotations on right. Quotations are in meters and they are purely esteemed.

The added ring on the right in **Fig. 5.3** provides a threaded connection with the body of the biosensor prototype illustrated in **Fig. 5.4** and **Fig. 5.5.** Eventually, in **Fig. 5.6** a complete view with quotations is present.

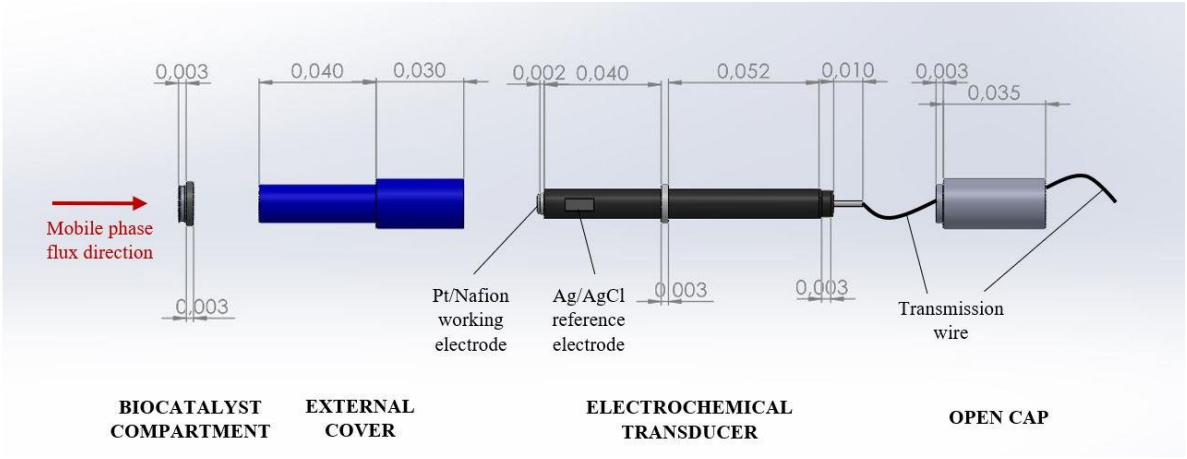

Fig. 5.4 Sketch of the tubular biosensor, lateral exploded view. Quotations are in meters and refer to calculation in subparagraph 5.2.2. Red arrow on left indicates the point where the solution to be analysed is inserted and the flux direction.

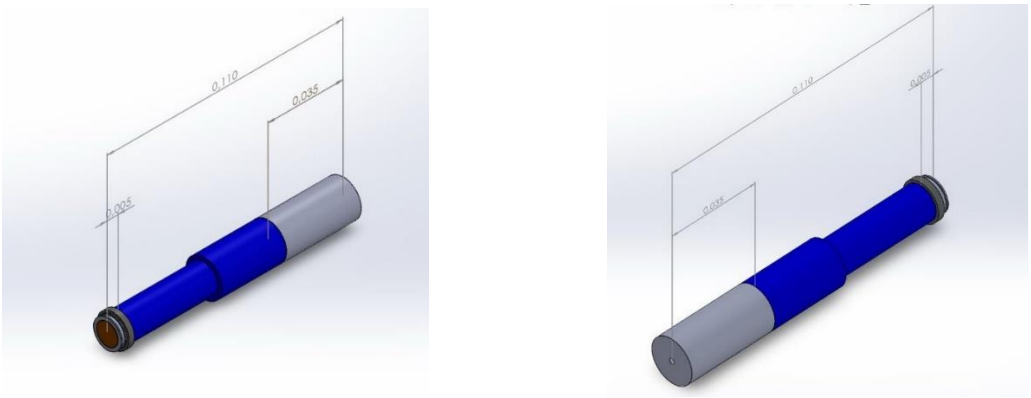

Fig. 5.5 Sketch of the tubular biosensor prototype, isometric assembled front (left) and back (right) views. Quotations are in meters and refer to calculation in subparagraph 5.2.2.

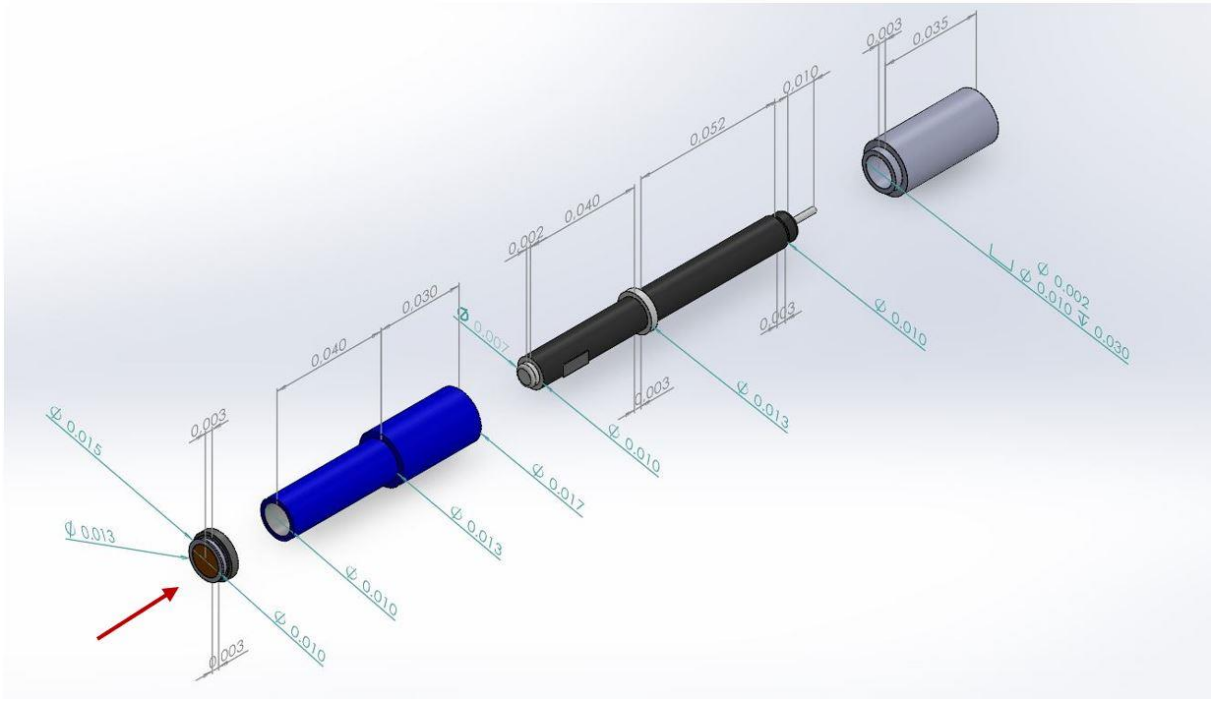

Fig. 5.6 Sketch of the tubular biosensor, isometric exploded view. Quotations are in meters and refer to calculation in subparagraph 5.2.2. Red arrow indicates the flow direction of the Mobile phase.

A series of improvements can be significant to enhance the performance of enzyme-based biosensors: (i) using a base electrode with a high sensitivity, such as a Pt electrode; (ii) using a host matrix with a large pore diameter; (iii) dispersing highly electrically conductive Pt, Au nanoparticles in host; and (iv) electrode composition in terms of relative quantities of enzyme and host on the electrode surface.

Potentiometric and amperometric transducer devices just presented will convert the chemical signal given from the analytes into an electrical signal that has to be read by the operator. The transduced signal is processed and transmitted to the electronic circuitry. The electrical signals obtained from the transducer are amplified and converted into digital form. The processed signals are then quantified by the display unit. This last is composed of a user interpretation system, such as a computer or a printer that generates the output so that the corresponding response can be readable and understandable by the user. Depending on the end-user prerequisite, the output can be in the form of a numerical, graphical, tabular value, or a figure. (**Fig. 5.7**)

Fig. 5.7 Electronic circuitry including Amplifier and processor devices and a display.

5.2 Studies and optimal parameters for a tubular biosensor prototype

5.2.1 Injecting volume and composition of the Mobile phase

The efficiency of the enzymatic biosensor prototype and the detector response rely on the flow rate and volume of the anti-cancer drug to be analysed. Lower flow is associated with bigger concentration differences of the LDH-A inhibitor. Therefore, the current response of the biosensor is the complex result of the influence of the flow rate on the sensor and the detector performance. The injection volume of an analyte can significantly affect such parameters as the sensitivity of measurements, the shape of the recorded curve, linear dynamic range, and in some cases also the enzyme activity.

In previously described inhibition tests, 30 µL of a 3.75 mM solution of NHI-2 has been employed for a biocatalyst quantity of 20 mg. The mobile phase to be inserted not only contains the enzyme inhibitor but must provide the substrate and cofactor for the reaction to occur. If utilizing the same reaction conditions as the inhibition test, the final mobile phase must have a volume of 151.5 mL and should be constituted by a solution of phosphate buffer pH 7.5 0.1 M, with a pyruvate concentration of 1.63 mM and a NADH concentration of 0.23 mM. Eventually, anti-cancer drug concentration in the mobile phase must be of 0.037 mM. If the inserted volume needs to be reduced, a more concentrated solution in its components may be used. Further analysis might be done on the inhibition efficiency concerning the anti-cancer drug concentration or the ratio between enzymatic load within the biocatalyst and the NHI-2 concentration.

5.2.2 Volume of the enzymatic compartment

The enzymatic compartment is commonly placed in front of the detector and it influences some important characteristics of biosensors, e.g., sensitivity, enzymatic capacity, lifetime of the reactor, peak parameters, etc. The powder of MCM-41/*h*LDH-A may be used for gradually filling a tube with a defined inner diameter and length. The powder quantity can be measured to obtain the desired volume or mass. The current response of the biosensor is expected to be proportional to the volume of the reactor. Some studies report a volume threshold beyond which the current response did not further vary. [98] Dimensions of this compartment for the biosensor prototype have been calculated referring to 100 mg of biocatalyst powder and the corresponding anti-cancer drug volume and concentration in the same proportions utilized in the inhibition test described in subparagraph 3.6.2. A diameter of 0.01 m of the compartment has been chosen arbitrarily. This biocatalyst mass occupies approximately 2.5e-6 m^3, which implies that the compartment should have a length of 3.2e-3 m.

5.2.3 Optimal residence time and flow rate

Another important parameter may be constituted by the optimal reaction time during which a maximum inhibition of the enzyme is operated by the anti-cancer drug and therefore a higher potential difference is recorded by the electrode due to the occurred redox reactions.

For this parameter calculus, the compartment containing the biocatalyst could be regarded as a fixed bed reactor, and thus, the reaction time coincides with the residence time of the mobile phase within the reactor. The inhibition tests have been carried on for 2 minutes, so this time interval will be assumed to be the residence time and utilized in the following calculations. Flow rate can be obtained from equation (5.3) and it results to be 2.1e-9 m^3/s. Eventually, after the insertion of the mobile phase, a volume of buffer equal to that of the catalytic bed has to be inserted to completely eject the reagents, or a more accurate cleaning has to be processed if the biocatalyst's regeneration is desired.

$$\text{Flow rate} = \frac{V_{reactor}}{\tau_{residence}} \tag{5.3}$$

5.2.4 Biosensor's materials

A brief description of the material employed for the electrode has been already provided in subsection *5.1*. For the part regarding materials employed for the external cover, it might be composed by polymeric or metallic materials. More attention has to be paid to the compartment in which the biocatalyst powder will be stored. First, polycarbonate membranes are provided at extremities: these can keep the powder entrapped within the compartment but are also permeable to the solution containing the anti-cancer drug to be tested to and to buffer solution needed to rinse the biocatalyst. Other material membranes might be suitable for this purpose, with the condition to possess a mesh compact enough to not allow loss of biocatalyst. From literature, the pore size for these membranes has to be of maximum 0.05 μm. [97]

The container's material must be neutral concerning the biocatalyst and must not interact with any functional group that characterises MCM-41 or LDH surfaces. From literature, it emerged that polytetrafluoroethylene (PTFE) might be employed for this role, as it is one of the most versatile plastic in terms of chemical compatibility. [98] Some basic properties that make it suitable for this biosensor are a good electrical insulating power in a hot and wet environment, good resistance to UV-light and weathering, low coefficient of friction, low dielectric constant/dissipation factor and low water absorption.

6. Conclusions

The initial project consisting of a biosensor-prototype's design is composed by several steps and involves a remarkable time lapse and research investments. Therefore, this thesis represents a section within this broader project having as a final goal the creation of a stable biosensor prototype based on *h*LDH-A for the screening of anti-cancer drugs. MCM-41 mesoporous silica has been implied as support for enzyme's immobilization due to its structural porous characteristics. It was then both hetero-functionalized with amino and aldehyde groups and mono-functionalized with only amino groups. FTIR analysis and characterization tests have been carried on to evaluate the actual presence of these functional groups on the matrix's surface. Changes in physical properties due to functionalization treatments were observed from N_2 physisorption analysis at 77 K and XRD. Drops in the specific surface area of MCM-41 hetero and amino-functionalized were observed, probably due to the functionalization processes. Moreover, an increase in the thickness of the channel walls of the functionalized silicas also emerged, which can be a consequence of the addition of organosilanes molecules on MCM-41's surface.

Among various immobilization procedure in absence and presence of different stabilizing agents, a distinguishable immobilization percentage of 92% and a *Retained activity* of 24.8% have been obtained from the immobilization of *h*LDH-A on hetero-functional MCM-41 in presence of 50 ppm PEG. The activity of this immobilized enzyme has been compared to that of the free enzyme as a function of pH and temperature to ascertain the stabilizing effect of the immobilization, obtaining an increase in enzymatic activity for a pH interval between 5 and 11. Eventually, anti-cancer drug NHI-2's inhibition effect has been tested on both immobilized and free enzyme, obtaining inhibition percentages of 35% and 89.4% respectively.

Among all the steps executed for this thesis' drafting, improvement research might be operated regarding the most critical steps: functionalization and immobilization. As the results can confirm, the immobilization processes lead to a significant activity of the immobilized enzyme, meaning the right direction has been taken. Further studies might be focused on innovative or more efficient stabilizing agents. A critical point which could be additionally analysed regards the choice of the support material and its functionalization, as during these procedures some of the fundamental features of MCM-41 might have been altered determining an inhomogeneous immobilization or deactivation of the enzyme. Different materials can be evaluated for a change in the pore dimension, factor that can significantly influence characteristics of the immobilized LDH. Other mesoporous silicas or a series of polymeric materials could be employed to define the most suitable for *h*LDH-A's immobilization.

Regarding the functionalization process, many factor still must be studied. A functionalization with only epoxy groups could be attempted or a less aggressive environment during functionalization reaction, avoiding toluene or H_2SO_4, may lead to improved characteristics of the final structure.

As a conclusion of this thesis, a design sketch of the biosensor prototype has been outlined, studying from literature parameters that might be fundamental for the development of its entire structure. Regarding the transducer, one of the most suitable solutions is constituted by an amperometric or a potentiometric electrochemical device, which focuses its measurements on the potential difference derived from electron transfer due to redox reactions

catalysed by LDH. Electrode configuration is one of the key points in determining biosensor's performance and many studies can be done to accomplish high sensitivity and precision. Many analyses could be executed to determine optimal parameters for the working biosensor, such as volume, flow rate and concentration of the anti-cancer drug to be tested and an optimal quantity of the employed biocatalyst as well, which will consequently identify more reasonable dimensions for the pieces composing the biosensor.

An eventual study might be focused on different configurations, as just a couple of them have been examined, mostly for their versatility and affordability.

Symbols and abbreviations

APTES	3-aminopropyl triethoxysilane
BET	Brunauer-Emmet-Teller
BJH	Barrett-Joyner-Halenda
BSA	Bovine serum albumin
$CuSO_4$	Copper sulphate
FTIR	Fourier-transform infrared spectroscopy
GPTMS	3-glycidyloxypropyltrimethoxysilane
H_2SO_4	Sulfuric acid
*h*LDH-A	Human Lactate dehydrogenase - A subunit
K	Kelvin
KI	Potassium iodide
LDH	Lactate dehydrogenase
MCM-41	Mobil Composition of Matter No. 41
N_2	Nitrogen
$NaBH_4$	Sodium borohydride
$NaHCO_3$	Sodium hydrogen carbonate
$NaIO_4$	Sodium periodate
NADH	Reduced form of Nicotinamide adenine dinucleotide
NAD^+	Oxidized form of Nicotinamide adenine dinucleotide
NHI	N-hydroxyindole compounds
NHI-2	Methyl 1-hydroxy-6-phenyl-4-(trifluoromethyl)-1*H*-indole-2-carboxylate
PEG	Polyethylene glycol
α	Asymptotic value of activity for an infinite time
a_0	Cell parameter *(nm)*
A	Activity
Abs	Fixed wavelength absorbance
A_{IE}	Immobilized enzyme activity *(IU/g_{sup})*
A_{FE}	Free enzyme activity *(IU/mg_{enz})*
ΔAbs	Absorbance variation

Δt	Time variation *(min)*
$\Delta Abs/\Delta t$	*Time course* mode absorbance *(1/min)*
$[E]$	Enzyme concentration *(mg/mL)*
$[IO_4^-]$	Sodium periodate solution concentration *(mmol/mL)*
d_0	Inter-lattice distance *(nm)*
D_{BJH}	Pore diameter evaluated with BJH method *(nm)*
δ	Wall thickness *(nm)*
ε	Molar extinction coefficient *(mM^{-1})*
g_{sup}	Support mass *(g)*
θ	Half of the diffraction angle *(°)*
$\%I$	Immobilization percentage (%)
k_D	Deactivation constant
K_m	Michaelis constant *(mM)*
λ	Wavelength *(nm)*
M	Total enzyme weight *(Da)*
m_{enzyme}	Enzyme mass in solution *(mg)*
m_{bio}	Biocatalyst mass *(mg)*
N_A	Avogadro number
q	Enzymatic loading *(mg_{enz}/g_{sup})*
R_{act}	Percentage Retained activity *(%)*
R_{min}	Enzyme minimum radius *(nm)*
$[S]$	Substrate concentration *(mM)*
S_{BET}	Specific surface area measured through BET method *(m^2/g)*
V	Reaction volume *(mL)*
$V_{IO_4^-}$	Sodium periodate solution volume *(mL)*
TEM	Transmission electron microscopy
XRD	X-ray diffraction

List of Figures and Tables

Bibliographic references

[1] H. Sung *et al.*, "Global Cancer Statistics 2020 : GLOBOCAN Estimates of Incidence and Mortality Worldwide for 36 Cancers in 185 Countries," vol. 71, no. 3, pp. 209–249, 2021, doi: 10.3322/caac.21660.

[2] D. Hanahan and R. A. Weinberg, "Hallmarks of cancer: The next generation," *Cell*, vol. 144, no. 5, pp. 646–674, 2011, doi: 10.1016/j.cell.2011.02.013.

[3] D. Hanahan, "Hallmarks of Cancer: New Dimensions," *Cancer Discov.*, vol. 12, no. 1, pp. 31–46, 2022, doi: 10.1158/2159-8290.CD-21-1059.

[4] M. L. Goodwin, L. B. Gladden, M. W. N. Nijsten, and K. B. Jones, "Lactate and Cancer: Revisiting the Warburg Effect in an Era of Lactate Shuttling," *Front. Nutr.*, vol. 1, no. January, pp. 2014–2016, 2015, doi: 10.3389/fnut.2014.00027.

[5] L. Brisson *et al.*, "Lactate Dehydrogenase B Controls Lysosome Activity and Autophagy in Cancer," *Cancer Cell*, vol. 30, no. 3, pp. 418–431, 2016, doi: 10.1016/j.ccell.2016.08.005.

[6] M. Manerba *et al.*, "Galloflavin (CAS 568-80-9): A Novel Inhibitor of Lactate Dehydrogenase," *ChemMedChem*, vol. 7, no. 2, pp. 311–317, 2012, doi: 10.1002/cmdc.201100471.

[7] X. Han *et al.*, "Evaluation of the anti-tumor effects of lactate dehydrogenase inhibitor galloflavin in endometrial cancer cells," *J. Hematol. Oncol.*, vol. 8, no. 1, pp. 2–5, 2015, doi: 10.1186/s13045-014-0097-x.

[8] C. Granchi *et al.*, "Discovery of N-hydroxyindole-based inhibitors of human lactate dehydrogenase isoform A (LDH-A) as starvation agents against cancer cells," *J. Med. Chem.*, vol. 54, no. 6, pp. 1599–1612, 2011, doi: 10.1021/jm101007q.

[9] G. Cheng, Z. Pi, Z. Zheng, S. Liu, Z. Liu, and F. Song, "Magnetic nanoparticles-based lactate dehydrogenase microreactor as a drug discovery tool for rapid screening inhibitors from natural products," *Talanta*, vol. 209, no. October, p. 120554, 2020, doi: 10.1016/j.talanta.2019.120554.

[10] N. Oshima *et al.*, "Dynamic Imaging of LDH Inhibition in Tumors Reveals Rapid In Vivo Metabolic Rewiring and Vulnerability to Combination Therapy," *Cell Rep.*, vol. 30, no. 6, pp. 1798-1810.e4, 2020, doi: 10.1016/j.celrep.2020.01.039.

[11] O. Warburg, "On the origin of cancer cells," *Science (80-.).*, vol. 10, no. 4, pp. 412–421, 1957, doi: 10.1016/0030-4220(57)90167-6.

[12] J. Li *et al.*, "Wild-type IDH2 promotes the Warburg effect and tumor growth through HIF1α in lung cancer," *Theranostics*, vol. 8, no. 15, pp. 4050–4061, 2018, doi: 10.7150/thno.21524.

[13] K. Offermans *et al.*, "Expression of proteins associated with the Warburg-effect and survival in colorectal cancer," *J. Pathol. Clin. Res.*, vol. 8, no. 2, pp. 169–180, 2022, doi: 10.1002/cjp2.250.

[14] X. Zhang *et al.*, "Analysis of key genes regulating the warburg effect in patients with gastrointestinal cancers and selective inhibition of this metabolic pathway in liver cancer cells," *Onco. Targets. Ther.*, vol. 13, pp. 7295–7304, 2020, doi: 10.2147/OTT.S257944.

[15] N. A. Kalkhoran, Sara; Benowitz, Neal L .; Rigotti, "Therapeutic targeting of the Warburg effect in pancreatic cancer relies on an absence of p53 function," *Rev. del Col. Am. Cardiol.*, vol. 72, no. 23, pp. 2964–2979, 2018, doi: 10.1158/0008-5472.CAN-15-0108.Therapeutic.

[16] J. E. Unterlass and N. J. Curtin, "Warburg and Krebs and related effects in cancer," *Expert Rev. Mol. Med.*, no. 1, 2019, doi: 10.1017/erm.2019.4.

[17] X. S. Chen, L. Y. Li, Y. Di Guan, J. M. Yang, and Y. Cheng, "Anticancer strategies based on the metabolic profile of tumor cells: Therapeutic targeting of the Warburg effect," *Acta Pharmacol. Sin.*, vol. 37, no. 8, pp. 1013–1019, 2016, doi: 10.1038/aps.2016.47.

[18] H. Sun, L. Chen, S. Cao, Y. Liang, and Y. Xu, "Warburg Effects in Cancer and Normal Proliferating Cells: Two Tales of the Same Name," *Genomics, Proteomics Bioinforma.*, vol. 17, no. 3, pp. 273–286, 2019, doi: 10.1016/j.gpb.2018.12.006.

[19] S. Benny, R. Mishra, M. K. Manojkumar, and T. P. Aneesh, "From Warburg effect to Reverse Warburg effect; the new horizons of anti-cancer therapy," *Med. Hypotheses*, vol. 144, no. August, p. 110216, 2020, doi: 10.1016/j.mehy.2020.110216.

[20] B. Bhattacharya, M. F. Mohd Omar, and R. Soong, "The Warburg effect and drug resistance," *Br. J. Pharmacol.*, vol. 173, no. 6, pp. 970–979, 2016, doi: 10.1111/bph.13422.

[21] C. Granchi, S. Bertini, M. Macchia, and F. Minutolo, "Inhibitors of Lactate Dehydrogenase Isoforms and their Therapeutic Potentials," *Curr. Med. Chem.*, vol. 17, no. 7, pp. 672–697, 2010, doi: 10.2174/092986710790416263.

[22] H. Tan *et al.*, "Identification of human LDHC4 as a potential target for anticancer drug discovery," *Acta Pharm. Sin. B*, vol. 12, no. 5, pp. 2348–2357, 2022, doi: 10.1016/j.apsb.2021.12.002.

[23] A. P. Acharya, M. Rafi, E. C. Woods, A. B. Gardner, and N. Murthy, "Metabolic engineering of lactate dehydrogenase rescues mice from acidosis," pp. 1–5, 2014, doi: 10.1038/srep05189.

[24] A. A. Khan, K. S. Allemailem, F. A. Alhumaydhi, S. J. T. Gowder, and A. H. Rahmani, "The Biochemical and Clinical Perspectives of Lactate Dehydrogenase: An Enzyme of Active Metabolism," *Endocrine, Metab. Immune Disord. - Drug Targets*, vol. 20, no. 6, pp. 855–868, 2019, doi: 10.2174/1871530320666191230141110.

[25] E. A.-R. a M. Adeva-Andany, M. López-Ojén, R. Funcasta-Calderón and J. R.-S. C. Donapetry-García, M. Vila-Altesor, "Comprehensive review on lactate metabolism in human health," *Mitochondrion*, 2014, doi: 10.1016/j.mito.2014.05.007.

[26] D. A. Bender, "Function and Metabolism," pp. 2904–2911, 2003.

[27] S. Passarella, "l -Lactate Transport and Metabolism in Mitochondria of Hep G2 Cells — The Cori Cycle Revisited," vol. 8, no. April, pp. 1–4, 2018, doi: 10.3389/fonc.2018.00120.

[28] J. M. Guisan and J. M. Walker, *Immobilization of Enzymes and Cells*, Third edit. 2013.

[29] N. R. Mohamad, N. H. C. Marzuki, N. A. Buang, F. Huyop, and R. A. Wahab, "An overview of technologies for immobilization of enzymes and surface analysis techniques for immobilized enzymes," *Biotechnol. Biotechnol. Equip.*, vol. 29, no. 2, pp. 205–220, 2015, doi: 10.1080/13102818.2015.1008192.

[30] D. Alagöz and N. E. Varan, “Effective immobilization of lactate dehydrogenase onto mesoporous silica,” no. August 2021, pp. 1–11, 2022, doi: 10.1002/bab.2304.

[31] N. Carlsson, H. Gustafsson, C. Thörn, L. Olsson, K. Holmberg, and B. Åkerman, “Enzymes immobilized in mesoporous silica: A physical-chemical perspective,” *Adv. Colloid Interface Sci.*, vol. 205, pp. 339–360, 2014, doi: 10.1016/j.cis.2013.08.010.

[32] J. Arnaldo *et al.*, “Microporous and Mesoporous Materials Recent progresses in the adsorption of organic , inorganic , and gas compounds by MCM-41-based mesoporous materials,” *Microporous Mesoporous Mater.*, vol. 291, no. July 2019, p. 109698, 2020, doi: 10.1016/j.micromeso.2019.109698.

[33] W. Alejandro, T. A. E. Patricia, A. Rafael, V. C. C. Alejandro, and F. Á. A. Á. Post-synthesis, “Effects of different amounts of APTES on physicochemical and structural properties of amino-functionalized MCM-41-MSNs,” 2016, doi: 10.1007/s10971-016-4163-4.

[34] E. Jackson, F. López-Gallego, J. M. Guisan, and L. Betancor, “Enhanced stability of L-lactate dehydrogenase through immobilization engineering,” *Process Biochem.*, vol. 51, no. 9, pp. 1248–1255, 2016, doi: 10.1016/j.procbio.2016.06.001.

[35] K. Xu, X. Chen, R. Zheng, and Y. Zheng, “Immobilization of Multi-Enzymes on Support Materials for Efficient Biocatalysis,” *Front. Bioeng. Biotechnol.*, vol. 8, no. June, pp. 1–17, 2020, doi: 10.3389/fbioe.2020.00660.

[36] H. Kim and J. Y. Kwon, “Enzyme immobilization on metal oxide semiconductors exploiting amine functionalized layer,” *RSC Adv.*, vol. 7, no. 32, pp. 19656–19661, 2017, doi: 10.1039/c7ra01615h.

[37] V. Solano-umaña and J. R. Vega-baudrit, “Micro , Meso and Macro Porous Materials on Medicine,” no. October, 2015, doi: 10.4236/jbnb.2015.64023.

[38] Z. A. Alothman, “A review: Fundamental aspects of silicate mesoporous materials,” *Materials (Basel).*, vol. 5, no. 12, pp. 2874–2902, 2012, doi: 10.3390/ma5122874.

[39] A. J. Schwanke, R. Balzer, and S. Pergher, “Microporous and Mesoporous Materials from Natural and Inexpensive Sources Microporous and Mesoporous Materials from Natural and Inexpensive Sources,” no. September, 2017, doi: 10.1007/978-3-319-68255-6.

[40] A. Kołodziejczak-Radzimska, L. D. Nghiem, and T. Jesionowski, “Functionalized Materials as a Versatile Platform for Enzyme Immobilization in Wastewater Treatment,” pp. 263–276, 2021.

[41] R. Mitran, S. Nastase, and D. Berger, “Tailoring the dissolution rate enhancement of aminoglutethimide by functionalization of MCM-41 silica : a hydrogen bonding propensity approach,” *RSC Adv.*, vol. 5, pp. 2592–2601, 2014, doi: 10.1039/C4RA11224E.

[42] A. Ghanbari and M. M. Attar, “A study on the anticorrosion performance of epoxy nanocomposite coatings containing epoxy-silane treated nano silica on mild steel substrate,” *J. Ind. Eng. Chem.*, 2014, doi: 10.1016/j.jiec.2014.08.008.

[43] H. Miao, M. Li, F. Wang, J. Li, Y. Lin, and J. Xu, “Surface Functionalization of SBA-15 for Immobilization of Myoglobin,” vol. 10, no. May, pp. 1–7, 2022, doi: 10.3389/fbioe.2022.907855.

[44] H. T. Imam, P. C. Marr, and A. C. Marr, “Enzyme entrapment, biocatalyst

immobilization without covalent attachment," *Green Chem.*, vol. 23, no. 14, pp. 4980–5005, 2021, doi: 10.1039/d1gc01852c.

[45] R. Fraas and M. Franzreb, "Reversible covalent enzyme immobilization methods for reuse of carriers," *Biocatal. Biotransformation*, vol. 0, no. 0, pp. 1–12, 2017, doi: 10.1080/10242422.2017.1344229.

[46] M. E. Hassan, Q. Yang, and Z. Xiao, "Covalent immobilization of glucoamylase enzyme onto chemically activated surface of κ -carrageenan," *Bull. Natl. Res. Cent.*, vol. 0, 2019.

[47] A. Böhm, S. Trosien, O. Avrutina, H. Kolmar, and M. Biesalski, "Covalent Attachment of Enzymes to Paper Fibers for Paper-Based Analytical Devices," *Front. Chem.*, vol. 6, no. June, pp. 1–10, 2018, doi: 10.3389/fchem.2018.00214.

[48] S. Smith, K. Goodge, M. Delaney, A. Struzyk, N. Tansey, and M. Frey, "A comprehensive review of the covalent immobilization of biomolecules onto electrospun nanofibers," *Nanomaterials*, vol. 10, no. 11, pp. 1–39, 2020, doi: 10.3390/nano10112142.

[49] D. Zhang, H. E. Hegab, Y. Lvov, L. D. Snow, and J. Palmer, "Immobilization of cellulase on a silica gel substrate modified using a 3 - APTES self - assembled monolayer," *Springerplus*, no. February, 2016, doi: 10.1186/s40064-016-1682-y.

[50] A. Buthe, S. Wu, and P. Wang, "Nanoporous silica glass for the immobilization of interactive enzyme systems.," *Methods Mol. Biol.*, vol. 679, pp. 37–48, 2011, doi: 10.1007/978-1-60761-895-9_5.

[51] J. S. Weltz, D. F. Kienle, D. K. Schwartz, and J. L. Kaar, "Reduced Enzyme Dynamics upon Multipoint Covalent Immobilization Leads to Stability-Activity Trade-off," *J. Am. Chem. Soc.*, vol. 142, no. 7, pp. 3463–3471, 2020, doi: 10.1021/jacs.9b11707.

[52] F. López-Gallego, J. M. Guisan, and L. Betancor, *Immobilization of Enzymes on Supports Activated with Glutaraldehyde: A Very Simple Immobilization Protocol*, vol. 2100. 2020.

[53] S. Moreno-Pérez *et al.*, "Intense PEGylation of Enzyme Surfaces: Relevant Stabilizing Effects," *Methods Enzymol.*, vol. 571, pp. 55–72, 2016, doi: 10.1016/bs.mie.2016.02.016.

[54] X. Wang, J. Bowman, S. Tu, D. Nykypanchuk, O. Kuksenok, and S. Minko, "Polyethylene Glycol Crowder's Effect on Enzyme Aggregation, Thermal Stability, and Residual Catalytic Activity," *Langmuir*, vol. 37, no. 28, pp. 8474–8485, 2021, doi: 10.1021/acs.langmuir.1c00872.

[55] J. K. Kaushik and R. Bhat, "Why is trehalose an exceptional protein stabilizer? An analysis of the thermal stability of proteins in the presence of the compatible osmolyte trehalose," *J. Biol. Chem.*, vol. 278, no. 29, pp. 26458–26465, 2003, doi: 10.1074/jbc.M300815200.

[56] C. Olsson, H. Jansson, and J. Swenson, "The Role of Trehalose for the Stabilization of Proteins," *J. Phys. Chem. B*, vol. 120, no. 20, pp. 4723–4731, 2016, doi: 10.1021/acs.jpcb.6b02517.

[57] L. Fiume, M. Manerba, M. Vettraino, and G. Di Stefano, "Inhibition of lactate dehydrogenase activity as an approach to cancer therapy," *Future Med. Chem.*, vol. 6, no. 4, pp. 429–445, 2014, doi: 10.4155/fmc.13.206.

[58] G. L. Kedderis, "Biotransformation of Toxicants," *Compr. Toxicol. Second Ed.*, vol. 1–

14, pp. 137–151, 2010, doi: 10.1016/B978-0-08-046884-6.00107-X.

[59] B. El Hassouni *et al.*, "The dichotomous role of the glycolytic metabolism pathway in cancer metastasis: Interplay with the complex tumor microenvironment and novel therapeutic strategies," *Semin. Cancer Biol.*, vol. 60, pp. 238–248, 2020, doi: 10.1016/j.semcancer.2019.08.025.

[60] B. El Hassouni *et al.*, "Lactate dehydrogenase A inhibition by small molecular entities: steps in the right direction," *Oncoscience*, vol. 8, no. September 2020, pp. 46–46, 2021, doi: 10.18632/oncoscience.529.

[61] E. C. Calvaresi *et al.*, "Dual targeting of the warburg effect with a glucose-conjugated lactate dehydrogenase inhibitor," *ChemBioChem*, vol. 14, no. 17, pp. 2263–2267, 2013, doi: 10.1002/cbic.201300562.

[62] F. M. Carlotta Granchi, Emilia C. Calvaresi, Tiziano Tuccinardi, Ilaria Paterni, Marco Macchia, Adriano Martinelli, Paul J. Hergenrotherb, "Assessing the differential action on cancer cells of LDH-A inhibitors based on the N-hydroxyindole-2-carboxylate (NHI) and malonic (Mal) scaffolds," vol. 11, no. 38, pp. 1–18, 2014, doi: 10.1039/b000000x/.

[63] N. V. Bhagavan and C.-E. Ha, "Enzymes and Enzyme Regulation," *Essentials Med. Biochem.*, pp. 63–84, 2015, doi: 10.1016/b978-0-12-416687-5.00006-3.

[64] K. Wang *et al.*, "Direct electrochemistry and electrocatalysis of glucose oxidase immobilized on glassy carbon electrode modified by Nafion and ordered mesoporous silica-SBA-15," *J. Mol. Catal. B Enzym.*, vol. 58, no. 1–4, pp. 194–198, 2009, doi: 10.1016/j.molcatb.2008.12.022.

[65] H. Fischer and I. Polikarpov, "Average protein density is a molecular-weight-dependent function," no. November, 2004, doi: 10.1110/ps.04688204.

[66] F. Jafary, M. R. Ganjalikhany, A. Moradi, and M. Hemati, "Novel Peptide Inhibitors for Lactate Dehydrogenase A (LDHA): A Survey to Inhibit LDHA Activity via Disruption of Protein-Protein Interaction," *Sci. Rep.*, no. January, pp. 1–13, 2019, doi: 10.1038/s41598-019-38854-7.

[67] H. P. Erickson, "Size and Shape of Protein Molecules at the Nanometer Level Determined by Sedimentation , Gel Filtration , and Electron Microscopy," vol. 11, no. 1, pp. 32–51, doi: 10.1007/s12575-009-9008-x.

[68] G. Pietricola, C. Ottone, D. Fino, and T. Tommasi, "Enzymatic reduction of CO2to formic acid using FDH immobilized on natural zeolite," *J. CO2 Util.*, vol. 42, no. June, p. 101343, 2020, doi: 10.1016/j.jcou.2020.101343.

[69] P. Vejayakumaran, I. A. Rahman, C. S. Sipaut, J. Ismail, and C. K. Chee, "Structural and thermal characterizations of silica nanoparticles grafted with pendant maleimide and epoxide groups," *J. Colloid Interface Sci.*, vol. 328, no. 1, pp. 81–91, 2008, doi: 10.1016/j.jcis.2008.08.054.

[70] C. Bernal, L. Sierra, and M. Mesa, "Improvement of thermal stability of β-galactosidase from Bacillus circulans by multipoint covalent immobilization in hierarchical macro-mesoporous silica," *J. Mol. Catal. B Enzym.*, vol. 84, pp. 166–172, 2012, doi: 10.1016/j.molcatb.2012.05.023.

[71] M. V. Lombardo, M. Videla, A. Calvo, F. G. Requejo, and G. J. A. A. Soler-Illia, "Aminopropyl-modified mesoporous silica SBA-15 as recovery agents of Cu(II)-sulfate solutions: Adsorption efficiency, functional stability and reusability aspects," *J. Hazard. Mater.*, vol. 223–224, pp. 53–62, 2012, doi: 10.1016/j.jhazmat.2012.04.049.

[72] J. M. Guisán, "Aldehyde-agarose gels as activated supports for immobilization-stabilization of enzymes," *Enzyme Microb. Technol.*, vol. 10, no. 6, pp. 375–382, 1988, doi: 10.1016/0141-0229(88)90018-X.

[73] M. D. Donohue and G. L. Aranovich, "Classification of Gibbs adsorption isotherms," *Adv. Colloid Interface Sci.*, vol. 76–77, pp. 137–152, 1998, doi: 10.1016/S0001-8686(98)00044-X.

[74] P. Bertier *et al.*, " On the Use and Abuse of N 2 Physisorption for the Characterization of the Pore Structure of Shales ," *Fill. Gaps – from Microsc. Pore Struct. to Transp. Prop. Shales*, vol. 21, pp. 151–161, 2016, doi: 10.1346/cms-wls-21-12.

[75] K. V. Kumar *et al.*, "Characterization of the adsorption site energies and heterogeneous surfaces of porous materials," *J. Mater. Chem. A*, vol. 7, no. 17, pp. 10104–10137, 2019, doi: 10.1039/c9ta00287a.

[76] Q. Xiong, K. Li, D. Yang, H. Yu, Z. Pan, and Y. Song, "Characterizing coal pore space by gas adsorption, mercury intrusion, FIB–SEM and μ-CT," *Environ. Earth Sci.*, vol. 79, no. 10, 2020, doi: 10.1007/s12665-020-08950-3.

[77] R. Kumar, "Nanoporous carbons derived from binary carbides and their optimization for hydrogen storage Nanoporous Carbons Derived from Binary Carbides and their Optimization for Hydrogen Storage A Thesis Submitted to the Faculty of by Ranjan Kumar Dash in partial fu," no. January 2006, 2015.

[78] T. Z. Forbes, "X-ray Diffraction," *Encycl. Earth Sci. Ser.*, pp. 1–4, 2016, doi: 10.1007/978-3-319-39193-9_25-1.

[79] Barrett, Joyner, and Halenda, "BJH analysis," *Vol. Area Distrib. Porous Subst.*, vol. 73, no. 1948, pp. 373–380, 1951.

[80] M. Dittrich, "Fourier Transform Infrared Spectroscopy for Molecular Analysis of Microbial Cells," *Methods Mol. Biol.*, no. May 2021, 2012, doi: 10.1007/978-1-61779-827-6.

[81] C. Y. Tang and Z. Yang, *Transmission Electron Microscopy (TEM)*. Elsevier B.V., 2017.

[82] Y. Matoba *et al.*, "An alternative allosteric regulation mechanism of an acidophilic L-lactate dehydrogenase from Enterococcus mundtii 15-1A An alternative allosteric regulation mechanism of an acidophilic L -lactate dehydrogenase from Enterococcus mundtii 15-1A," *FEBS Open Bio*, no. January, 2015, doi: 10.1016/j.fob.2014.08.006.

[83] N. A. Pronina, "Functional Properties of Lactate Dehydrogenase from Dunaliella salina and Its Role in Glycerol Synthesis," no. May, 2014, doi: 10.1023/A.

[84] C. J. Valvona, H. L. Fillmore, P. B. Nunn, and G. J. Pilkington, "The Regulation and Function of Lactate Dehydrogenase A : Therapeutic Potential in Brain Tumor," 2015, doi: 10.1111/bpa.12299.

[85] T. Saba, J. W. H. Burnett, J. Li, P. N. Kechagiopoulos, and X. Wang, "A facile analytical method for reliable selectivity examination in cofactor NADH regeneration," pp. 1231–1234, 2020, doi: 10.1039/c9cc07805c.

[86] G. Pietricola *et al.*, "Synthesis and characterization of ordered mesoporous silicas for the immobilization of formate dehydrogenase (FDH)," *Int. J. Biol. Macromol.*, vol. 177, pp. 261–270, 2021, doi: 10.1016/j.ijbiomac.2021.02.114.

[87] F. López-gallego, G. Fernandez-lorente, J. R.- Martin, J. M. Bolivar, C. Mateo, and J. M. Guisan, "Stabilization of Enzymes by Multipoint Covalent Immobilization on

Supports Activated with Glyoxyl Groups," no. November 2016, 2013, doi: 10.1007/978-1-62703-550-7.

[88] A. C. Diesing, "Reduction of Schiff Bases with Sodium Borohydride," pp. 1068–1070, 1956.

[89] "Product Information : ATTO NHS-Esters," pp. 1–4, 2021.

[90] "Product Information Sheet: ATTO 488," p. 2, 2017, [Online]. Available: https://www.atto-tec.com/fileadmin/user_upload/Katalog_Flyer_Support/ATTO_488.pdf.

[91] S. Ma, W. Liu, Z. Wei, and H. Li, "Mechanical and thermal properties and morphology of epoxy resins modified by a silicon compound," *J. Macromol. Sci. Part A Pure Appl. Chem.*, vol. 47, no. 11, pp. 1084–1090, 2010, doi: 10.1080/10601325.2010.511522.

[92] S. Azarshin, J. Moghadasi, and Z. A Aboosadi, "Surface functionalization of silica nanoparticles to improve the performance of water flooding in oil wet reservoirs," *Energy Explor. Exploit.*, vol. 35, no. 6, pp. 685–697, 2017, doi: 10.1177/0144598717716281.

[93] H. Gustafsson, E. M. Johansson, A. Barrabino, M. Odén, and K. Holmberg, "Immobilization of lipase from Mucor miehei and Rhizopus oryzae into mesoporous silica-The effect of varied particle size and morphology," *Colloids Surfaces B Biointerfaces*, vol. 100, no. 100, pp. 22–30, 2012, doi: 10.1016/j.colsurfb.2012.04.042.

[94] N. Yusoff, *Graphene-polymer modified electrochemical sensors*. Elsevier Inc., 2018.

[95] R. A. S. Couto, J. L. F. C. Lima, and M. B. Quinaz, "Recent developments, characteristics and potential applications of screen-printed electrodes in pharmaceutical and biological analysis," *Talanta*, vol. 146, pp. 801–814, 2016, doi: 10.1016/j.talanta.2015.06.011.

[96] S. Damiati and B. Schuster, "Electrochemical biosensors based on S-layer proteins," *Sensors (Switzerland)*, vol. 20, no. 6, pp. 1–22, 2020, doi: 10.3390/s20061721.

[97] M. R. Romero, F. Ahumada, F. Garay, and A. M. Baruzzi, "Amperometric Biosensor for Direct Blood Lactate Detection," vol. 82, no. 13, pp. 5568–5572, 2010.

[98] O. Josypčuk, J. Barek, and B. Josypčuk, "Electrochemical Biosensors Based on Enzymatic Reactors Filled by Various Types of Silica and Amalgam Powders for Measurements in Flow Systems," *Electroanalysis*, vol. 28, no. 12, pp. 3028–3038, 2016, doi: 10.1002/elan.201600273.

[99] M. Sharifi, S. M. Robatjazi, M. Sadri, and J. M. Mosaabadi, "Immobilization of organophosphorus hydrolase enzyme by covalent attachment on modified cellulose microfibers using different chemical activation strategies: Characterization and stability studies," *Chinese J. Chem. Eng.*, vol. 27, pp. 191–199, 2019, doi: 10.1016/j.cjche.2018.03.023.

[100] S. R. Patel, M. G. S. Yap, and D. I. C. Wang, "Immobilization of l -lactate dehydrogenase on magnetic nanoclusters for chiral synthesis of pharmaceutical compounds," vol. 48, pp. 13–21, 2009, doi: 10.1016/j.bej.2009.07.017.

[101] G. Cheng, Z. Pi, Z. Zheng, S. Liu, Z. Liu, and F. Song, "Talanta Magnetic nanoparticles-based lactate dehydrogenase microreactor as a drug discovery tool for rapid screening inhibitors from natural products," *Talanta*, vol. 209, no. November 2019, p. 120554, 2020, doi: 10.1016/j.talanta.2019.120554.

Appendix A

Graphene is a flat single-layer formed by carbon atoms tightly packed into honeycomb lattice. Among its properties, those which make it suitable for enzyme immobilization are a large specific surface area and the diversity of functional groups on its surface (epoxy, hydroxyl, carboxyl and carbonyl groups). There are many ways of producing graphene but the most common is graphite oxidation-reduction method. Among all the derivatives, graphene oxide and partially reduced graphene oxide, rather than pristine graphene, are the common-used supports for enzyme immobilization due to the abundant functional groups. [35]

CNTs are nanoscale circular tubes consisting of a hexagonal arrangement of hybridized carbon atoms, which are formed by a single or multi-layer graphene sheet coiled around the central axis at a certain rotation angle. There exist single-walled carbon nanotubes (SWCNTs) and multi-walled carbon nanotubes (MWCNTs). Properties as high specific surface area, large aspect ratios, mechanical strength and chemical stability are typical of CNTs. In this case, immobilization occurs mostly through physical adsorption or cross-linking. [35]

MOFs are porous network structures with tridimensional crystallinity, which are constructed by linking metal ions or clusters and organic ligands via coordination bonds. They are characterized by large specific surface area (typically ranging from 1,000 to 10,000 m^2/g), high porosity (pores' diameter typically ranging from 1 to 10 nm) and adjustable structure. Simple, gentle, and eco-friendly synthesis method make them a valid solution for the future of enzyme immobilization. [35]

DNA origami refers to the self-assembly of highly complex nanostructures by combining a long single strand of DNA with a series of short and engineered DNA fragments via the specific interaction between complementary base pairs. Immobilization of enzymes onto the DNA scaffold with precise positions is a promising approach for the self-organization of enzyme-DNA origami composite nanostructures. [35]

Polymers with flexibility and diversity can be rationally designed based on the enzyme characteristics, which have been proved as one of the most promising materials for enzyme immobilization. Their characteristics are tailored permeability together with colloidal and mechanical strength. Polymers nanostructures has also been used as carriers for enzyme and multi-enzyme immobilization. Natural polymers, in particular, are inert, non-toxic, biodegradable and biocompatible. As well as, they can be treated with different functional groups easily by chemical reactions that occur under gentle conditions in absence of impurities. Their multiple applications are also due to their low prices and great availability. Carriers based on cellulose, as the cheapest natural polymer on the earth for enzyme immobilization, were noticeable because of their ideal properties like hydrophilicity, renewability, and low contamination risk to the environment. Cellulose could be plant-based or synthesized by algae, tunicates, and some bacteria. Additionally, three hydroxyl groups exist in every monomeric unit (glucose) of cellulose chemical structure with the potential of making covalent bonds with amino acids of biocatalysts. [35] [99]

Metal [36], TiO_2, magnetic nanoparticles [9] [100] and other natural polymers have been used for the fabrication of efficient enzyme systems. Magnetic beads exploiting covalent bonding have also been used for magnetic immobilization of LDH on nanoparticles or

nanoclusters.[101][100] Glyoxyl-agarose beads have been used mostly for their good biocompatibility, low price and biodegradability. [34] [35]

Paper and paper-based materials have attracted significant interest mainly because of cellulose constitution, which is the most abundant, renewable biopolymer on earth. [47]

Eventually, silica (SiO_2) materials are one of the widely used porous structures with various applications. They possess ordered pore structure, narrow pore size distribution, large specific surface area (~1,000 m^2/g) and high stability. The ordered mesoporous materials arise from the efforts to obtain materials with larger pores, which can process larger molecules than the microporous channels of the zeolites synthesized thus far.

Acknowledgements

Ringraziamenti

In questi mesi, alcune persone mi hanno sostenuta e aiutata nella realizzazione della tesi dal punto di vista didattico e non. Persone che in questa occasione ci tengo a ringraziare.

Devo un sentito ringraziamento al relatore Professor Marco Piumetti, determinante nella realizzazione di questa tesi. Alla correlatrice, Professoressa Valentina Alice Cauda va un altrettanto significativo "Grazie".

Il mio impegno non sarebbe stato di per sé sufficiente senza la guida della dottoranda Clarissa Cocuzza, che ha saputo avere la pazienza di condurmi in questo percorso, consigliandomi e dedicandomi il suo tempo.

Ringrazio di cuore i miei genitori, i cui immensi sacrifici non potrò mai ripagare. Alle loro parole di conforto con cui mi hanno fatto e continueranno a farmi da pilastri ogni giorno.

A Valerio, compagno, amico, fisioterapista e psicoterapeuta personale, grazie per i preziosi consigli che mi riservi e grazie per la forza ed il coraggio con cui credi in ogni mia scelta. Grazie anche per criticarmi (quasi sempre) costruttivamente.

Un enorme grazie ad Anna Maria, collega per quasi tutti questi 5 anni, e grazie a tutti gli amici che mi hanno accompagnata credendo nelle mie capacità più di quanto lo facessi io stessa, avete arricchito questo percorso di ricordi preziosi.